Development and Screening of Targeted Anticancer Nanomedicines

by

James W. Gillespie

A dissertation submitted to the Graduate Faculty of
Auburn University
in partial fulfillment of the
requirements for the Degree of
Doctor of Philosophy

Auburn, Alabama
August 1, 2015

Keywords: Cancer, Nanomedicines, Phage Display, Molecular Recognition

Approved by

Valery A. Petrenko, Chair, Professor of Pathobiology
Frank F. Bartol, Professor of Anatomy, Physiology and Pharmacology
R. Curtis Bird, Professor of Pathobiology
Mark E. Byrne, Associate Professor of Chemical Engineering
Calvin M. Johnson, Professor of Pathobiology
Stuart B. Price, Associate Professor of Pathobiology

ABSTRACT

Cancer remains a significant healthcare burden worldwide and novel strategies to improve treatment outcomes with improved patient quality of life are needed. Recently, nanomedicines, which encapsulate a therapeutic drug within a protected core, have been added to the repertoire of therapeutic options for a number of diseases. Nanomedicines provide increased circulation time and bioavailability for their encapsulated cargo, and can enhance the toxicity profile of therapeutic molecules in cancer cells. However, there are still significant dose-limiting and off-target toxicities that lead to poor clinical outcomes. Active targeting of nanomedicines to malignant cells may improve the therapeutic index of otherwise non-targeted nanomedicines. Phage display, a tool that uses a bacteriophage or 'phage' vector to display randomized peptide fusions within a structural protein of the parent vector, has been used by a number of research groups to identify ligands that interact specifically with the target cancer cells.

In this project, two landscape phage display libraries were used to identify a number of novel ligands that interact specifically with overexpressed cell surface receptors on a non-small cell lung cancer (NSCLC) cell line. Two predominate phage clones, ANGRPSMT and VNGRAEAP, were shown to be selective for their target cells and the amino acids surrounding the common NGR motif can modulate the endocytic pathway of uptake and subcellular distribution of intact phage clones. The utility of these two peptides to increase cytotoxicity of a liposomal nanomedicine (Lipodox) by incorporation of the full-length phage major coat protein, pVIII, which displays the cell-specific fusion peptide on the exterior of the liposome membrane after insertion, was demonstrated. The VNGRAEAP-modified Lipodox performed better than ANGRPSMT-modified Lipodox. This showed that internalization of the targeting ligand is required for improved drug delivery. The increase in toxicity was determined to be due to an increased rate of intracellular doxorubicin uptake when compared to untargeted Lipodox.

It was hypothesized that this actively-targeted drug delivery system could be translated into a functional screening assay in which selected ligands from either of the landscape phage display libraries could be screened for improved toxicity in the context of a common nanomedicine core. This strategy would prove more advantageous in comparison to a system developed through rational design based on binding data alone. Additionally, a novel pVIII

protein isolation procedure, which allows for rapid modification of a common nanomedicine core (Lipodox) with minimal modifications to the liposome integrity and drug retention, was developed. In this context, a novel characterization assay for quantification of protein modification to targeted liposomes using flow cytometry and characterization of protein orientation using a novel dot blot assay was also established. Using this screening assay, seven ligands that displayed increased functional activity when compared to unmodified Lipodox were identified. In a doxorubicin-sensitive cell line (breast cancer; MCF-7), four ligands – DMPGTVLP, ANGRPSMT, VNGRAEAP, and ANDVYLD – were determined to be functionally active. Similarly, in a doxorubicin-resistant cell line (pancreatic cancer; PANC-1), three ligands with structurally similar YL motifs increased toxicity at least 2-fold in comparison with unmodified Lipodox. Results provide evidence of the utility of this platform for large scale functional screening of targeted nanomedicine preparations in a number of cancer phenotypes.

ACKNOWLEDGEMENTS

I would like to thank Dr. Valery Petrenko for his excellent mentoring during my project and for the many professional development opportunities that I was given to improve the quality of my research-training program. I thank my committee members: Dr. Frank Bartol, Dr. R. Curtis Bird, Dr. Mark Byrne, Dr. Calvin Johnson, and Dr. Stuart Price for their encouragement, discussions, and advice throughout this project.

I thank Dr. Tao Wang, Dr. Abraham Abouzeid, and Dr. Vladimir Torchilin of Northeastern University for their intellectual contributions and preparation of various liposomes for this project. I also thank the intellectual contributions of my co-authors: Dr. Deepa Bedi, Dr. Lixia Wei, Dr. Anatoliy Puzyrev, and Mrs. Amanda Gross.

I would like to thank Dr. John Dennis and the College of Veterinary Medicine Department of Anatomy, Physiology, and Pharmacology for the use of their confocal microscope and assistance with confocal microscopy image acquisition/analysis. I thank Dr. R Curtis Bird and Allison Church Bird (Flow Cytometry Facility at Auburn University) for their assistance with collection and interpretation of flow cytometry data. I would also like to thank Dr. Robert Arnold, Dr. Peter Panizzi, Mr. Matthew Eggert, Mr. Andrew Brannen, and Mr. Ben Nie for their contributions and discussions leading to future developments of the work presented here.

I also thank my family and friends for their continued support throughout the duration of my training experience.

I declare that the research was conducted in the absence of any commercial or financial relationships that could be construed as a potential conflict of interest. This work was supported by the National Cancer Institute at the National Institutes of Health. [U54 CA151881 to V.A.P.] and funding support from the Auburn University Research Initiative in Cancer (AURIC) to V.A.P.

TABLE OF CONTENTS

Abstract ii

Acknowledgements iv

List of Tables vi

List of Figures vii

List of Abbreviations ix

Chapter 1: Active Targeting of Anticancer Nanomedicines 1

Chapter 2: Selection of Lung Cancer-Specific Landscape Phage for Targeted Drug Delivery 28

Chapter 3: Combinatorial synthesis and screening of cancer cell-specific nanomedicines targeted via phage fusion proteins 62

Chapter 4: Conclusions 96

Appendix I: Techniques in Phage Protein-Based Nanomedicines 97

References 142

LIST OF TABLES

Table I: Actively targeted nanomedicines with ongoing or completed clinical trials. 26

Table II: Families of peptides identified from f8/8 library 41

Table III: Families of peptides identified from f8/9 library 42

Table IV: Representative selectivity data for select phage clones from the f8/9 library 47

Table V: Cancer-interacting motifs 58

Table VI: Phage Major Coat Protein (pVIII) Properties 68

Table VII: Phage Protein-Modified Lipodox Characterization 88

LIST OF FIGURES

Figure 1: Disorganized endothelial cell junctions in a tumor model 6
Figure 2: Schematic of actively targeted nanomedicines via the EPR effect 8
Figure 3: Schematic of nanomedicine deposition by passive and/or active targeting 11
Figure 4: Schematic of nanomedicine deposition with a complex tumor microenvironment 14
Figure 5: Schematic of a pegylated liposomal nanomedicine targeted via three targeting ligands 23
Figure 6: Selection of multi-domain ligands for cancer cell-specific targeting 24
Figure 7: Schematic of f8 type landscape phage display libraries 30
Figure 8: Selection scheme to identify lung cancer cell-specific phage clones 33
Figure 9: Recovery of phage following each round of selection 38
Figure 10: Recovery of phage following each round of selection 39
Figure 11: Histogram of the change in information content after four rounds of selection 44
Figure 12: Representative selectivity and specificity assay for select phage clones from the f8/8 library 46
Figure 13: Phage mode of interaction with Calu-3 cells 49
Figure 14: Change of phage endocytosis in Calu-3 cells by chemical inhibition 52
Figure 15: Confocal microscopy of phage associated with Calu-3 cells 53
Figure 16: Cell viability of Calu-3 cells after treatment with Lipodox or modified Lipodox 55
Figure 17: Doxorubicin cell-associated uptake after 4 hours in Calu-3 cells 56
Figure 18: Phage fusion protein-targeted nanoparticles 66
Figure 19: UV/Vis spectrum of pVIII major coat protein solubilized in 75% 2-propanol 74
Figure 20: SDS-PAGE of pVIII major coat protein solubilized in 75% 2-propanol 75
Figure 21: Purification and characterization of DMPGTVLP-modified Lipodox 77
Figure 22: Schematic of phage protein orientation assay 79
Figure 23: N-terminal orientation assay in DMPGTVLP-modified Lipodox 80
Figure 24: Phage protein orientation assay by dot blot analysis 82

Figure 25: Flow cytometry analysis of unmodified Lipodox and 488-labeled-DMPGTVLP-modified Lipodox 84

Figure 26: MTT viability assay of MCF-7 cells treated with Lipodox or DMPGTVLP-modified Lipodox 85

Figure 27: Doxorubicin uptake assay in MCF-7 cells treated Lipodox or DMPGTVLP-modified Lipodox 86

Figure 28: MTT viability assay of MCF-7 cells treated with dilutions of phage protein-modified Lipodox 88

Figure 29: MTT viability assay of PANC-1 cells treated with dilutions of phage protein-modified Lipodox 89

Figure 30: Spontaneous insertion of the major coat protein into lipid membranes 93

LIST OF ABBREVIATIONS

ABC – ATP-binding cassette

ABC – accelerated blood clearance

API – active pharmaceutical ingredient

APN – aminopeptidase N (CD13)

AT-II – angiotensin II

BBB – blood brain barrier

CPPs – cell penetrating peptides

DNA – deoxyribonucleic acid

DOX - doxorubicin

ECM – extracellular matrix

EMEM – Eagle's minimal essential medium

EPR – enhanced permeation and retention

IV – intravenous

JAM-1 – junctional adhesion molecule-1

MMPs – matrix metalloproteases

MPS – mononuclear phagocyte system

NO – nitric oxide

NSCLC – non-small cell lung cancer

Phage – bacteriophage

PEG – polyethylene glycol

R8 – octa-arginine

RES – reticuloendothelial system

RRR – remove, recentrifuge, remove

SCLC – small cell lung cancer

siRNA – silencing ribonucleic acid (RNA)

TAT – *trans*-acting activator of transcription

TKIs – tyrosine kinase inhibitors

VEGF – vascular endothelial growth factor

CHAPTER 1

ACTIVE TARGETING OF ANTICANCER NANOMEDICINES

1. Failure of Classic Small Molecule Chemotherapies

Significant progress has been made in the management and treatment of malignant neoplasms; however cancers are still recognized as a leading cause for mortality in the United States and worldwide (Mathers et al. 2008). Classically, efforts in tumor management using different cytotoxic drugs rely primarily on the specificity of a given drug to selectively kill cells undergoing mitosis. In general, chemotherapeutic drugs accumulate non-specifically in all reachable cells. Once high enough concentrations of the cytotoxic drugs accumulate within the cells, most classic chemotherapies will act by interfering with progression of a cell through the cell cycle and cause cell death by apoptosis or other mitotic catastrophes. Several common classes of chemotherapies that are classified by their mechanism of action, including: alkylating agents (Bignold 2006), anti-metabolites (Kaye 1998), anti-tumor antibiotics (Galm et al. 2005; Abdella & J. Fisher 1985), topoisomerase inhibitors (Pommier 2006), and mitotic inhibitors (Chan et al. 2012). Each class of chemotherapy is intended to interfere with a certain defined process within the cell cycle or to cause direct damage to DNA molecules, thereby inhibiting cell replication. Once these cells accumulate in a stalled cell state, and if they are unable to repair the damage or bypass the defect, they will begin the process of programmed cell death or apoptosis. Thus, commonly used chemotherapy drugs provide an initial level of cell cycle-specific targeting by inhibition of specific processes within the normal cell cycle. Combinations of several different classes of small molecule drugs have been used successfully in the clinic for decades. However, despite the effects achieved by cell cycle-specific targeting, there are significant side effects and/or increased risk factors for increases in toxicity due to non-specific accumulation of these drugs. For example, doxorubicin is commonly known for its severe cardiotoxicity, and as a result, patients are limited to a maximum lifetime treatment dose that is considered safe in order to prevent severe complications (Chlebowski 1979). Improvements in small molecule drugs have led to the development of a new class of tyrosine kinase inhibitors (TKIs), such as Gleevec, which act by modulating growth signaling pathways aberrantly expressed in certain cancers. TKIs have shown significant improvements in cancer management, however tumors are still prone to develop drug resistance and lack treatment response in the general, unselected patient population (Arora & Scholar 2005).

Several limitations have been observed with traditional small molecule therapies, apart from the non-specific cell accumulation. These include: 1) rapid blood clearance, 2) poor aqueous solubility for certain hydrophobic molecules, 3) inherent susceptibility to ATP-binding cassette (ABC) transporters, and 4) rapid degradation/modification into a non-toxic, non-active metabolite (Z. G. Chen 2010). These limitations have traditionally been overcome by altering dosing schedules and/or increasing doses, administration of the small molecule with a biologically-compatible excipient (Buggins et al. 2007; Gardner et al. 2008), or modulation of ABC transporter activity (Shukla et al. 2011). Despite these improvements, it is common for these drugs to have a low therapeutic index – typically defined to be the ratio of the highest exposure of drug that results in no toxicity to the exposure that produces the desired effect (P. Y. Muller & Milton 2012). Drugs that have a low therapeutic index often result in sub-optimal patient quality of life. There is a critical need for improvements in cancer drug delivery systems that would result in improved patient care with increased survival time post-treatment.

2. Rise of Nanomedicines and Drug Delivery Systems

The last few decades have witnessed significant advances in nanotechnology, which deals with particles in the scale of 1-1,000 nm in any single dimension (Ferrari 2005). Nano-scale devices have been developed for a number of applications that fall broadly into three categories: diagnostic (Grodzinski et al. 2006), therapeutic (Petros & DeSimone 2010), or theranostic. The latter is an emerging treatment paradigm that combines disease diagnostics with therapeutics into a single device (Xie et al. 2010). Following is a brief discussion of therapeutic nanoparticles. Many of the same principles that apply to nanomedicines also apply to diagnostic nanoparticles. Therapeutic nanoparticles, or nanomedicines, are composed primarily of two major components: a therapeutic molecule and a drug delivery system/nanocarrier. Nanomedicines can also be modified to contain additional components including a polymer coating, like polyethylene glycol (PEG), a targeting molecule(s), or a reactive linker molecule. Drug conjugates, nanoparticles composed of a therapeutic molecule covalently attached to one or more of the additional component like PEG, are also classified as nanomedicines because of their nano-scale size and similar biological properties even though they lack a defined nanoparticle core.

A common characteristic of nanomedicines is their ability to improve the systemic bioavailability of small molecule drugs and subsequently improve their therapeutic effect by providing prolonged circulation of such molecules in a patient (Ventola 2012). It is clear that nanomedicines increase the circulation time of a therapeutic molecule when compared to non-encapsulated forms (Gabizon et al. 1994). In general, encapsulation of a

therapeutic molecule within a nanomedicine core greater than ~10 nm in diameter prevents rapid renal clearance (Longmire et al. 2008) and provides protection against metabolic degradation (Paolino et al. 2010; Immordino et al. 2004). Both of these mechanisms lead to loss of activity. However, because of the inactivation of renal clearance mechanisms, nanomedicines, such as liposomes, are rapidly cleared in the liver or through actions of the mononuclear phagocyte system (MPS)[1]. Therefore, modifications must be made to the nanocarrier to prevent such rapid clearance (Gabizon & Papahadjopoulos 1988). Traditionally, this is achieved by coating the nanomedicine with a biologically unreactive polymer coating such as PEG to prevent binding of serum opsonins (Gabizon et al. 2003; Lankveld et al. 2011). Despite improvements in bioavailability provided by polymer coatings, nanomedicines are still rapidly removed after repeated doses by a phenomenon referred to as accelerated blood clearance (ABC) (Ishida et al. 2003; Ishida & Kiwada 2008). This emphasizes the need for improved therapeutics with increased activity in a single dose to prevent therapeutic intolerance. Untargeted nanomedicines alone increase the therapeutic index compared to their unencapsulated counterparts via mechanisms discussed above. However, dose limiting toxicities still remain and non-specific accumulation of nanomedicines in the liver, spleen and other components of the MPS produce undesired side effects.

In the early 1900s Paul Ehrlich pioneered the concept of a therapeutic "magic bullet" and ushered in the era of modern chemotherapy research (Strebhardt & Ullrich 2008). This idea that a therapeutic molecule could be delivered specifically to diseased cells within an organism, serves as the foundation upon which various research groups have built for the past hundred years. Once delivered, the therapeutic molecule was envisioned to provide curative treatment of the disease by either correction of the disease state or removal of the diseased cells. While leaving the healthy cells unharmed. Ehrlich proposed that this could be achieved through specific interactions of an antigen interacting with a side chain or receptor molecule expressed on the surface of a cell (Strebhardt & Ullrich 2008). This led to the general hypothesis that nanomedicines could be targeted specifically to cancer cells by a process termed active targeting, a term that describes the accumulation of a nanocarrier in a target due to cell-specific, ligand-receptor interactions (Bae & K. Park 2011). Following is a short review of the field of actively targeted anti-cancer nanomedicines with a specific focus on the benefits and properties achieved through active

[1] Also referred to as the Reticuloendothelial System (RES) in older literature, but has been replaced for the term MPS as it is now understood that most endothelial cells do not possess phagocytic activities like macrophages (Singh 2006).

targeting of peptide ligands. Included is a brief summary of future directions and areas requiring additional study in this rapidly developing field.

3. Present Trends in Actively Targeted Nanomedicines

Active targeting can be achieved by a variety of different reactive moieties including those provided by small molecules, peptides and proteins, DNA aptamers, antibody fragments, or even whole antibodies. These ligands can be generated from a number of sources including naturally derived products, phage display libraries (G. P. Smith & Petrenko 1997), aptamer libraries (Cerchia & de Franciscis 2010), or engineered antibodies (Attarwala 2010). Regardless of the type of ligand used, there are a number of factors that affect the delivery of a nanocarrier including ligand density, ligand charge and ligand orientation/availability (Bertrand et al. 2014). These ligands can be attached to one of the components of the drug delivery system in a number of methods including covalent linkages, hydrophobic interactions or non-covalent interactions, such as the streptavidin-biotin system.

3.1. Systemic Interactions

3.1.1. Circulatory system

Following IV infusion of a nanomedicine, any exposed targeting ligand will be immediately subjected to serum proteases, DNAses, and RNAses. Free peptides (< 50 amino acids) show very rapid serum degradation and clearance from circulation by the kidneys. Attachment of peptides to a high molecular weight PEG or nanocarrier delivery system results in increased circulation time and decreased renal clearance (Pollaro & Heinis 2010). Several strategies have been used to increase resistance of protein ligands to degradative effects of serum proteases including: optimization/selection of cleavage-resistant primary sequences, introduction of secondary structure to reduce substrate recognition, shielding of functionally active domains, derivatization of cleavable sites, and functionalization of peptide termini. For example, using mRNA display, protease-resistant peptides were generated with increased serum stability as much as 400-fold higher when compared to peptides selected in the absence of a protease selective pressure (Howell et al. 2014). Protein ligands can also be synthesized as inactive precursors that display the active targeting ligands following enzymatic cleavage with serum proteases.

Ligands can also be susceptible to certain spontaneous or enzyme-mediated chemical reactions that modify the final binding interactions with the desired cell targets. For example, peptide ligands containing asparagine are susceptible to deamination and isomerization at physiological conditions (37ºC and pH 7.4) that result in either aspartic acid or L/D-iso-aspartic acid residues (Wakankar & Borchardt 2006). The reactivity of asparagine residues

can modify the resulting charge of a ligand under certain physiological conditions, resulting in undesired alterations in peptide binding (Corti & Curnis 2011).

3.1.2. Immune Reactivity and Clearance

Nanomedicines promote a number of immune responses *in vivo* because they are recognized as foreign substances that must be removed to prevent damage to the host (Dobrovolskaia & McNeil 2007). Targeting ligands are subject to the same general problems of immunogenicity as untargeted nanomedicines. However, targeted ligands are more of a concern for immunogenicity and design considerations that limit adverse immune responses are required to improve bioavailability. In some situations, proteolytic cleavage of protein ligands by serum proteases prior to cellular uptake can result in higher immunogenicity by cytotoxic T cells following presentation of the MHC class I complex (Falo et al. 1992). This results in increased nanomedicine clearance with repeated doses. Nanomedicines and their impact on the immune system was discussed in a previous review (Zolnik et al. 2010) and focused on the immunotoxicity of nanoparticles rather than the immunoreactivity of nanomedicines with active targeting moieties.

3.2. Microenvironment-Specific Interactions

3.2.1. Interactions of Non-targeted Nanomedicines with Diseased Vasculature

The circulatory system can be regarded as the primary route for nanomedicine dispersion throughout the body. However, to exert their biological effect they must escape from circulation and enter into the cancer microenvironment. Physiologically normal capillaries are composed of three major components: endothelial cells, pericytes, and a basement membrane. These three components work together to provide a continuous conduit for the circulatory system and serves as a primary barrier for erythrocytes, plasma proteins, and other circulating cells/molecules from diffusing into the surrounding environment under normal physiological conditions. As shown in Figure 1 (left), physiologically normal blood capillaries contain tight endothelial junctions between neighboring cells. However, capillaries within a tumor tissue are more disorganized and contain large gaps between neighboring endothelial cells (Figure 1, right). These gaps, or fenestrations, are commonly observed in rapidly growing neovasculature of tumor tissues due to the secretion of vascular endothelial growth factor (VEGF) into the surrounding tissues by neoplastic cells. Rapid capillary growth results in highly fenestrated capillaries instead of a properly formed, continuous capillary bed (Roberts & Palade 1997). Fenestrated capillaries are typically characterized as having gaps ≤100 nm in diameter. However, in tumor xenografts, such capillaries can allow

liposomes of up to ~600 nm in diameter to extravasate out of the capillaries and into the tumor microenvironment (Yuan et al. 1995). Increased vessel leakiness is a single feature in a collection of interrelated processes referred to as the enhanced permeation and retention (EPR) effect. Nanomedicines designed to rely on passive accumulation within the tumor microenvironment by virtue of the EPR effect showed promising results in the clinic with liposomes drug delivery systems such as Doxil (Gabizon et al. 2003).

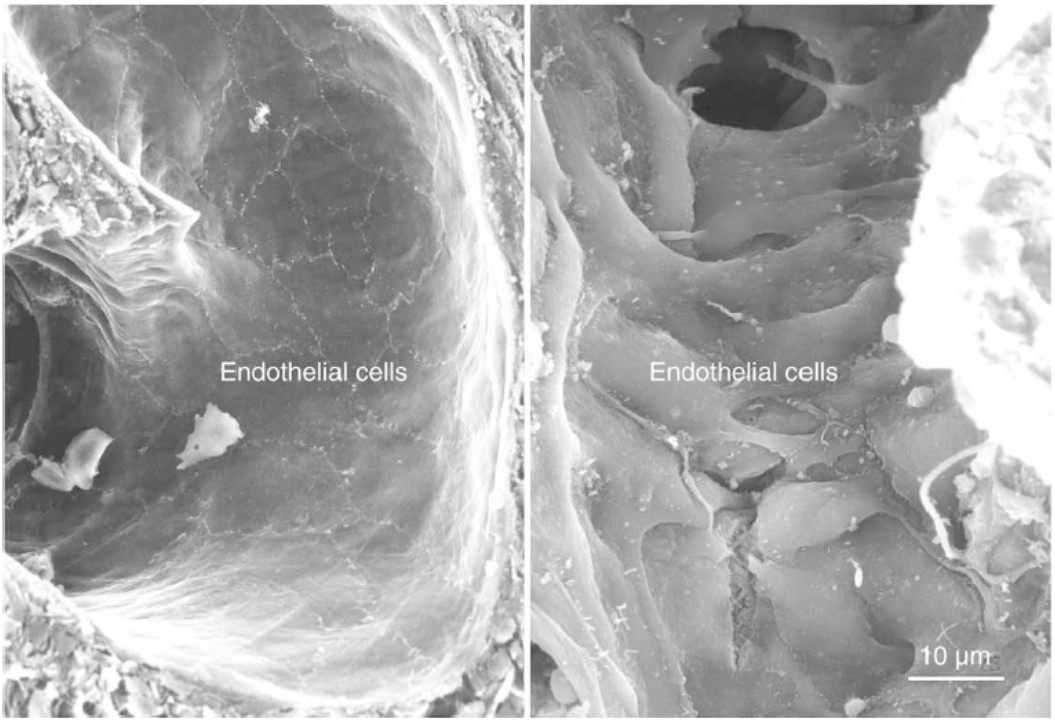

Figure 1: Scanning electron micrograph of the luminal side of (*Left*) tight endothelial cell junctions in normal blood capillaries and (*Right*) disorganized endothelial cell junctions in a tumor model. Reprinted with permission from (Baluk et al. 2005).

3.2.2. Interactions of Targeted Nanomedicines with Diseased Vasculature

The vascular bed of normal and diseased tissues is highly heterogeneous and expresses a number of different cell surface receptors based on the tissue site (Rajotte et al. 1998) and disease state (Arap, Pasqualini & Ruoslahti 1998a; Ruoslahti 2000; Ruoslahti 2002). This can be exploited to deliver therapeutics specifically to a diseased site by attachment of a homing peptide (Arap, Pasqualini & Ruoslahti 1998a). Actively targeted nanomedicines may be recruited specifically to vasculature around the tumor microenvironment (Figure 2) through a mechanism similar to that observed with leukocyte accumulation at specific sites. During leukocyte accumulation, rolling adhesion interactions are formed between leukocytes and specific integrins or selectins expressed on

endothelial cell surfaces (Berlin et al. 1995). Blood rheology studies show that a transported nanomedicine should follow the path of greatest effective diffusion, which is reduced as a particle moves from larger to smaller vessels. Further, as the size of a nanomedicine increases, the smaller its diffusion coefficient becomes. This can create a physiological barrier preventing delivery of nanomedicines from the microcirculation (Gentile, Ferrari, et al. 2008b). Spherical particles of small size (<200 nm) will only marginate to the capillary wall under the effects of external field forces such as gravity or electromagnetic fields (Gentile, Curcio, et al. 2008a). However, non-spherical particles have a greater propensity to marginate to vessel walls than spherical particles due to more dynamic/stochastic particle movements within the vessels (Carboni et al. 2014). Collectively, these observations indicate that a low-affinity, vascular-specific targeting ligand will allow selective partitioning of nanomedicines out of the central blood flow and towards the outer edges of capillary walls. Once nanomedicines are marginalized and slowed, the number of interactions with the vascular fenestrations is increased resulting in enhanced accumulation of particles by the EPR effect. Cancer vasculature-specific proteins have been identified including aminopeptidase N, integrins, and cell surface expressed nucleolin as discussed below.

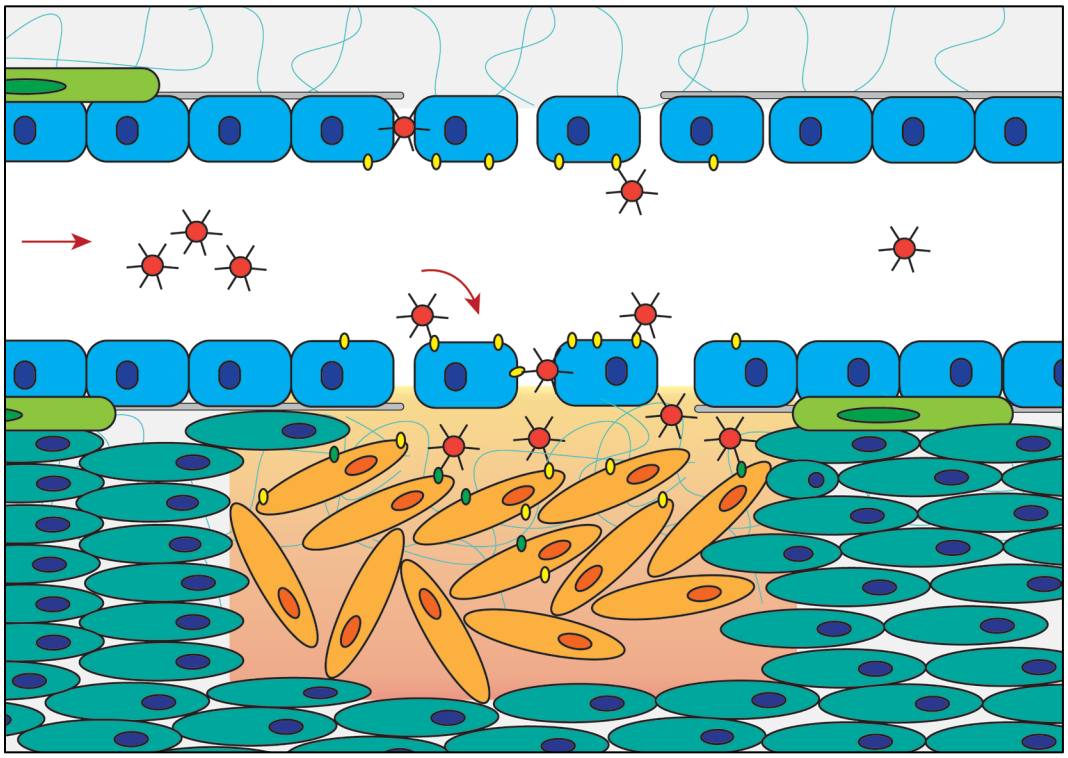

Figure 2: Schematic of actively targeted nanomedicines to penetrate into the complex tumor microenvironment. Active targeting allows marginalization of nanomedicines to sites of diseased vasculature followed by extrusion through fenestrations present in the endothelial capillary cells via the EPR effect.

Aminopeptidase N (APN/CD13), a type II integral membrane protein composed of 967 amino acids that exists as a homodimer, is responsible for the catalytic removal of neutral amino acids from small peptide fragments. CD13 plays an important role in tumor cell invasion (Ishii et al. 2001), extracellular matrix degradation (Saiki et al. 1993), and angiogenesis (Rangel et al. 2007). It is selectively expressed by vascular endothelial cells (Fukasawa et al. 2006) liver cancer stem cells (Haraguchi et al. 2010), and in a number of disease states including breast cancer (Dixon et al. 1994), colon cancer (Hashida et al. 2002), melanoma (Menrad et al. 1993), non-small cell lung cancer (Tokuhara 2006), and pancreatic cancer (Ikeda et al. 2003). CD13 may serve as a marker of poor clinical prognosis for diseases such as non-small cell lung cancer (Tokuhara 2006), and is expected to identify poor prognosis for additional cancer phenotypes. Ligands containing an exposed Asn-Gly-Arg (NGR) motif were suggested to interact specifically with CD13 (Corti et al. 2008; Pasqualini et al. 2000).

Integrins are a class of type I transmembrane glycoproteins that exist as heterodimers composed of α and β subunits that are responsible for cell-cell and cell-extracellular matrix (ECM) interactions. In mammals, there are 18 α subunits and 8 β subunits that display inter-species structural conservation (Carson-Walter et al. 2001). Combination of α and β subunits produces the 24 known heterodimer assemblies (R. O. Hynes 2002). Integrins activate cell signaling pathways that affect a number of physiological responses and conditions including: cell cycle progression (Giancotti 1997; Moreno-Layseca & Streuli 2014), cell shape (Boudreau & P. L. Jones 1999), composition of the ECM, and cell motility (Huttenlocher & Horwitz 2011). Tumor endothelial cells express a number of different integrins. Such expression can indicate angiogenesis, which may result in metastasis and a poor prognosis (Desgrosellier & Cheresh 2010). For example, most proliferative endothelial cells within tumor-associated blood vessels express elevated levels of integrin $\alpha_v\beta_3$. This is identified as a poor prognostic marker for breast cancer patients (Gasparini et al. 1998). Ligands containing an exposed Arg-Gly-Asp (RGD) motif can interact with a number of integrin heterodimers including: $\alpha_5\beta_1$, $\alpha_8\beta_1$, $\alpha_v\beta_1$, $\alpha_v\beta_3$, $\alpha_v\beta_5$, $\alpha_v\beta_6$, $\alpha_v\beta_8$, and $\alpha_{IIb}\beta_b$ (Ruoslahti 1996; Pytela et al. 1985). The amino acids surrounding an RGD motif and peptide conformation (linear vs. cyclic) can have significant functional properties that change binding specificity or activation of certain downstream signaling cascades (Pfaff et al. 1994; Fani et al. 2006).

Nucleolin, a soluble phosphoprotein composed of 707 amino acids that corresponds to an apparent molecular mass of ~100-110 kDa (77 kDa predicted molecular mass), is primarily involved in nucleosome remodeling (Angelov et al. 2006), pre-rRNA processing (Ginisty et al. 1998), and the nuclear-cytoplasmic shuttling of ribosomal proteins/subunits (Ginisty et al. 1999). However, nucleolin may have additional functions (Tajrishi et al. 2011). Initially, nucleolin was described as a predominantly nuclear protein comprising up to 5-10% of the total nuclear protein mass and expressed in large quantities during exponential cell growth (Lapeyre et al. 1987). However, recent data showed constant expression of nucleolin on the surface of cancer cells, where it acts to internalize bound ligands in a calcium- and temperature-dependent mechanism (Hovanessian et al. 2010). Nucleolin is constitutively expressed on the surface of neovascular endothelial cells (Christian 2003) and also on tumor cells (Hovanessian et al. 2010). Cell surface nucleolin was implicated in cell behaviors including enhanced cell proliferation (Srivastava & Pollard 1999; Hovanessian et al. 2010), tumorigenesis (Di Segni et al. 2008), angiogenesis (Y. Huang et al. 2006) and acting as a molecular shuttling protein from the cell surface to the nucleus. A number of ligands including the F3 (AKVKDEPQRRSARLSAKPAPPKPEPKPKKAPAKK) peptide (Christian

2003), HB-19 pseudopeptide (Krust et al. 2011), and the fusion phage protein DMPGTVLP (Fagbohun 2010) were identified as targeting ligands for cell surface expressed nucleolin.

3.2.3. Transport Across Endothelial Cell Barriers

Current active targeting mechanisms rely heavily on the EPR effect to promote accumulation within the tumor microenvironment. However, extensive debate remains on the clinical presentation of the EPR effect that is observed in preclinical models. This raises concerns about the feasibility of designing nanomedicines seeking to therapeutically exploit leaky vascular found in tumors (Taurin et al. 2012; Prabhakar et al. 2013). Some active targeting systems could fail because of the assumption of the EPR effect being present in the tumor microenvironment. As shown in Figure 3, the passive accumulation of non-ligand-targeted nanomedicines results in increased deposition of particles within the tumor microenvironment as a result of the leaky vasculature. This allows the delivery of the therapeutic molecule to the tumor. Similarly, as described above, active targeting of a nanomedicine together with passive targeting supported by the EPR effect allows for increased marginalization toward the outer capillary walls. This, in turn, allows for increased penetration of nanomedicines into the tumor microenvironment via leaky vasculature. As discussed above, the receptor being targeted may be expressed on endothelial cells. However, the receptor may also be overexpressed on cancer cells resulting in increased accumulation and penetration. Overall, active targeting of a nanomedicine in the presence of the EPR effect is hypothesized to improve the biologic effect of the nanomedicine when compared a system relying only on passive targeting. Alternatively, if the same actively targeted nanomedicine is applied to a biological system without an observed EPR effect, in which there are no leaky blood vessels, the nanomedicines will likely marginalize but fail to cross the endothelial cell barrier and reach the tumor microenvironment. This results in failure of the nanomedicine to induce a biologic response and explains some of the discrepancies observed in active targeting data obtained in *in vitro* versus *in vivo* studies (Gray et al. 2013).

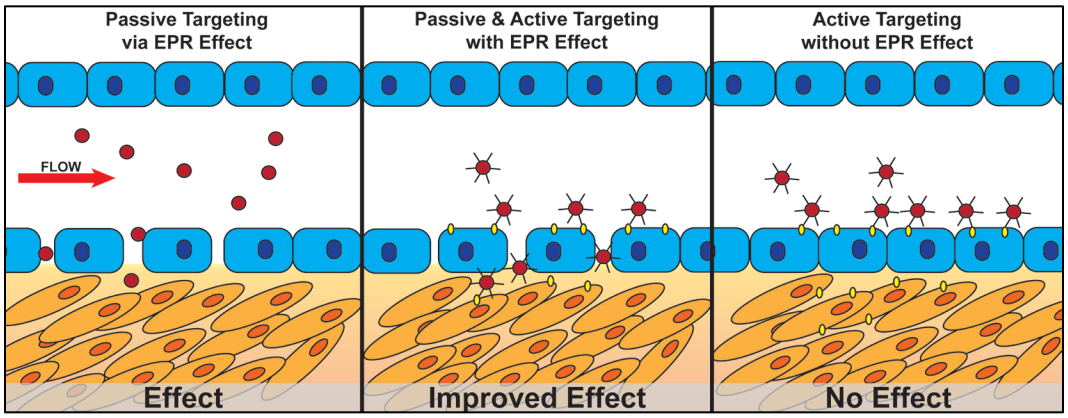

Figure 3: Schematic of nanomedicine deposition by passive and/or active targeting in the presence or absence of an EPR effect (leaky vasculature). *Left*: Passive targeting of non-ligand targeted nanomedicines results in delivery and a biologic effect. *Center*: Passive targeting of an actively targeted nanomedicine results in enhanced delivery and an improved biologic effect. *Right*: Active targeting of a nanomedicine in the absence of leaky vasculature results in marginalization of nanomedicines without delivery into the tumor microenvironment resulting in no biologic effect.

To overcome an intact endothelial cell barrier, three mechanisms that may enable nanomedicines within a blood capillary to escape/extravasate into the tumor microenvironment are being explored, including: 1) transcytosis through the intact endothelial cell layer, 2) paracellular transport by extravasation between the tight junctions of neighboring endothelial cells as seen during leukocyte extravasation, and 3) modulation of the EPR effect.

Transcytosis, which involves the specific, bidirectional transport of molecules across an endothelial cell barrier, occurs in all continuous and fenestrated vascular endothelium (Tuma & Hubbard 2003). The transcellular transport route is supported by caveolin-mediated endocytosis (see below). Active transport mechanisms of the vasculature system are bidirectional, however most proceed in an apical-to-basolateral direction based on typical concentration gradients (Tuma & Hubbard 2003). Transport proceeding in the apical-to-basolateral direction is required for ideal nanomedicine transport from the blood to the tumor interstitium. Theoretically, therefore, nanomedicines should be able to escape the vascular system to reach the interstitium of any tissue; however this is not observed. A major question in transcytosis transport is – how does the endothelial cell recognize particles for transcytosis versus degradation? It is envisioned that, upon endocytosis, certain cell surface receptors will route vacuoles to different subcellular locations that promote degradation, while other receptors will route the vacuoles across the cell. For example, the low density lipoprotein (LDL) receptor supports specific transcytosis of LDL

across the blood brain barrier (BBB) in a receptor-mediated mechanism (Dehouck et al. 1997). Another major concern here is – how does a cell recognize cargo to be used within the cell versus that destined for transport for use by other cells? Here it is hypothesized that post-translational modifications, such as ubiquitination of a cytoplasmic domain, mark vacuoles for degradation, while unmodified protein domains are marked for transport (Haglund et al. 2003). Identification of ligands that promote transcytosis for improved rational design of drug delivery systems are ongoing (Ivanenkov & Menon 2000). However, progress has been made in the transcellular delivery of nanomedicines. For example, using an antibody (TX3.833) developed to target lung caveolae, up to 89% accumulation of an IV injected drug dose was identified in the lungs within 30 minutes. Following their accumulation studies, antibody-drug conjugates were delivered to the underlying cells via transendothelial transport and increased specific drug delivery up to 170-fold when compared to untargeted drug (McIntosh et al. 2002).

In normal blood vessels, neighboring endothelial cells are held in close contact to each other through a combination of adherens junctions, tight junctions, and gap junctions (Hartsock & Nelson 2008). Adherens junctions form through the interaction of two VE-cadherin molecules expressed extracellularly on adjoining cells (Vestweber 2008). Intracellular components of these molecules (α-, β-, and gamma-catenins and p120) interact with the cytoplasmic domain of VE-cadherins to modulate adhesive strength and regulate vessel homeostasis and/or angiogenesis (Lampugnani & Dejana 2007). Tight junctions are primarily composed of the occludins, claudins, and junctional adhesion molecule-1 (JAM-1) that are involved in membrane permeability and cell polarity required to maintain vascular integrity (Bazzoni & Dejana 2004). Gap junctions are primarily involved with intercellular communication and molecule transport, however they may also function as a physical barrier that limits nanomedicine extrusion (M. W. M. Li et al. 2012).

The paracellular transport route is restricted to molecules < 6 nm in diameter (Komarova & Malik 2010). However, under proper conditions, this barrier can be traversed by much larger objects, as is observed during leukocyte extravasation and diapedesis (W. A. Muller 2009; Petri & Bixel 2006). Few nanomedicine drug delivery systems are reported to increase paracellular transport. Still, chitosan treatment was used to disrupt JAM-1 interactions reversibly and increased penetration of a tracer molecule into the tumor microenvironment (Sonaje et al. 2012; J. Zhang et al. 2014). Treatments involving irreversible tight junction modifications designed to increase nanomedicine penetration should not be used as a treatment strategy. Loss of paracellular transport barrier functions were implicated in an increased number of metastatic lesions (Martin & Jiang 2009). Extensive work on the BBB,

which is commonly used as a model of endothelial tight junctions, is ongoing with strategies involving direct modification of tight junction integrity or use of positively charged nanoparticles to increase delivery (Lockman et al. 2004). However, no targeting ligands have been identified to increase paracellular transport *in vivo*. Recently, two peptides, PIP 640 and PIP 250, were designed to reversibly open tight junctions of polarized intestinal epithelial cells allowing minor increases in insulin uptake into the portal vein following a direct injection into the lumen of the distal jejunum. The PIP 640 peptide, RKKRRVEVKYDRR, increased paracellular permeability for molecules up to 70 kDa *in vitro*, while the PIP 250 peptide was less effective, only enabling a maximum of 4 kDa proteins to traverse the cell barrier. (Taverner et al. 2015) Because mechanisms that regulate tight junction permeability in epithelial and endothelial cells are similar (Shen et al. 2010), active targeting with ligands containing these peptides may increase paracellular transport activity.

An alternative method of crossing endothelial barriers, independent targeting ligands, involves the chemical modulation of interactions between intercellular tight junctions of neighboring cells (J. Fang et al. 2011). One method to increase the EPR effect in tumor tissues is to increase leakiness of tumor blood vessels by causing a systemic constriction, or hypertension, in normal blood vessels. For example, angiotensin II (AT-II) can be used to cause systemic vasoconstriction of the pericytes surrounding blood vessels. However, because of the lack of pericytes in tumor vessels, there is no constriction in these vessels (M. Suzuki et al. 1981). The resulting constriction in normal vessels causes an increase in blood volume locally within the tumor and enables deposition of additional nanomedicines within the microenvironment (J. Fang et al. 2011). A second method used to increase the EPR effect involves use of nitric oxide (NO)-releasing compounds at specific sites that cause selective vasodilation of the nearby blood vessels. Nitroglycerin, a commonly used vasodilator, was used in combination with a small molecule anthracycline, which resulted in enhanced delivery of the anthracycline in the tumor and showed an improved therapeutic response (Seki et al. 2009). This method requires the use of additional small molecule therapies to modulate the EPR effect and enhance passive targeting rather than using active targeting to overcome the barrier. Further discussion of this strategy is available in an excellent review provided elsewhere (J. Fang et al. 2011).

3.2.4. Microenvironment Penetration

It is hypothesized that the failure of numerous nanomedicines could be associated with the inability of nanomedicines to penetrate through the complex tumor microenvironment into the core of certain tumors. The tumor microenvironment is composed of three major compartments: 1) the interstitial fluid; 2) the non-cellular interstitial

components, such as the extracellular matrix (ECM); and 3) the cellular components or stromal cells (Wiig et al. 2010). Owing to the complex tumor microenvironment, it is commonly observed that larger nanomedicines will fail to penetrate into the tumor and only reach the first few layers of tumor cells, as suggested in Figure 4 (Stapleton et al. 2013). This causes nanomedicines to release their therapeutic drug within the first layer of cells and results in loss of nanomedicine activity and minimal objective response to the treatment.

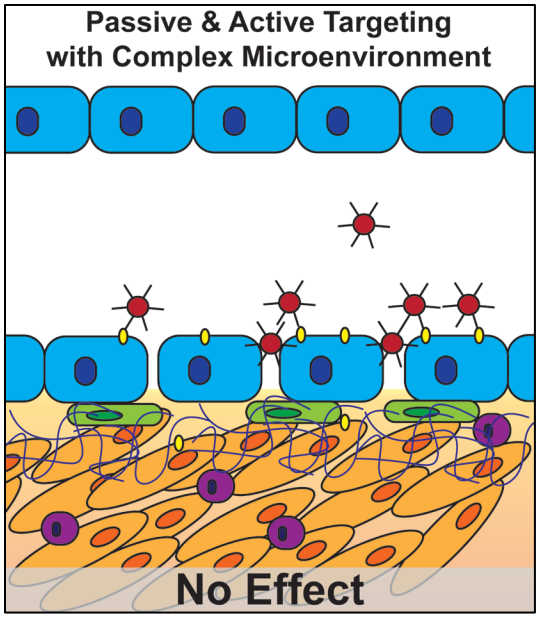

Figure 4: Schematic of nanomedicine deposition by passive and active targeting with a complex tumor microenvironment.

Tumor interstitial fluid is composed of various regulatory molecules, growth factors, waste products generated from tumor cells, and a number of soluble, tumor-associated biomolecules (Gullino et al. 1964). Another physiological characteristic commonly associated with the EPR effect is poor lymphatic drainage, which results in pooling of interstitial fluid within the tumor microenvironment. This increase in non-cellular components and a decreased rate of lymphatic drainage results in increased interstitial pressure within the tumor microenvironment, which subsequently creates a barrier to deep tumor penetration (Ferretti et al. 2009). Normalizing and repairing the dysfunctional blood and lymphatic vessels in the tumor microenvironment by modulating angiogenic signaling pathways can result in decreased tumor interstitial pressure. Normalization of tumor vasculature with improved lymphatic drainage can be a useful approach to increase the penetration of nanomedicines into the tumor

microenvironment (Heldin et al. 2004). Reduction of tumor interstitial pressure reduced the proliferation rate of tumors cells in preclinical models, which may provide an alternative treatment strategy (Hofmann et al. 2006).

Several tumor-specific proteases, or cancer-associated proteases, found in interstitial fluid are involved in tumor cell invasion or metastasis. These include: urokinase, several types of cathepsins, and various matrix metalloproteases (MMPs) (Duffy 1996). Thus, targeting ligands will be exposed to increasing concentrations of these proteases as the disease progresses and as the nanomedicine comes in closer contact with the tumor microenvironment. Consequently, active targeting ligands must be designed to withstand increasing protealytic activity. Similarly, nanomedicines can be developed with an inactivated form of targeting ligand that becomes activated in the presence of specific cancer-associated proteases. In this regard, a responsive targeting system can be used to improve drug delivery. In this system a secondary targeting motif can be exposed upon treatment with a tumor-associated protease or alternatively, a drug carrier can be dissociated upon proteolytic cleavage (X.-X. Zhang et al. 2012), thereby increasing the concentrations of drug specifically within the tumor microenvironment.

The extracellular matrix (ECM) of the tumor microenvironment is an important structural component of the tumor interstitial space composed primarily of collagen fibers, glycosaminoglycans (ex. hyaluronan and chondroitin sulfate), and proteoglycans (Wiig et al. 2010). This ECM forms an effective barrier to systemically administered nanomedicines. Active targeting seeks to reduce non-specific ECM interactions that prevent delivery of nanomedicines. Consequently, strategies to improve delivery have focused on degradation of the ECM using specific enzymes that results in improved interstitial pressure and promotes fluid flow (Jie Wang et al. 2011a). Given the dynamic role of the ECM in promoting cellular growth and cell morphology (Lu et al. 2011; Senoo & Hata 1994), the possibility that degradation/remodeling of the ECM may promote increased proliferation and metastatic spread of the tumor and tumor cells to alternative locations must be considered (M. Fang et al. 2014). Therefore, alternative strategies should be sought to increase penetration of nanomedicines through the ECM.

The remaining cellular components of the tumor microenvironment consist primarily of stromal cells, such as cancer-associated fibroblasts and pericytes; and immune cells, such as cancer-associated lymphocytes and myeloid-derived suppressor cells (MDSCs) (H. Li et al. 2007a). These cellular components are often considered to co-evolve with malignant cells as the tumor progresses, resulting in a self-sustaining microenvironment that promotes increased tumor growth. While these supportive cells are typically non-malignant, they exert significant effects on the tumor microenvironment. Consequently, these cells may serve as targets for new therapies (H. Li et al.

2007a; Bijlsma & van Laarhoven 2015). Tumor stromal cells can account for a vast majority (>50%) of the tumor-associated cells, especially for certain tumors like pancreatic cancer. These cells may limit effective delivery of nanomedicines and even small molecule therapies and prevent an effective treatment response (Feig et al. 2012). Targeting nanomedicines with a tumor-penetrating peptide could significantly improve delivery into more central regions of the tumor. Tumor-infiltrating cytotoxic ($CD8^+$) T cells are primarily associated with the removal of non-self-identified malignant cells. This is used as an indicator of improved prognosis for breast (Ali et al. 2014), colorectal (Naito et al. 1998), esophageal (Cho et al. 2003) and ovarian cancers (Sato et al. 2005). However, the tumor microenvironment will accumulate a large number of immunoregulatory cells, such as MDSCs and regulatory T cells (T_{regs}) that allow malignant cells to escape detection by $CD8^+$ T cells and continue to grow (Oleinika et al. 2013). This decrease in active immune cells within the tumor microenvironment can have an impact on treatment if the therapeutic molecule relies on the activity of functional $CD8^+$ T cells. Alternatively, actively targeting nanomedicines to immunoregulatory cells can remove the immunosuppressive phenotype in the microenvironment allowing $CD8^+$ T cells to identify and remove malignant cells (Ha 2009). Given the dynamic nature of the tumor microenvironment and the role it can play in disease progression, actively targeting nanomedicine to specific components within the tumor microenvironment may help modulate tumor growth (Tsai et al. 2014). Alternatively, identification of ligands that promote tumor penetration and navigation through the tumor microenvironment to the malignant cell population should be used.

3.3. Cell-Specific Interactions

Once a given nanomedicine has been deposited within the tumor microenvironment, its journey is not complete. For nanodiagnostics or nanoimaging systems, specific deposition within the tumor environment and identification of cancer cells by surface protein expression may be sufficient to complete the desired task. However, for therapeutic activity of a nanomedicine to occur, it must deliver its cargo specifically to the cancer cells displaying the diseased phenotype. Indeed, even specific delivery of a therapeutic molecule to an appropriate subcellular organelle is generally desired. Cell-specific delivery of nanomedicines can reduce doses given to a patient, thereby decreasing the total cumulative dose and undesired side effects in the patient.

3.3.1. Cancer Cell-Specific Binding

Once within the tumor microenvironment, an actively targeted particle must navigate successfully through a number of cellular and extracellular components, discussed above, to reach the desired target cell. At the cell

surface, an actively targeted nanomedicine must be able to discriminate between phenotypically normal cells and diseased cells. A byproduct commonly observed with neoplastic transformation of cancer cells is the aberrant expression numerous cell surface proteins as the result of a various subcellular abnormalities including: altered gene expression (Baylin et al. 2001) or altered post-translational protein modification. Alterations in gene expression are often caused by altered DNA methylation patterns (Das & Singal 2004), alternative intron splicing (J. Chen & Weiss 2015; Venables 2004), or changes in microRNAs (miRNAs) expression (H. Suzuki et al. 2013; Croce 2009). Post-translational protein modifications observed in cancer cells include alterations in glycosylation patterns (Christiansen et al. 2014). However, alternative post-translational modifications are also thought to play a role. As neoplastic transformation progresses from early stage to metastatic disease, surface protein profiles continue to change (Luque-García et al. 2010). Therefore, identification of an appropriate cell-targeting ligand that is present and persistent throughout the course of treatment must be identified. Another issue that is becoming apparent for active tumor targeting is the presence of intertumor heterogeneity between patients and between patients with the same type of cancer, as well as intratumor heterogeneity found within tumors of a single patient (R. Fisher et al. 2012; Burrell et al. 2013). This tumor heterogeneity requires identification of a ligand(s) that can be used to target tumors with different cell surface phenotypes.

3.3.2. Cancer Cell-Specific Receptors

A number of cell surface proteins/receptors are recognized as cancer cell-specific markers based on their aberrant expression compared to normal cells within the same tissue. These molecules are often exploited for use in actively targeted nanomedicines in a disease specific manner. Examples of these include: *HER2*, folate receptor, transferrin receptor, and nucleolin. The human epidermal growth factor receptor 2 (*HER2*), also known as receptor tyrosine-protein kinase ERBB-2, is one of the most commonly utilized biomarkers. Increased *HER2* expression was observed for ~20-30% of breast cancer patients (Slamon et al. 1989; Kennecke et al. 2010) and often signals poor patient prognosis with significant decreases in disease-free and overall survival rates (Tsutsui et al. 2002). The ERBB superfamily of receptors includes four structurally related members – ERBB-1, ERBB-2, ERBB-3, and ERBB-4. Each of the ERBB receptors are composed of three functional domains: an extracellular ligand-binding domain, a single transmembrane domain, and a cytoplasmic tyrosine kinase domain for activation of intracellular tyrosine signaling pathways (N. E. Hynes & Lane 2005). The ERBB receptors were implicated in a number of processes involved in malignant transformation including increased cell proliferation/survival, angiogenesis, cell

migration and metastatic invasion (Holbro et al. 2003). Anti-*HER2* immunoliposomes increased the therapeutic response in ERBB-2 expressing models when compared to unencapsulated or free drug preparations. This treatment resulted in significant objective response in preclinical models (J. W. Park et al. 2002). Despite high expression levels that can be exploited for targeting in some patients, expression of ERBB-2 is dynamic and can show inverse expression compared to other common breast cancer receptors like the estrogen receptor (Lopez-Tarruella & Schiff 2007). Therefore, certain active targeting strategies that target ERBB-2 may lose their efficacy in clinical studies due to the dynamic nature of certain receptor families, which transition to alternative redundant signaling pathways, as suggested with targeted antibodies like trastuzumab (Gutierrez & Schiff 2011) or small molecule inhibitors like lapatinib (F. L. Chen et al. 2008).

Transferrin receptor (CD71) is an essential membrane protein involved in intracellular iron uptake and regulation of cell growth (T. R. Daniels, Delgado, Rodríguez, et al. 2006b). There are two isoforms of the transferrin receptor (transferrin receptor 1 and 2) that import iron intracellularly through receptor-mediated endocytosis of a transferrin-iron complex. Due to its involvement with cell proliferation, CD71 is overexpressed in a number of malignant cell types including: brain (Recht et al. 1990), breast (Habashy et al. 2010), ovarian (Calzolari et al. 2007), and pancreatic (Ryschich et al. 2004) cancers. A number of different nanomedicines were targeted using transferrin or an anti-transferrin receptor conjugate (T. R. Daniels, Delgado, Helguera, et al. 2006a; T. R. Daniels et al. 2012). The success of actively targeted nanomedicines via the transferrin receptor-mediated endocytosis pathway is reflected by the number of transferrin conjugates currently in clinical trials as discussed below.

The folate receptor (FR) is another essential membrane protein involved in intracellular uptake of tetrahydofolate, which is then processed into alternative forms and commonly used as a biological cofactor (Kamen & A. K. Smith 2004; Antony 1996). Two predominate forms of the folate receptor (FR-α and FR-β) are expressed in human tissues, with FR-α being overexpressed in epithelial cancer cells and FR-β being expressed in non-epithelial cancer cells (Ross et al. 1994). Folate receptor overexpression was implicated as a marker of poor clinical outcome for breast (Hartmann et al. 2007) and ovarian cancers (Kalli et al. 2008). The folate receptor was also exploited as a target by conjugating folate-derivatives to different nanomedicines, resulting in increased intracellular delivery (Zwicke et al. 2012).

3.3.3. Subpopulation Targeting

Two major hypotheses were proposed for the generation, establishment, and expansion of a tumor: 1) the clonal evolution theory (Nowell 1976) and 2) the cancer stem cell theory (Tan et al. 2006). The clonal evolution theory states that tumors arise from the accumulation of spontaneous mutations in normal cells that give rise to a cell with an enhanced survival phenotype. These mutations occur through progression of the disease and generate a number of genotypically and phenotypically unique clones within the growing tumor. Each subclone will then propagate itself by clonal division in a highly competitive microenvironment in which the subclone(s) with greatest growth potential will outgrow other clones or eventually metastasize to distant locations. Under the cancer stem cell theory, a cancer stem cell with unlimited proliferative potential produces a daughter cell that differentiates into a mature cancer cell after a single round of cell division. This cancer stem cell division continues unregulated and the tumor mass continues to grow and expand by clonal expansion. Under this theory, the cancer stem cell-of-origin may either be a resident adult stem cell that accumulates a number of oncogenic mutations or be the result of dedifferentiation of a cell after an oncogenic mutation into a cancer stem cell with increased proliferative potential (Visvader 2011). Cancer stem cells were proposed to be intrinsically resistant to many forms of chemotherapy because of their higher expression levels of drug efflux pumps (Hirschmann-Jax et al. 2004) and their slower cell cycle, which enables the cell to avoid accumulation of cytotoxic drug during the progression of the normal cell cycle (Moore & Lyle 2011).

Irrespective of tumor expansion model, there is a subpopulation of cells within some tumors with a higher propensity to promote tumor growth. Active targeting of nanomedicines to specific subpopulations of tumor cells with a highly aggressive phenotype or other tumor-initiating properties could prevent continued growth and expansion of a developing neoplasm. For example, a number of ligands have been identified that allow identification of the tumor-initiating subpopulation of a glioblastoma xenograft model. These ligands could subsequently be added to a nanomedicine to specifically enhance delivery of a therapeutic drug to the driving population of a tumor mass (J. K. Liu et al. 2014). This therapeutic strategy was suggested by specific targeting of the tumor-initiating subpopulation within a bladder cancer model through inhibition of CD47, a cell surface receptor responsible for inhibiting macrophage phagocytosis, using a monoclonal antibody. This resulted in elimination of the aggressive subpopulation *in vitro* (Chan et al. 2009). However, studies using an actively targeted nanomedicine to deliver a drug specifically to the tumor-initiating cell population are lacking. Two significant problems in targeting the tumor-

initiating population are their low occurrence within a tumor population (~1-5% of the total population) and their central location within the tumor, which then requires mechanisms to increase tumor penetration as discussed previously (Visvader & Lindeman 2008; LaBarge 2010).

3.3.4. Cell Internalization

In the absence of nanomedicine internalization, a therapeutic molecule must be released extracellularly and is rapidly redistributed to surrounding cells within the tissue microenvironment. This results in loss of cell-specific drug targeting. Extracellular release of therapeutic molecules results in a decreased overall dosage accumulated per cell and can increase drug resistant phenotypes by increasing expression of drug transporters following low-dose sensitization of cells (Schuurhuis et al. 1993). With continued treatment, drug resistant cell subpopulations become enriched within the tumor leading to poor clinical outcomes. Alternatively, delivery of a nanomedicine intracellularly results in higher doses of therapeutic drug being reached within the desired cell targets, which leads to increased cytotoxicity and improved therapeutic indices. For example, delivery of a doxorubicin immunoliposome with a cell-internalizing antibody resulted in an increased survival time compared to the same preparation targeted with a non-internalizing antibody (Sapra & Allen 2002). Following appropriate discrimination of cells with a neoplastic phenotype, nanomedicines must therefore be internalized to deliver their therapeutic payload by one of two major pathways: 1) direct penetration through the cytoplasmic membrane and delivery into the cytoplasm, or 2) endocytosis and escape from endosomes.

A number of cell penetrating peptides (CPPs) have been identified that promote intracellular delivery, including the octa-arginine (R8), TAT, pHLIP and polyhistidie peptides (PHPs) (Gupta et al. 2005; Weiqin Wang et al. 2015). The TAT peptide (GRKKRRQRRRPQ), a peptide derived from the human immunodeficiency virus-1 (HIV-1) *trans*-acting activator of transcription (TAT), has been shown to rapidly translocate through the plasma membrane and accumulate within the nucleus, however extensive debate on the mechanism of internalization remains (Brooks et al. 2005). The pH Low Insertion Peptide (pHLIP), a peptide derived from the bacteriorhodopsin C transmembrane helix, was found to be water soluble at physiological pHs with an unstructured state. However, a rapid change in conformation allows it to insert across a membrane when there is a change in pH to a slightly acidic pH (7.0 – 6.5 or less) (Andreev et al. 2010).

Conjugation of a CPP to a therapeutic molecule or drug delivery system can increase the intracellular accumulation of a drug compared to an untargeted drug (Torchilin 2008). For example, the pHLIP peptide was

conjugated to PEGylated liposomes, which results in fusion of liposome and cell membranes under acidic conditions typically found in the tumor microenvironment. Subsequently, the targeted liposomes delivered an encapsulated therapeutic molecule to the cancer cells within an acidic microenvironment (Yao, J. Daniels, Wijesinghe, et al. 2013b). Similarly, the pHLIP peptide was conjugated to gold nanoparticles for diagnostic imaging of cancer cells using a similar mechanism (Yao, J. Daniels, Danniels, et al. 2013a). A number of pHLIP peptides have been generated with refined peptide-lipid bilayer interactions allowing rational design of peptides that can modify tumor specificity, distribution, and blood clearance properties (Weerakkody et al. 2013). Recently, a polyhistidine peptide containing 16 histidine residues (H16) showed a 15-fold increase in cell penetrating activity when compared to the R8 peptide in a charge-independent mechanism under physiological conditions (Iwasaki et al. 2015). The mechanism of CPP uptake is still under debate, however several critical factors have been identified that influence effective uptake including: temperature (Richard et al. 2003), the clustering of negatively charged phospholipids (Bechara & Sagan 2013), and activation of endocytosis for certain types of CPPs (Madani et al. 2011). As suggested previously, a CPP can be combined with an enzyme-cleavable domain to prepare a targeting ligand that is active only when certain enzymes are present in the microenvironment. For example, lysine residues found in the TAT peptide, which are responsible for translocation of the peptide through the membrane, were modified with a blocking dipeptide. To promote tumor specific accumulation, the dipeptide was cleaved by APN or dipeptidyl peptidse IV, which are highly expressed on tumor cells, allowing the TAT peptide to translocate into the cell membrane (Bode et al. 2015).

Endocytosis is the primary mechanism used for penetration of nanomedicines and delivery of therapeutic molecule into the cytoplasm. Two broad classes of endocytosis pathways are phagocytosis, which typically involves the uptake of large solid particles, and pinocytosis, which are a collection of fluid phase uptake pathways. Several pinocytosis pathways were discovered and have been reviewed extensively (Sahay et al. 2010). Briefly, pinocytosis uptake pathways can be mediated by clathrin (clathrin-mediated endocytosis, CME), caveolae (caveolae-mediated endocytosis), or other clathrin- and caveolae-independent mechanisms. Ligands shown to promote CME are mannose-6-phosphate, transferrin, and nicotinic acid. In this pathway, receptors are engulfed in a clathrin-coated invagination of the cytoplasmic membrane through the use of a number of accessory proteins. The CME pathway is the most utilized mechanism for cellular uptake of essential nutrients and is functional in all active mammalian cells (Sahay et al. 2010). Attachment of an endocytosis-promoting ligand to a nanomedicine scaffold can promote

changes to the primary route of intracellular trafficking. Ligands promoting transport via caveolae-mediated endocytosis pathway include the Shiga toxin and cyclic RGD peptide, which interacts with the $\alpha_v\beta_3$ integrin as discussed previously. Caveolae-mediated transport is reported to be the major pathway involved in transcytosis and is one of the only pathways that does not lead to degradation by lysosomes. Extensive work is still proceeding identify ligands that promote delivery of nanomedicines to a specific endocytosis pathway.

3.4. Combination/Multiple Targeting

The use of multiple, unique ligands decorated on the surface of a nanomedicine core (as in Figure 5) was shown to result in synergistic targeting, in which the combination of targeting ligands will outperform the efficiency of treatment when compared to the individual targeting ligands alone (Ringhieri et al. 2015; H.-W. Yang et al. 2012; Y. Liu et al. 2011; Kluza et al. 2012; Kontermann 2012). For example, dynamic signaling pathways like the ERBB superfamily of receptors can develop treatment resistance through modification of expression levels. Combination targeting that uses two cell-specific binding ligands is hypothesized to decrease the occurrence of acquired resistance, as was shown using a combination of ERBB-2 small molecule drugs. To overcome the dynamic nature of these receptors, a combination of EGFR targeting and FR targeting was used with a common liposomal core to increase delivery of doxorubicin to cells that overexpress either type of receptor (Saul et al. 2006). A 10-fold increase in nanomedicine toxicity could be achieved through the use of two different targeting ligands. However, the use of multiple/combination targeting can result in an increased antigenicity. Similarly, the complexity of each preparation would be increased with each additional ligand added to the drug delivery system.

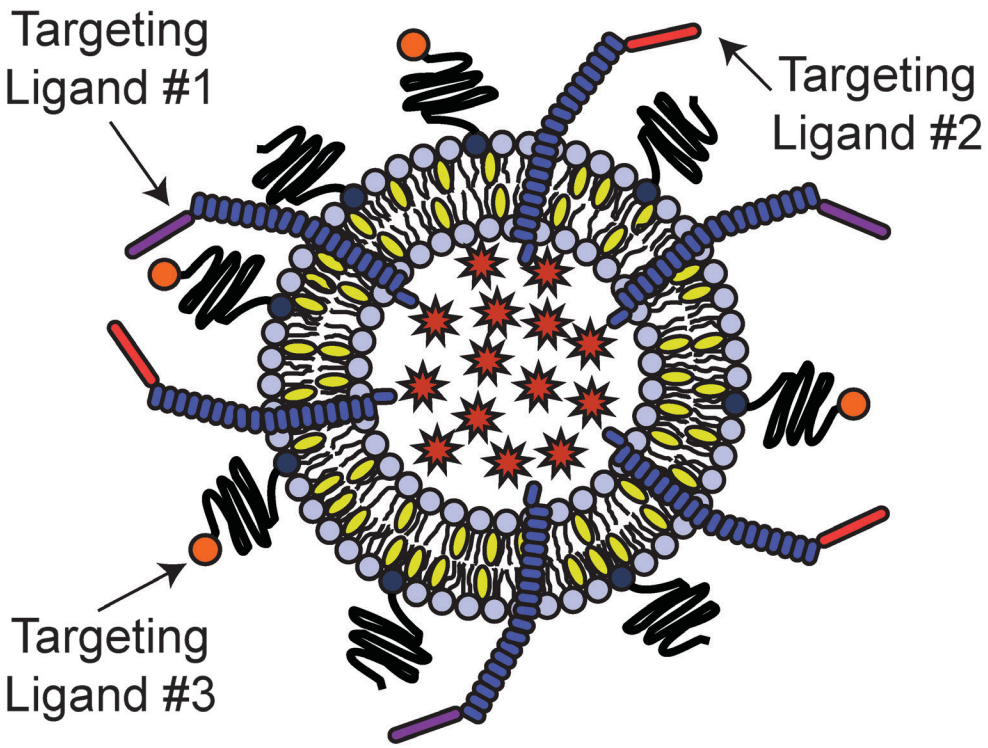

Figure 5: Schematic of a PEGylated liposomal nanomedicine targeted via a combination of three targeting ligands.

Combining multiple motifs into a single-targeting ligand or identification of ligands with a desired functional activity can be used to overcome the increased complexity of multi-targeted nanomedicines. Phage display can be used to enrich for clones with specificity to multiple cancer types with highly different phenotypes, which results in the generation of ligand fusions containing two functional domains as show in Figure 6. These multi-functional ligands, which contain multiple functional domains within the same targeting ligand, were shown to increase the inherent selectivity of the peptide to multiple cellular phenotypes (Gross et al. n.d.). These ligands were shown to increase the toxicity of nanomedicines across multiple cell lines when compared with a nanomedicine targeted with a ligand containing a single peptide motif. Similarly, bispecific antibodies, in a number of formats, have been developed to specifically target two different targets with a single targeting ligand (Kontermann 2012).

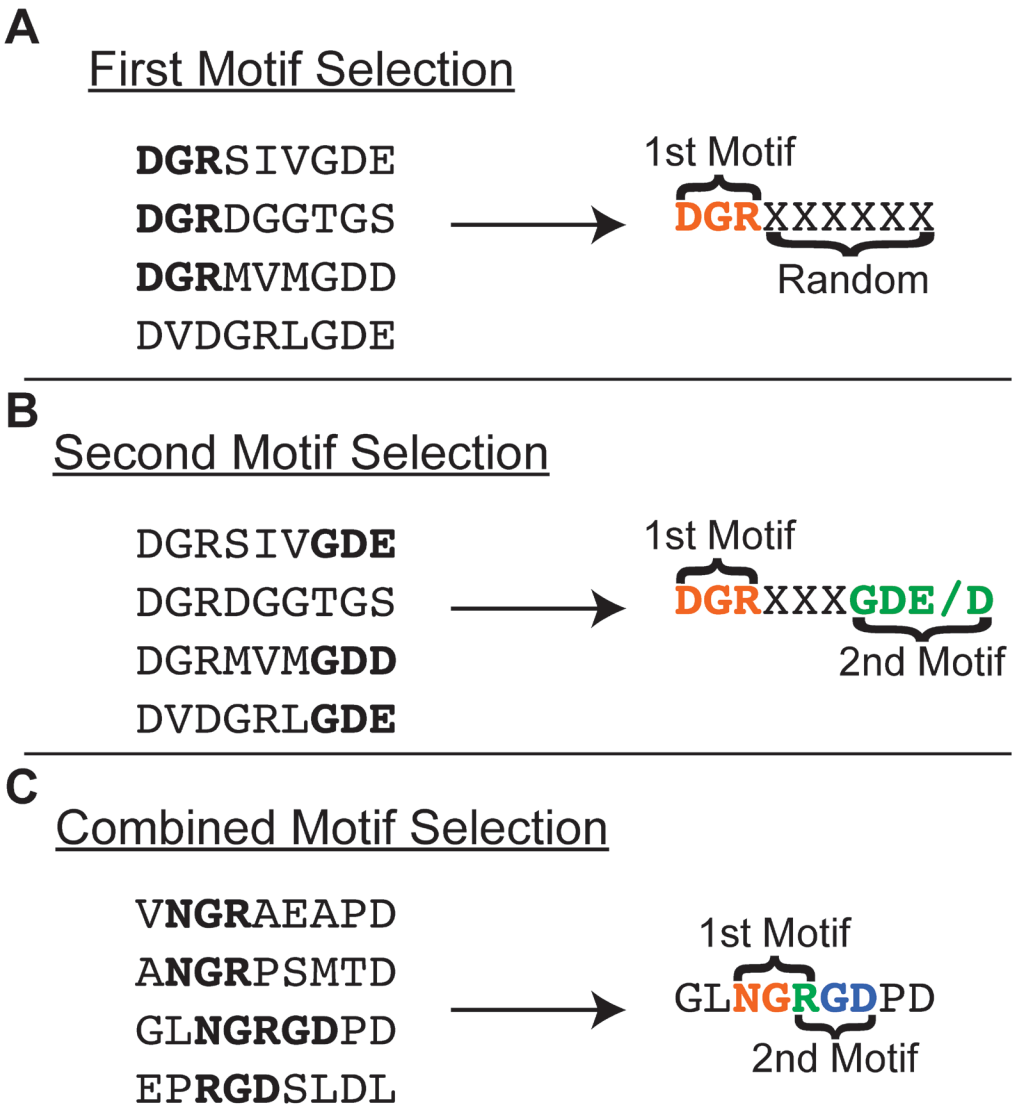

Figure 6: Selection of multi-domain ligands for cancer cell-specific targeting. Motif 1 was identified from a selection against lung cancer cells (A) and motif 2 was identified from a continued selection against pancreatic cancer cells (B) to generate a single ligand with multiple targeting domains. Similarly, multi-domain ligands with over-lapping functional motifs can be enriched as shown from a selection against lung cancer cells (C).

3.5. Clinical Progress in Actively Targeted Nanomedicines

Six actively targeted nanomedicines are under evaluation in phase I or II clinical trials, as summarized in Table I below. However, the FDA has not approved any actively targeted nanomedicines for general use at this time. Of the six actively targeted nanomedicines, 66% (4/6) were based on a liposomal nanocarrier, with the remaining

33% (2/6) based on polymer assemblages. The same proportion of nanocarriers was observed to enter into phase II clinical trials. The active pharmaceutical ingredients (API) studied in these trials were traditionally well-characterized cytotoxic chemotherapy drugs. However two nucleic acid-based APIs were also studied – a silencing RNA (siRNA) and a corrective gene product. These trials show that only a small number of targeting ligands (4 different ligands) were studied for therapeutic activity in a clinical setting. Of the 4 ligands, only 2 have successfully passed into a phase II trial where efficacy of targeting can be evaluated, with the predominant ligand being transferrin.

From available data on these nanomedicines reported at the conclusion of their respective phase I trials, all formulations were identified as safe in patients and showed less systemic toxicity compared to the unencapsulated version of the API. For example, the doxorubicin immunoliposomes, MCC-465 and C225-ILS-DOX, showed no signs of palmar-planter erythrodysaesthesia (hand-foot syndrome), or cardiotoxicity in the patient group. These symptoms are commonly observed, dose-limiting toxicity profiles associated with free doxorubicin. An objective response to either doxorubicin immunoliposome was not observed (1 of the 26 patients in the C225-ILS-DOX study showed complete response, while a second patient showed partial response), however 40-55% of the patients presented with stable disease by the end of the study (Mamot et al. 2012; Matsumura et al. 2004). Pharmacokinetic data were not available from either study to allow quantification of drug deposition within the tumor. Phase II trials have not been planned for either doxorubicin immunoliposome.

Similarly, the SGT-53 nanocomplex was shown to be non-toxic following systemic infusion up to 3.6 mg of DNA per infusion, which resulted in significant expression levels of the delivered $p53^{wt}$ gene. Preferential delivery of SGT-53 to tumor tissues, including metastatic lesions, was shown in comparison to normal tissue biopsies. Quantification of the gene transcript successfully delivered to the tumors was not estimated. However, even at the lowest administered dose of SGT-53, there was still expression of the $p53^{wt}$ gene in target cells. SGT-53 was shown to promote stable disease in 66% (8/12) of the patients after 6 weeks of treatment. Unlike the immunoliposomes, SGT-53 was not intended for use as a single therapeutic agent, rather it is intended to be used as a combination with standard treatment regimens (Senzer et al. 2013). SGT-53 was well tolerated, but no phase II trials are planned.

Table I: Actively targeted nanomedicines with ongoing/completed clinical trials. Adapted from (Sanna et al. 2014).

Name (Identifier)	**Nanocarrier**	**Ligand**	**API**	**Condition**
Phase I				
BIND-014 (Hrkach et al. 2012) (NCT01300533)	PL(G)A-PEG polymers	Anti-PSMA small molecule	Docetaxel	Advanced solid tumors
C225-ILS-DOX (Mamot et al. 2012) (NCT01702129)	Liposomes	Fab' of cetuximab (anti-EFGR)	Doxorubicin	Advanced solid tumors
CALAA-01 (Davis et al. 2010) (NCT00689065)	Cyclodextrin-containing polymers	Transferrin	siRNA; anti-ribonucleotide reductase	Various solid tumors
MBP-426 (Phan et al. 2007) (NCT00355888)	Liposomes	Transferrin	Oxaliplatin	Advanced or metastatic solid tumors
MCC-465 (Matsumura et al. 2004) (N/A)	Liposomes	$F(ab')_2$ of GAH	Doxorubicin	Advanced or metastatic gastric cancer
SGT-53 (Senzer et al. 2013) (NCT00470613 & NCT02354547)	Liposomes	scFV to Transferrin Receptor	p53 plasmid (+docetaxel or +topotecan & cyclophosphamide)	Various solid tumors (adults & children)
Phase II				
BIND-014 (NCT01812746, NCT01792479 & NCT002283320)	PL(G)A-PEG polymers	Anti-PSMA small molecule	Docetaxel	Prostate, NSCLC, or $KRAS^{+}$/Squamous NSCLC
MBP-426 (Senzer et al. 2009) (NCT00964080)	Liposomes	Transferrin	Oxaliplatin	Gastric, Gastroesophageal, or Esophageal adenocarcinomas
SGT-53 (NCT02340156 & NCT02340117)	Liposomes	scFV to Transferrin Receptor	p53 plasmid (+temozolomide or +nab-paclitaxel & gemcitabine)	Glioblastoma or metastatic pancreatic cancer

All nanomedicines that have successfully reached phase II trials are ongoing and will not be discussed in this review since all data has not been collected and processed. However, all formulations were tolerable by patients and the nanomedicine form reduced non-specific toxicities compared to the unencapsulated API.

4. Conclusions

Active targeting of nanomedicines was shown to significantly increase the therapeutic index of an unencapsulated therapeutic molecule in preclinical settings. There are increasing concerns that actively targeted nanomedicines are not showing significant improvements in tumor accumulation compared to their passively targeted counterparts as originally hypothesized. The extensive work that is unfolding on the complexity of the

tumor microenvironment has provided the research community with additional challenging factors to overcome with targeting. At this time, a number of barriers that current active targeting strategies fail to overcome leads them to perform similarly to their non-targeted equivalents. As suggested, combination of multiple ligands with appropriate functions to overcome specific barriers will likely prevail as a necessity for success of actively targeted nanomedicines. Subsequently, an understanding of the underlying biological and/or physical barriers that caused many actively targeted drug delivery systems to fail must be identified and appropriate ligands must be generated to overcome these barriers. A phage protein-modified liposome system was previously described and was used as a model to allow direct comparison between different ligands in a common nanomedicine (Petrenko & Jayanna 2014). The use of phage display to generate cancer cell-specific ligands that can increase delivery of a commonly used liposomal doxorubicin (Doxil) without prior knowledge of the expressed cell surface proteins is presented in the following chapters. A paradigm shift from rational development of active targeting systems based on binding activity to non-rational development of nanomedicines based on a combinatorial ligand-screening assay that allows identification of active targeting nanomedicines based on the desired functional activity is presented.

CHAPTER 2

SELECTION OF LUNG CANCER-SPECIFIC LANDSCAPE PHAGE FOR TARGETED DRUG DELIVERY

1. Abstract

Cancer cell-specific diagnostic or therapeutic tools have been hypothesized to significantly increase the success rate of lung cancer diagnosis and targeted therapies. Using two landscape phage display libraries, f8/8 and f8/9, which display an 8- or 9-mer random peptide fusion respectively, a number of novel peptide families that are specific to non-small cell lung cancer cells were identified that will significantly increase the repertoire of available lung cancer cell-specific peptides. Using a phage capture assay, two of the selected phage clones, ANGRPSMT and VNGRAEAP, were shown to be selective for NSCLC cells and distribute into unique subcellular fractions. Phage ANGRPSMT uptake was inhibited by treatment with endocytosis inhibitors chlorpromazine (27.6%) or genistein (27.8%) and phage VNGRAEAP was inhibited by genistein (42.5%) or cytochalasin D (41.8%). Phage ANGRPSMT is internalized primarily by receptor-mediated transport while VNGRAEAP is internalized by caveolae-mediated endocytosis or macropinocytosis. These results show that amino acid residues surrounding a positionally constrained Asn-Gly-Arg (NGR) motif modulate the endocytic uptake route and subcellular distribution of phage displaying these peptide sequences across their surface. The application of VNGRAEAP-modified Lipodox to significantly increase the intracellular doxorubicin accumulation, thereby increasing the cytotoxicity profile of unmodified Lipodox, was shown. Results from this study provide numerous ligands suitable for NSCLC cell targeting and identifies ligands that can modify the route of cell penetration of targeted therapeutics.

2. Introduction

Respiratory neoplasms remain a significant health problem in the United States accounting for an estimated 14% of new cancer cases and approximately 30% of cancer mortalities for both men and women in 2014 (Siegel et al. 2014). Lung cancer is classified into two major groups based on observed histological differences: non-small cell lung cancer (NSCLC) and small cell lung cancer (SCLC) (Vescio et al. 1990). Both NSCLC and SCLC display a high level of heterogeneity within the tumor (Fraire et al. 1987) that may limit successful therapeutic responses due to a small population of cells escaping the effects of treatment and causing recurrent diseases demonstrating resistance to the treatment. This observation suggests a modification of therapeutic strategies and a need for novel diagnostic and therapeutic probes to overcome the shift in the lung cancer molecular phenotype towards NSCLC.

Several strategies have been suggested to overcome drug resistance including the use of nanomedicines to deliver lethal concentrations of drug to cancer cells before resistance develops (Modok et al. 2006; Markman et al. 2013). The use of nanomedicines, encapsulated forms of existing cytotoxic drugs, has resulted in significant increases in therapeutic index of existing drugs and will concurrently reduce dose-limiting side effects commonly associated with non-encapsulated forms of the drugs. Nanomedicines accumulate at the site of tumor pathology by the enhanced permeation and retention (EPR) effect, which involves their passive diffusion through vascular defects commonly associated with rapidly forming blood vessels in certain tumor types (Torchilin 2011). Even with passive targeting, chemotherapy resistance and tumor relapse are still observed clinically for numerous cancer types. It was suggested that the tumor-specific effects achieved by passive targeting could be enhanced by attachment of targeting molecule to nanomedicines (Nobs et al. 2004). However, a limited number of targeting ligands are available to be used in conjunction with a passively targeted nanomedicine. Therefore, a need for novel ligands remains a challenge for adequate active tumor targeting.

Phage display (G. P. Smith & Petrenko 1997) has been used extensively over the past three decades for generation of protein ligands interacting with cellular components or surface receptors across a wide range of diverse sources including isolated molecules, intact bacterial cells, and mammalian cells (*in vitro*, *in vivo,* or *ex vivo)*. In particular, vectors based on filamentous bacteriophages of the class Ff (M13, fd, and f1), supporting a variety of different display formats depending on the host protein used, have been used extensively for displaying foreign peptides and proteins (G. P. Smith & Petrenko 1997). Structurally, filamentous phage consist of a small, ~9 kb single-stranded, circular genome surrounded by 5 structural proteins (pIII, pVI, pVII, pVIII, and pIX) to produce long, filamentous particles (Marvin et al. 2014). Phage display on the Ff class of bacteriophage vectors has produced numerous libraries with large structural complexities on the order of $\geq 10^9$ unique sequences. These libraries contain a number of constrained and/or randomized structures which provides a rich source of targeting ligands for numerous applications (Kuzmicheva, Jayanna, Sorokulova, et al. 2009b). Thus, phage display in minor coat protein p3 has been used to identify cancer specific peptides for a variety of tumor types including lung cancer (McGuire et al. 2014).

Landscape phage libraries of type f8 (Kuzmicheva, Jayanna, Eroshkin, et al. 2009a; Petrenko et al. 1996; G. P. Smith 1993) designed on the filamentous bacteriophage vector fd-tet, consist of a collection of phage with random inserts introduced at the N-terminal end of every copy of the pVIII major coat protein of the phage vector

and are subsequently expressed in ~4,000 copies across the length of the phage particle (Figure 7). This layout dramatically alters the physical properties of the phage surface so that each phage particle is structurally unique compared to the remainder of the library and each phage possesses a specific ability to interact with the surrounding environment.

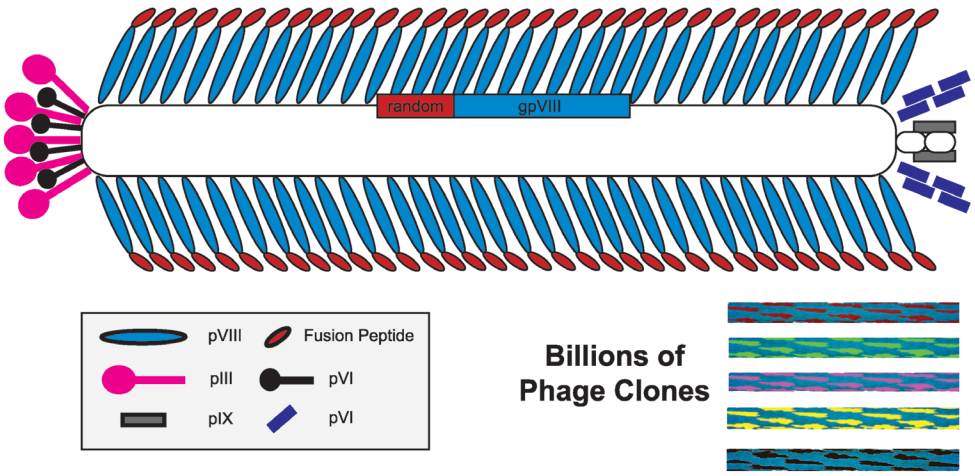

Figure 7: Schematic of f8 type landscape phage display libraries. Diverse fusion derivatives of filamentous phage fd-tet from f8/8 and f8/9 libraries consist of phage with dimensions of 1.2 μm × 6.5 nm and contain a randomized peptide (red) fused to every copy of the N-terminus of the major coat protein pVIII (blue). The major coat proteins cover the length of the single-stranded DNA accommodated at the core of the phage particle. The ends of phage particles are closed by minor coat proteins pIII, pVI, pIX, & pVI. Phage composed of different random peptide fusions create a library of billions of different phage variants with unique surface landscapes.

Landscape phages are an ideal targeting material compared to traditional antibodies as large quantities of pure phage or phage proteins can be produced inexpensively while retaining high product purity and shelf-storage stability. Numerous platforms derived from the protein products of the fd-tet vector have been developed over the past decade for various diagnostic and therapeutic applications. These platforms include targeted nanoparticles for gene delivery to specific cells (Gandra et al. 2013; Mount et al. 2004), MRI probes for cancer diagnostics (Deutscher 2010), cancer-specific liposomes or micelles containing various therapeutic payloads (Petrenko & Jayanna 2014; Tao Wang, Petrenko, et al. 2010b), cancer-specific siRNA nanoparticles (Bedi et al. 2013), and nanorods for

photothermal therapy (Jing Wang et al. 2012a). Given the wide number of platforms being targeted with phage display-derived peptides, there is an increasing need for diverse collections of targeting ligands that possess tumor cell specificity and also capable of intracellular delivery.

A NSCLC cell line, Calu-3, was explored due to its derivation from a metastatic site in a patient receiving prior chemotherapy and used to mimic the advanced stage disease commonly treated as a recurrent or metastatic disease. In this study, two previously characterized 8- and 9-mer landscape phage display libraries, f8/8 and f8/9, was used as a source of novel protein ligands identified against a NSCLC cell line *in vitro* to expand the collection of available ligands with specificity to NSCLC. Two novel phage clones, containing a commonly identified NGR motif, were identified that display unique subcellular distributions and showed that these ligands significantly increased the toxicity of liposomal doxorubicin.

3. Materials and Methods

3.1. Cells

All cell lines were purchased from the American Type Culture Collection (ATCC, Manassas, VA) as a frozen vial and maintained as described in the technical bulletins. All cell passages were cultured in 25-cm^2 cell culture treated flasks (Corning, Corning, NY) in a humidified 37ºC incubator with 5% CO_2. Cells were subcultured when they reached 80-90% confluence by trypsin-EDTA treatment and reseeded at a density of ~4×10^4 cells/cm^2.

3.2. Phage Display Libraries

As a source of diverse binding ligands we used multibillion clone landscape phage display libraries f8/8 and f8/9, constructed from the fd-tet type vectors f8-1 and f8-6 (Petrenko & G. P. Smith 2005), which respectively display an 8- or 9-mer peptide fusion at the N-terminus of every copy of the pVIII major coat protein (Petrenko et al. 1996; Kuzmicheva, Jayanna, Sorokulova, et al. 2009b). Phage derived from these landscape libraries have a 55 amino acid mature pVIII major coat protein sequence of NH_2-A**XXXXXXXX**[**D/X**]PAKAAFDSLQASATEYIGYAWAMVVVIVGATIGIKLFKKFTSKAS-COOH rather than a 50 amino acid wild-type protein, where X can be any random amino acid (coded by NNK codons, where N is any base and K is G or T bases). The 10th position of the pVIII protein fusion is D for phage derived from the 8-mer library and X for phage derived from the 9-mer library. Herein, phage are commonly identified by their fusion peptide sequence, however all protein references refer to the full-length, 55 amino acid protein sequence unless specified otherwise. All general phage handling, propagation, purification, titering, and DNA sequencing procedures

have been described previously (Brigati et al. 2008). The number of phage particles was estimated using either spectroscopy to measure the number of physical phage particles (virions) or by titering phage in a bacterial host as colony forming units (CFU). Physical titering of phage was performed when phage concentrations were higher than 10^{12} virions/mL by measuring the absorbance at 269 nm and converted to vir/mL by the following formula for f8/8 and f8/9 libraries (9198 nucleotide genome) as derived previously (Kuzmicheva, Jayanna, Eroshkin, et al. 2009a):

$$1 \text{ Absorbance Unit } (AU)_{269} = 6.5\times10^{12} \text{ virions/mL} \quad (1)$$

3.3. Selection of Lung Cancer Specific Phage

3.3.1. *First Round Selection*

Calu-3 and SAE cells were cultured in 25-cm^2 flasks until ~90% confluent. An aliquot of each library containing 1.2×10^{11} virions, with each unique fusion sequence being represented by ~100 copies, was diluted in blocking buffer (0.5% BSA + EMEM with 10% FBS) and transferred to an empty, cell culture treated 25-cm^2 flask for one hour incubation at room temperature to remove phage binding to the treated plastic. Unbound phage were recovered and transferred to a flask that had been treated overnight with EMEM/10% FBS for one hour at room temperature to remove medium and serum binding phage. The f8/8 library underwent a single round of serum depletion, while the library f8/9 underwent two rounds of serum depletion. The unbound phage were recovered and then incubated with normal lung airway epithelial cells (SAE cells) for 1 hour at room temperature. The resulting depleted libraries were then transferred to flasks containing target Calu-3 lung cancer cells and allowed to incubate for one hour at room temperature. Cells were washed and phage recovered as in Chapter 2, Section 3.3.3.

3.3.2. *Second to Fourth Rounds of Selection*

For further rounds, an aliquot of 1.0×10^{11} virions from each of the eluate and lysate sublibraries generated from the previous round was incubated with confluent Calu-3 cells in EMEM with 10% FBS in an incubator at 37ºC and 5% CO_2 for 1 hour. A schematic of selection is presented in Figure 8. Cells were washed and phage recovered as in Chapter 2, Section 3.3.3.

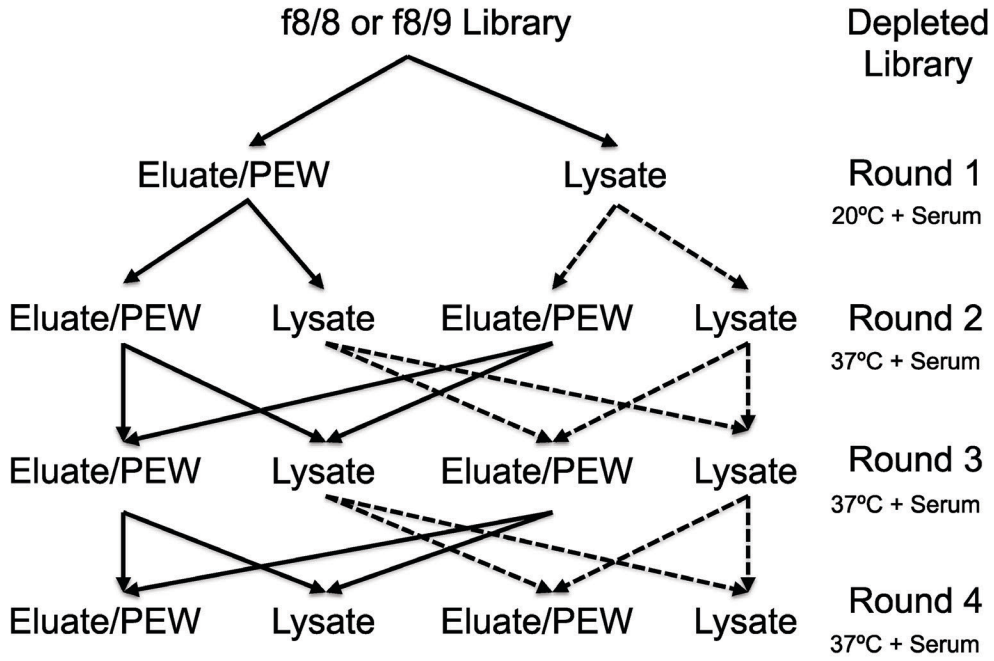

Figure 8: Selection scheme to identify lung cancer cell-specific phage clones. Two input sublibraries were used beginning with second round, identified as an eluate input (solid line) and a lysate input (dashed line). Each input sublibrary was split into two library fractions consisting of eluate and lysate phage that were amplified as individual fractions. In subsequent rounds of selection, the eluate input sublibrary was prepared by combining the eluate fractions generated from both the eluate and lysate output sublibraries from the previous round of selection. A similar scheme was followed for the lysate input.

3.3.3. Washing and Sublibrary Generation

Unbound phage were recovered from the flasks and saved for titering. The Calu-3 cells were washed ten times with cold washing buffer (0.1% Tween 20/0.5% BSA in EMEM) for 5 minutes each to remove low binding phage. Washes were collected and saved for titering. Surface bound phages were recovered by addition of elution buffer (200 mM glycine, pH 2.2/0.1% BSA in EMEM) followed by neutralization with neutralizing buffer (1 M Tris-HCl, pH 9.1). Adherent cells were washed with washing buffer two times at room temperature and collected as "post-elution washes" for titering. The remaining cell monolayers were scrapped from the bottom of the culture flask and transferred to a centrifuge tube. Cells were pelleted and the remaining cell pellets were lysed with lysis buffer (2% w/v sodium desoxycholate/10 mM Tris-HCl, pH 8.0/2 mM EDTA) for 10 minutes at room temperature

to isolate internalized phage. Recovered surface bound and post-elution wash phage were concentrated to ~0.2 mL with Amicon 100 kDa MWCO concentrators (EMD Millipore, Billerica, MA). Concentrated phages from eluate and post-elution wash fractions were combined as a single eluate sublibrary. Phage from eluate and lysate sublibraries were infected into K91BluKan *E. coli* cells, amplified, and purified by PEG/NaCl precipitation the following day for future rounds of selection. All recovered fractions were titered and quantified as described previously (Brigati et al. 2008).

3.3.4. Sequencing of Sublibraries

A portion of the amplified library was spread on an NZY/Tet agar plate after 45 minutes of growth and placed in an in 37ºC incubator overnight. Individual clones were gridded on NZY/Tet agar plates and incubated at 37ºC overnight. The sequence of gpVIII was amplified by PCR as described previously (Brigati et al. 2008). PCR products were purified and sequenced by dye-terminator sequencing at the Massachusetts General Hospital (MGH) DNA Core (Cambridge, MA). Unique clones were propagated in 2 mL scale and concentrated by a double PEG/NaCl precipitation for storage and future experiments.

3.4. Computational Analysis

The gpVIII sequence from unique phage clones was translated to their corresponding pVIII protein sequences using the EditSeq tool (DNASTAR, ver. 11; Madison, WI). Phage clones were manually curated for common structural motifs and subsequently grouped into families of related peptide motifs based on an identified consensus motif. Unique phage clones isolated from both phage libraries were analyzed for information content using the INFO tool found within the RELIC suite of programs designed for the statistical analysis of combinatorial peptide libraries such as the two phage libraries studied here (Mandava et al. 2004). A histogram showing the relative change in information content between both libraries was constructed by subtracting the relative abundance of information observed at a given information content in the selected library from the relative abundance of information observed in a random sampling of the unselected phage libraries. The overall diversity of the two libraries before and after four rounds of selection was calculated using the AADIV tool also found within the RELIC suite of programs.

Using MimoDB (ver. 4.2, updated April 2014), a manually curated, publicly accessible database of peptides identified following selection with random phage display libraries (J. Huang et al. 2012), unique phage clones that we identified were submitted to the optimized MimoDB BLAST tool designed for identification of

conserved structural motifs within short peptides and compared to the latest released version of the database. Resulting peptide motifs identified following selection against other cancer cell lines or known cell surface receptors were manually compiled into a single table and conserved peptide motifs were grouped and reported in Table V.

3.5. Phage Capture Assay - Selectivity and Specificity

The ability of unique phage clones to bind to their target lung cancer cells, Calu-3, in comparison to other control cells and serum was studied by a phage capture assay described previously (Fagbohun et al. 2012). In this assay, small airway epithelial cells were used as phenotypically normal lung epithelial cells and MCF-7 breast cancer cells were used as a non-related cancer. Briefly, 5.0×10^4 cells per well of each cell type was plated in triplicate for each phage in a 96-well plate in EMEM and allowed to grow to 90% confluence. Triplicate wells containing EMEM was also prepared for each phage clone to be used as a negative control. After overnight incubation, cells were incubated for 1 hour with serum-free medium at room temperature. Individual phage clones were added to corresponding wells at ~10^6 CFU per well in blocking buffer (0.5% BSA in EMEM) for 1 hour in a 37ºC/5% CO_2 cell culture incubator. Unbound phages were removed by washing with washing buffer (0.5% BSA/0.1% Tween 20 in EMEM) for 5 minutes for a total of eight washes. Cells were lysed with CHAPS (3-[(3-Cholamidoproply)dimethylammonio]-1-propanesulfonate) lysis buffer (2.5% CHAPS/0.5% BSA in EMEM) for 10 minutes with gentle shaking on a rocker. The remaining cell lysis was then titered for phage with K91BluKan *E. coli*. A previously identified phage displaying an unrelated peptide, VPEGAFSSD that binds streptavidin (Petrenko & G. P. Smith 2000), was used as a negative control in all assays. Phage recovery was calculated as the ratio of recovered phage versus the input phage as follows:

$$\text{Percent Recovery (\%)} = \frac{\text{Phage}_{\text{Output}}}{\text{Phage}_{\text{Input}}} \times 100 \quad (2)$$

3.6. Phage Capture Assay - Mode of Interaction

Interactions between phage clones displaying a fusion peptide with high target specificity to their target Calu-3 cells were studied by tracking the uptake of intact phage particles. Phage capture assay was performed as above, however phages bound to the surface were recovered by eluting with elution buffer (200 mM glycine, pH 2.2/0.1% BSA in EMEM), neutralized with neutralizing buffer (1 M Tris-HCl, pH 9.1), and saved for titering. Cells were then washed twice with washing buffer and saved for titering. The remaining cell monolayer was lysed with lysis buffer to recover internalized phage and saved for titering. All recovered fractions were titered as described previously (Brigati et al. 2008). Recoveries were reported as a percentage of the total number of input phage. Cell

uptake percentages were calculated as the number of phage recovered in a particular fraction by the sum of all recovered phage from all fractions as follows:

$$\text{Percent Recovered}_{\text{fraction}}(\%) = \frac{\text{Phage}_{\text{fraction}}}{\text{Phage}_{\text{eluate}} + \text{Phage}_{\text{PEW}} + \text{Phage}_{\text{lysate}}} \times 100 \quad (3)$$

3.7. Inhibition of Phage Uptake with Endocytosis Inhibitors

Intracellular uptake of phage clones into target Calu-3 NSCLC cells was studied using a modified phage capture assay in the presence of different endocytosis inhibitors. Calu-3 cells were seeded at 5.0×10^4 cells per well in a 96 well plate and allowed to grow until reaching 90% confluence. Prior to treatment with isolated phage clones, cells were pretreated at room temperature with either 1) 10 μg/mL chlorpromazine for 30 minutes, 2) 1 μg/mL genistein for 30 minutes, 3) 30 mM cytochalasin D for 30 minutes, 4) 450 mM sucrose for 1 hour, or 5) fresh medium as an untreated control. Endocytosis inhibitor concentrations were identified from literature that displayed no reported toxicity to the cells. Following drug treatment, individual phage clones were added to corresponding wells (~10^6 CFU) in blocking buffer (0.5% BSA in EMEM) for 1 hour in a 37ºC/5% CO_2 cell culture incubator. Cells were washed and remaining phages were recovered and titered as in the phage capture assay. Endocytosis inhibition was reported as the percent change between phage uptake in the presence of an inhibitor compared to an untreated control as follows:

$$\text{Uptake Inhibition}_{\text{Inhibitor}}(\%) = \frac{\text{Phage}_{\text{Inhibitor}} - \text{Phage}_{\text{Control}}}{\text{Phage}_{\text{Control}}} \times 100 \quad (4)$$

3.8. Confocal Microscopy

Calu-3 cells were seeded in 4-well chamber slides in fresh culture medium. CellLight Early Endosome-RFP reagent (Molecular Probes, Carlsbad, CA) was added to exponentially growing Calu-3 cells and incubated overnight in a 5% CO_2 incubator at 37ºC as recommended by the manufacturer. The following day, culture medium was aspirated and replaced with fresh medium containing ~10^7 virions (~10^6 CFU) for 1 hour at 37ºC. Unbound phages were removed and cells were washed for 5 minutes with wash buffer three times. Cells were fixed with 4% formaldehyde for 15 minutes at 37ºC. The cell plasma membrane was stained with Wheat Germ Agglutinin (WGA) conjugated with Alexa Fluor 555 (Molecular Probes, Carlsbad, CA) for 10 minutes at room temperature. Cells were washed twice with 1X Hank's balanced salt solution and permeabilized with 0.2% Triton X-100 at room temperature for 10 minutes. Cells were then washed three times with 1X TBS, pH 7.4 for 5 minutes at room temperature followed by incubation with blocking buffer for 30 minutes at room temperature. Cells were incubated

with a polyclonal rabbit anti-fd IgG diluted in blocking buffer for 1 hour at room temperature. Cells were washed three times with washing buffer, followed by treatment with a goat anti-rabbit IgG conjugated with Alexa Fluor 488 for 30 minutes at room temperature. Cells were again washed three times with washing buffer. Cell nuclei were labeled with TOPO-3 stain (Molecular Probes, Carlsbad, CA) according to the manufacturer's recommendations and overlaid with ProLong Gold anti-fade reagent (Molecular Probes). Slides were cover-slipped and sealed with nail polish. Slides were imaged by confocal microscopy with a Nikon Eclipse TE 2000-E and analyzed with NIS Elements (Nikon Instruments)

3.9. Preparation of Phage Protein-modified Liposomal Doxorubicin

Phage protein-modified liposomal doxorubicin (Lipodox; SUN Pharmaceutical Ind. Ltd. Gujaat, India) was modified by cholate-solubilized major coat proteins at a lipid-to-protein mass ratio of 200:1 at 37ºC followed by dialysis in 1X PBS, pH 7.4 as described previously (Tao Wang et al. 2014).

3.10. Cell Viability Assay and Doxorubicin Uptake Assay

Calu-3 cells were seeded into a 96-well plate at a density of 5,000 cells/well and exposed to different concentrations of doxorubicin-loaded liposomes for 36 hours of treatment. Cell viability was estimated by measurement with MTT assay as described previously (Bedi et al. 2014). Cell associated doxorubicin was estimated after 4 hours of doxorubicin exposure by extraction of total associated doxorubicin with acidified isopropanol followed by quantification by fluorescent signal (ex 470/em 590) as described previously (Bedi et al. 2014)

4. Results

4.1. Selection of Lung Cancer Cell-Specific Phage

To identify a collection of phage and phage protein probes that interact specifically with novel or aberrantly overexpressed receptors of unknown identity present on the surface of NSCLC cells, two proprietary landscape phage libraries were used that display a randomized 8- or 9-mer fusion peptide in the N-terminus of every copy of the pVIII major coat protein of fd-tet phage. These phage libraries consist of phage clones containing random DNA oligomers inserted into a specific region of the pVIII gene of the wild-type phage. When expressed during phage morphogenesis, this fusion allows the translated peptide to be expressed at the N-terminus of the mature major coat protein, pVIII. When phage from these libraries are propagated, they express ~4,000 copies of a single, modified protein containing a fusion between the protein encoded by the randomized DNA insert and the N-terminus of the wild-type pVIII major coat protein.

To identify phage particles that interact specifically with NSCLC, first phage interacting with unrelated targets such as: 1) plastic, 2) cell culture medium, 3) serum components, and 4) phenotypically normal lung cells, were removed. After these depletion steps, each phage library was enriched for phage interacting at room temperature with the surface receptors of a NSCLC cell line and binding phage were separated into eluate and lysate library fractions that would theoretically contain cell surface-binding and cell-internalizing phage respectively, as depicted in the flow chart in Figure 8. As expected, a moderate recovery of phage from the eluate fractions of both libraries (Figure 9) and lower recovery of phage from the lysate fractions (Figure 10) was observed for the first round of selection.

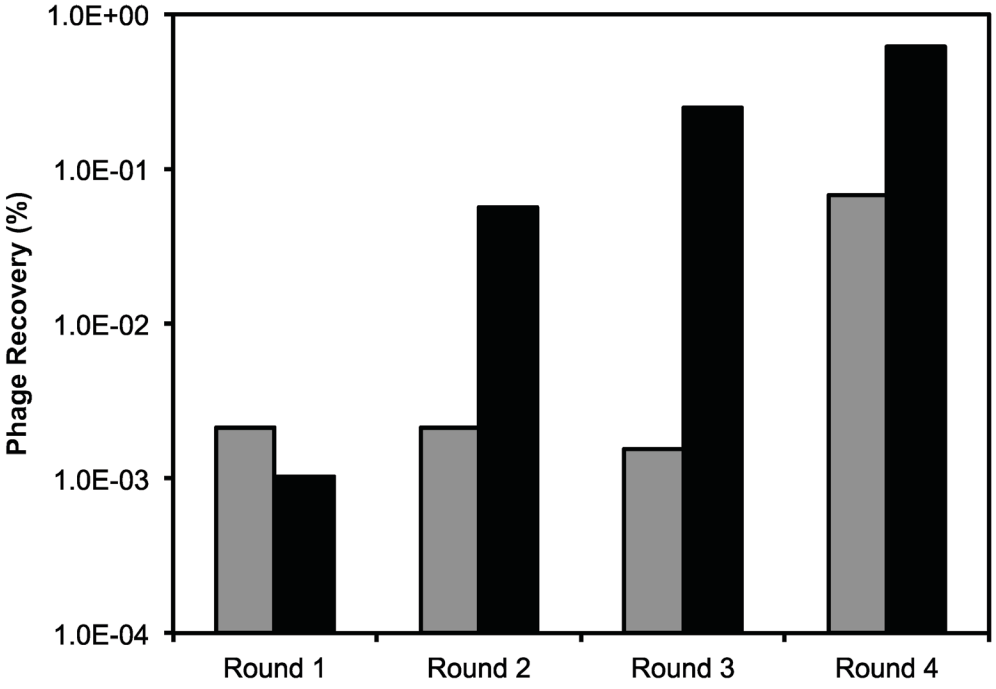

Figure 9: Recovery of phage following each round of selection. Output phage generated from the eluate selection scheme (solid line from Figure 8), isolated from the depleted f8/8 library (gray bars) and f8/9 library (black bars). (Phage yield = output phage/input phage, %)

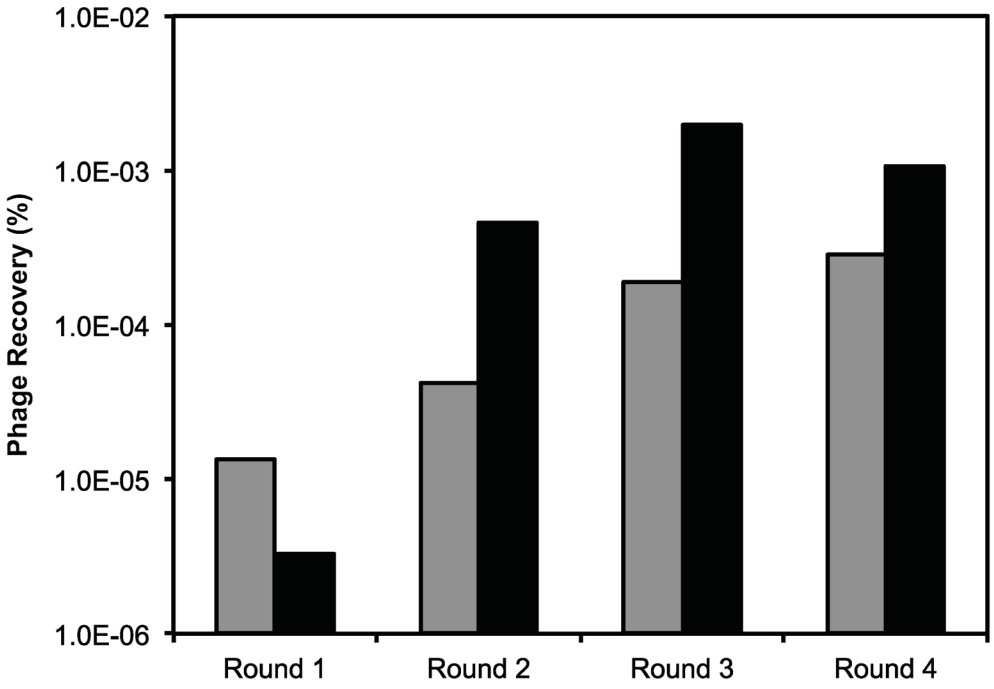

Figure 10: Recovery of phage following each round of selection. Output phage generated from the lysate selection scheme (dashed line from Figure 8), isolated from the depleted f8/8 library (gray bars) and f8/9 library (black bars). (Phage yield = output phage/input phage, %)

The temperature of phage incubation was increased from room temperature to a more physiologically relevant temperature of 37ºC to increase the stringency of the following rounds of selection, as depicted in the flow chart (Figure 8). It was hypothesized that the increase in temperature would increase the yield of the phage recovered in the lysate fraction, irrespective of input library used, due to increased endocytosis and other metabolically active transport mechanisms. The increased temperature leads to enrichment of the phage library for NSCLC specific phages that are internalized by active transport mechanisms. Beginning with the second round of selection, the input was prepared by combining eluate fractions prepared in the previous round of selection as depicted in Figure 8. For example, the eluate input was prepared as a combination of phage from both eluate and lysate fractions. An approximate 10-fold increase in phage recovery was observed for each subsequent round of selection for both fractions in both libraries (Figure 9 & Figure 10), with the exception for the final round of selection with the f8/9 library lysate fraction that resulted in a slight decrease in recovered phage. These results suggest enrichment of the recovered phage population for the peptide sequences that interact specifically with their target NSCLC cells. The significant enhancement of phage yield recovered in the lysate fraction after increasing the

incubation temperature may suggest that active transport mechanisms are probably used to increase intracellular phage penetration.

Approximately 100 clones from each library were sequenced after four rounds of selection to identify the corresponding fusion peptide sequence of each recovered phage clone and determine the overall diversity present in the libraries after selection. Several families of phage containing common linear motifs were identified with the f8/8 library (Table II) and with the f8/9 library (Table III). Also a few common motifs between both libraries were identified, including EPG[Q/E], NGR, RGD and DGR, most families were unique within their respective library of origin due to the differences in amino acid diversity in each library before selection. A family of sequences containing the motif DxDY[S/T] that had been identified in previous screening of an 8-mer phage library against the MCF-7 breast cancer cell line (Fagbohun et al. 2012) was identified suggesting a common receptor could be identified between the two types of cancer. A phage clone, VEEGGYIAA, isolated during selection against lung cancer cells, was also selected and had also been reported previously in selection against breast cancer (Fagbohun et al. 2012) and pancreatic cancer cells (Bedi et al. 2014) using the same library suggesting a common receptor between all three cancer types.

Table II: Families of peptides identified from f8/8 library. Lung cancer-specific phage clones recovered after the fourth round of selection with the f8/8 library in target Calu-3 cells. Phage were grouped into nine different peptide families based on a common consensus sequence (shown in bold) identified between phage clones. Orphan phage clones that did not contain a common consensus sequence between any identified clones were grouped into another family.

ASP-----	**----GTS-**	**V/AD-DYS/T**
ASPLAAPA	ASLP**GTS**Q	GT**AD**Q**DYS**
ASPMDVNS	DPT**GTS**AP	**VD**P**DYT**SP
AS/TL----Q	**--LWS---**	Other
ASLPGTS**Q**	AT**LWS**LGQ	ANEHPMSQ
ATLWSLG**Q**	A**LWS**DSGA	DAGPMWSG
		DNGTFREM
----EPGQ	**-NGRP--**	DTSLTTDE
AMLM**EPGQ**	V**NGR**AEAP	EMSYNADA
ATLM**EPGQ**	A**NGRP**SMT	ETMMPYGT
VTIP**EPGQ**	A**NGRP**THL	VTDPSAST
ATVI**EPG**E	AT**GRP**THL	
VTGH**EPG**E		
---FSG--	**--P-LS-E**	
APG**FSG**QP	AR**P**I**LS**S**E**	
DNP**FSG**TQ	GT**P**L**LS**P**E**	

Table III: Families of peptides identified from f8/9 library. Lung cancer-specific phage clones recovered after the fourth round of selection with the f8/9 library in target Calu-3 cells. Phage were grouped into sixteen different peptide families based on a common consensus sequence (shown in bold) identified between phage clones. Orphan phage clones that did not contain a common consensus sequence between any identified clones were grouped into another family.

AP---D-DT	**-EY-E-VNA**	**------MDQ**	Other
APAHEYGYD	A**EY**G**ES**V**NA**	ESYPMH**MDQ**	ANDVYLD
APMFS**D**H**DT**	G**EY**V**EL**V**NA**	GVSYVD**MDQ**	DIPWYGDES
APYSF**D**A**DT**			AYDPDLGGD
	----EYG--	**----RGD--**	EDARTAAMA
D/E-S-SYIDQ	APAH**EYG**YD	GLNG**RGD**PD	ADYDFMVDN
DESISYIDQ	A**EYG**ESVNA	EP**RGDS**LDL	DPLAEVTTL
DSSLSYIDQ			DPRVESMSG
DASFMAV**DQ**	**------GDS/M**	**----SYI--**	DYPNEYSSA
EGMNYH**IDQ**	DGESWG**GDS**	**DMSYI**ASED	EFYAESTSL
	DHVWAE**GDS**	DESI**SYI**DQ	EHVYDEGSN
	DMERYS**GDM**	DSSL**SYI**DQ	EYSPYAGDT
	VESGAL**GDM**		GNATLSSME
		------VDS	VDIAEQSTA
DGR------	**---GES---**	G**VDS**EIVSL	
DGRDHDAEN	AEY**GES**VNA	VGDYDV**VDS**	
DGRFDSETS	D**GES**WGGDS		
DGRSYTGED	DWMPVE**GES**		
V**DGR**TGTDS			
----EASTL	**GYD--L---**	**---VEE---**	
ADTS**EASTL**	**GYD**FN**L**TDQ	EVN**VEE**INL	
EIDP**EASTL**	**GYD**LD**L**NAD	**VEE**GGYIAA	
---EPGL--	**GSLEE-S-L**		
EPF**EPGL**AS	**GSLEE**V**S**T**L**		
GMVM**EPGL**D	**GSLEE**S**S**N**L**		

After selection with the f8/8 library, a common EPG[Q/E] motif that was enriched in 18% (5/28) of the total unique sequences identified was observed. Previous results showed that phage clones containing an EPGX motif often interact non-specifically with an unidentified component in serum (Fagbohun et al. 2012). As a result of this data, a reduction in the number of serum-binding clones isolated during screening of the f8/9 library was sought. To accomplish this, a second step of serum depletion was performed during the selection scheme of the f8/9 library. After four rounds of selection with the f8/9 library, only 4% (2/47) of clones were observed to contain this motif suggesting an enhanced depletion of serum-binding clones during the added depletion step.

The RELIC suite of statistical analysis programs, which was developed specifically for the analysis of combinatorial peptide libraries such as the two landscape phage libraries used in this study, was used to study the evolution of the libraries during selection and identify functionally significant clones. Briefly, the information content of any random phage displayed peptide can be generally defined as the probability of an amino acid appearing following selection versus the probability of the amino acid appearing by chance in an unselected library in a defined position. Thus, phage with high information content contain a fusion peptide with amino acids statistically underrepresented in the unselected library and often indicate the presence of a selective pressure to maintain the rare amino acid. The change in total information associated with each phage library before and after four rounds of selection against Calu-3 NSCLC cells was sought. It was hypothesized that following selection, there would be enrichment of phage clones with high information content and a decrease in phage clones with low information content. After four rounds of selection with the f8/8 library against a NSCLC cell line, 30 unique phage clones were analyzed for their information content compared to a collection of 73 random, unselected clones from the f8/8 library. A decrease in phages with low information content and a decrease in some phages with moderate information content was observed. There was an increase in some moderate information containing phage as well as an increase in high information content phage that was also observed (Figure 11, solid line). Overall, selection with the f8/8 library produced clones with higher information content than the unselected population suggesting a successful selection experiment and enrichment of lung cancer specific phage in the generated output library. Similarly, 53 unique phage clones recovered after four rounds of selection with the f8/9 library were analyzed and compared to a collection of 64 random clones from the unselected f8/9 library. A larger decrease in moderate information containing phage as well as a larger increase in high information content phage was observed (Figure 11, dashed line). An increase in low information content phage compared to an unselected population was also observed. Thus, the results suggest there was enrichment of lung cancer specific phage clones in the f8/9 library.

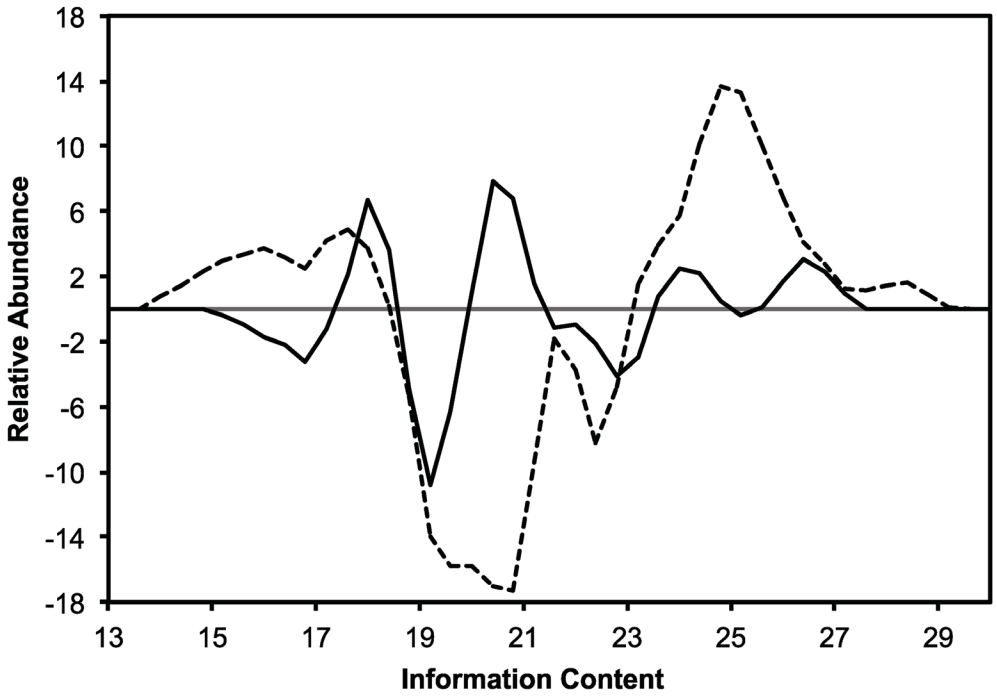

Figure 11: Histogram of the change in information content available in each sublibrary generated after four rounds of selection against a NSCLC cell line, Calu-3. Information content from clones in f8/8 (black line) and f8/9 (dashed line) are presented. Positive values indicate an increase in total information content, while negative values indicate a decrease in total information content. More detailed information is given in the results section.

Another common characteristic used to measure the quality and utility of a phage display library is the calculation of the peptide diversity, also referred to as the completeness of sequence representation within the libraries. Next, the observed protein diversity of our two generated libraries (composed of the eluate and lysate clones after the fourth round of selection) was determined using the AADIV tool found in the RELIC analysis suite. It was hypothesized that following selection there should be a decrease in the overall population diversity compared to an unselected library due to the selective enrichment of cell-binding motifs identified through the selection procedure and a loss of non-specific peptides. There was a 2.42 fold decrease in overall peptide diversity from $9.14\times10^{-3} \pm 4.49\times10^{-3}$ in the unselected f8/8 library to $3.77\times10^{-3} \pm 2.76\times10^{-4}$ ($P < 0.0001$) following four rounds of selection against Calu-3 lung cancer cells. Similarly, there was a 4.51 fold decrease in overall peptide diversity from $2.67\times10^{-3} \pm 1.44\times10^{-3}$ in the unselected f8/9 library to $5.93\times10^{-4} \pm 3.53\times10^{-4}$ ($P < 0.0001$) following four rounds of selection. After selection, there was a significant decrease in overall diversity per amino acid from 55.6% to 37.3%

in the f8/8 library and from 51.8% to 43.8% in the f8/9 library. From these data, it is shown that there was enrichment of both phage libraries for clones with high information content and a decrease in overall amino acid diversity as expected following selection against our target cells. As suggested previously (Kuzmicheva, Jayanna, Sorokulova, et al. 2009b), each of the two f8-type libraries biopanned here occupy different sequence spaces resulting in different populations of ligands following the same selection protocol.

4.2. Interaction of Phage with Lung Cancer Cells

Ideal ligands for targeted drug delivery should have the ability to interact specifically with their target cancer cells and not with phenotypically normal cells surrounding the tumor. A phage capture assay was used to determine if the enrichment of phage clones observed during our final round of selection produced lung cancer cell-specific phage clones. In Figure 12, the binding specificities of a representative collection of identified phage clones from the f8/8 and f8/9 libraries are presented.

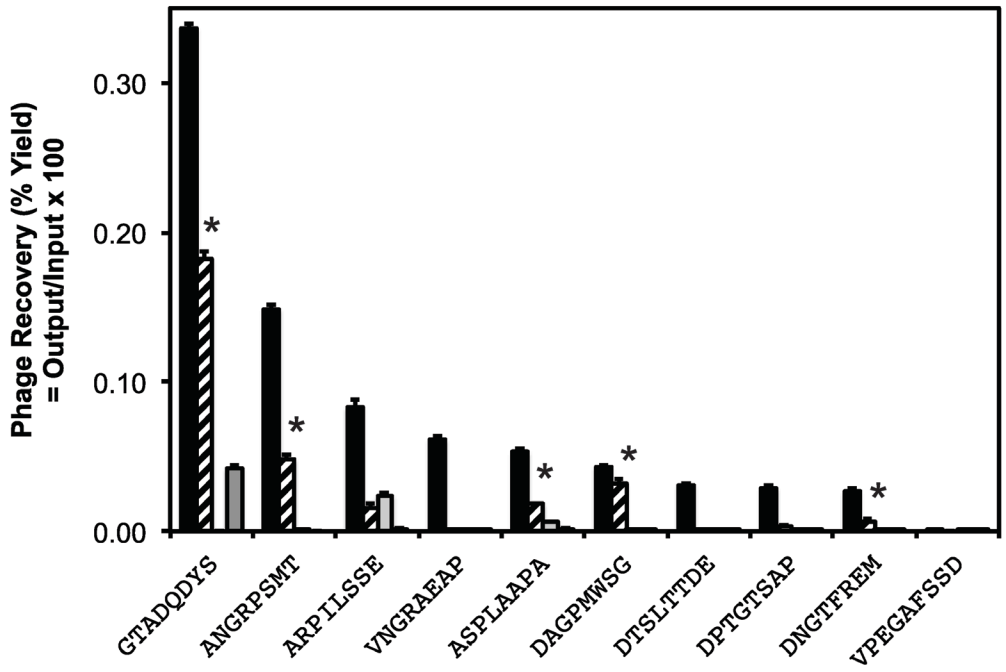

Figure 12: Representative selectivity and specificity assay for select phage clones from the f8/8 library. Individual phage clones were incubated at a constant concentration with: 1) target Calu-3 cells (black), 2) non-related MCF-7 cancer cells (striped), 3) phenotypically normal lung small airway epithelial cells (white), and 4) culture medium with 10% serum (grey). After washing, mammalian cells were lysed and the remaining phage were titered as described in the methods section. Percent recovery was plotted as the number of recovered phage per number of input phage particles for each phage clone. All phage clones binding Calu-3 cells were statistically different from an unrelated phage ($P < 0.0001$) and also different from paired phage samples with different targets ($P < 0.0001$). Phage interactions with MCF-7 cells were compared between paired phage samples with different targets and significant interactions were marked (* $P < 0.0001$).

Clones were screened from the f8/9 library according to their associated information content compared to an unselected library (Table IV). As expected, all representative clones showed a statistically significant increase in binding to Calu-3 cells compared to a non-related phage containing the guest fusion sequence of VPEGAFSSD, which was shown previously to have an affinity to streptavidin and possess little ability to bind cancer cells ($P < 0.0001$). The ratio of phage yield (output/input) obtained for each clone bound to Calu-3 cells by phage yield of non-related phage (VPEGAFSSD) is referred to as a phage's specificity. Alternatively, for each clone the ratio of phage

yield to Calu-3 cells by yield to another cell line is referred to as a phage's selectivity. A number of clones studied showed minimal binding to normal lung epithelial cells or serum components (high specificity), however some of the phage clones identified from the f8/9 library showed equal or better binding to serum under identical conditions. Clones such as VNGRAEAP, DTSLTTDE, and DESISYIDQ show specific interactions with only the target Calu-3 cells ($P < 0.0001$). Some identified clones such as EVNVEEINL, and DAGPMWSG, show moderately high interaction with the target cells and possess the ability to interact with other non-related cancer cells more than normal cells (Tukey-Kramer HSD test, non-related cancer vs. normal cells; $P = 0.0198$ and $P < 0.0001$ respectively). However some phage clones, like ARPILSSE, were shown to have moderately high interactions with the target cells (Tukey-Kramer HSD test, target vs. non-related cancer cells, $P < 0.0001$), but also showed minor interacts with a non-related cancer type and phenotypically normal cells that were statistically equally to each other. (Tukey-Kramer HSD test, non-related cancer vs. normal cells; $P = 0.0587$). It was also observed that some clones, such as ANGRPSMT, ASPLAAPA, DAGPMWSG, and GTADQDYS, were selective to a non-related breast cancer cell line, MCF-7, when compared to a non-related phage described in materials section ($P < 0.0001$). Two prominent phage clones that showed high relative selectivity and specificity at the studied concentration were ANGRPSMT and VNGRAEAP that both contain a conserved NGR motif shown to interact with aminopeptidase N (CD13), a commonly overexpressed marker on tumor cells and vascular endothelium around tumor tissues (Corti et al. 2008).

Table IV: Representative selectivity data for select phage clones from the f8/9 library. Information content refers to a statistic generated by RELIC comparing the probability of amino acid occurrence in a selected clone compared to an unselected library. Selectivity refers to the ability of a clone to identify the target compared to an unrelated clone. Specificity refers to the ability of a clone to discriminate between two cell types, here Calu-3 cells compared to phenotypically normal lung cells (SAE).

Phage	Information Content	Specificity	Selectivity (Calu-3/SAE)
EVNVEEINL	28.245	76.91	3.31
GEYVELVNA	26.867	145.12	2.40
GMVMEPGLD	26.092	62.49	2.29
GVSYVDMDQ	25.452	119.53	1.15
AEYGESVNA	25.054	48.11	1.73
DESISYIDQ	25.029	24.04	14.01
VPEGAFSSD	-	2.23	4.11

Most drug delivery applications requiring a cell-specific ligand not only need to discriminate the desired target cell from a collection of normal cells, but also be able to be internalized for successful treatment. Thus, the relative uptake distribution for a select number of lung cancer specific phage was sought. It was hypothesized that selective phage clones would undergo different mechanisms of transport based on the specific interaction between their fusion peptide and their currently unidentified receptors. The interaction of intact phage with Calu-3 cells using a modified phage capture assay, in which phage were recovered from phage-treated cells using different extraction buffers, was sought to determine a general subcellular distribution of phage probes within the NSCLC cells. Phages were split into three representative subcellular fractions as performed during selection (eluate, post-elution wash, and lysate) and titered. From the studied phage clones, there were three distinct classes of phage interactions observed with lung cancer cells: 1) clones that predominately bind to the surface of the cells and remain restricted to the cell surface; 2), clones that are internalized and associate with an internal membrane or membrane bound organelle; and 3) clones that internalize and remain in the cytoplasm (Figure 13A-C).

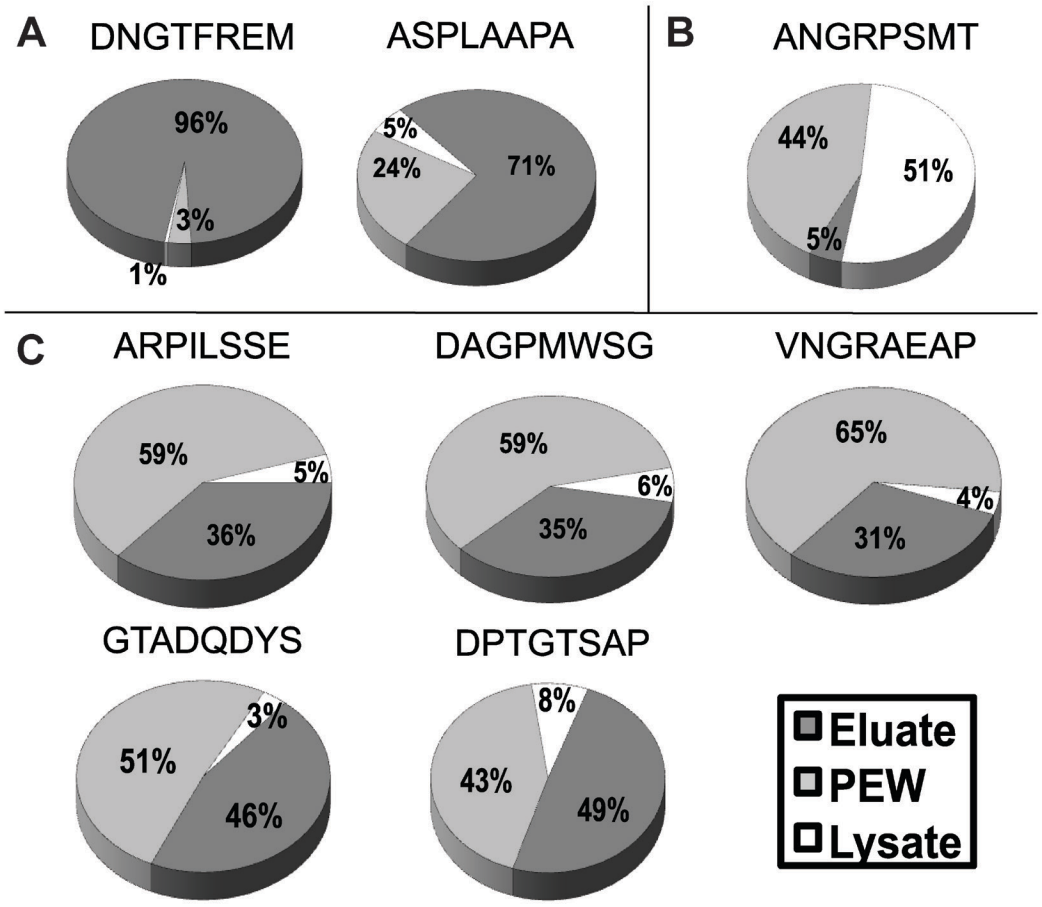

Figure 13: Phage mode of interaction with Calu-3 cells after recovery of cell-associated phage by different elution steps with acid and detergent. Cells were split into three general subcellular fractions and the amount of phage associated with each fraction was determined by titering in K91BluKan *E. coli*. The portion of each fraction was calculated as the part of each fraction per total recovered phage. Three different classes of phage were identified based on binding distribution: A) surface bound, B) membrane bound, and C) cytoplasmic.

The first class of phage was represented by phage clones, DNGTFREM and ASPLAAPA, which show greater than 70% of phage recovery in the eluate fraction (Figure 13A). It was hypothesized that these phage clones interact with surface restricted receptors that do not undergo endocytosis or have a slow rate of endocytosis, which leads to minimal phage uptake. The second class of phage was represented by phage clone, ANGRPSMT, which showed greater than 50% of phage recovery in the lysate fraction and <10% recovery in the eluate fraction (Figure 13B). It was hypothesize that these phage either interact with receptors that undergo rapid endocytosis or are able to

directly penetrate through the cell membrane upon interaction with a surface receptor. Similarly, it was hypothesized that this class of phage clones are internalized and protected from the post-elution washes by a membrane bound organelle or other hydrophobic compartment/membrane. The third and most common class of phage clones was represented by phage clones: ARPILSSE, DAGPMWSG, VNGRAEAP, GTADQDYS, and DPTGTSAP, which were identified by a composition of ~40% of phage recovered in the eluate fraction, ~5% in the lysate fraction, and ~60% in the post-elution wash fraction (Figure 13C). It was hypothesized that this class of phage interacts with a receptor that undergoes endocytosis and resides primarily in the cytoplasm of the cells. It was shown previously that phage recovered from the post-elution wash fractions are released from the cytoplasm after activation of phospholipases during pH shock, resulting in membrane defects and subsequent release of internalized phage (Jayanna, Bedi, DeInnocentes, et al. 2010a). The observed rapid cytoplasmic release can also be contributed to the instability of the endosomal membrane after accumulation of certain phage particles during intracellular trafficking that leads to the collapse and subsequent leakage of infectious phage particles from the endosomal compartment to the cytoplasm. Increased endosomal escape activity of phage proteins was demonstrated previously for phage proteins with the fusion peptide DMPGTVLP that were incorporated into liposomal nanomedicines (Tao Wang, S. Yang, et al. 2010c). Nanoparticles that enhance endosomal escape and avoid degradation of their encapsulated payload are becoming a requirement for nanomedicines. The identification and classification of ligands that promote endosomal escape is an important consideration for effective ligand selection in many therapeutic applications.

4.3. Mechanism of Phage Uptake into Lung Cancer Cells

The amino acid residues surrounding a consensus motif, such as RGD, have been shown to play a vital role in the functional activity of cell binding motifs. Due to the relatively high binding and the observed difference in cellular distribution between the two phage clones with a conserved NGR motif (A**NGR**PSMT and V**NGR**AEAP), it was hypothesized that the observed difference in phage uptake could be explained by a difference in primary endocytic route. To determine the endocytic routes used during cell penetration, a modified phage capture assay was performed in which different endocytosis inhibitors, used at sublethal concentrations, were pre-incubated with Calu-3 cells prior to addition, recovery and titering of phage. Chlorpromazine, a cationic amphiphilic drug commonly used to inhibit the formation of clathrin-coated pits, was used to inhibit clathrin-mediated endocytosis (L H Wang et al. 1993; Vercauteren et al. 2010). Genistein, a tyrosine-kinase inhibitor that causes disruption of the actin network (Parton et al. 1994) and inhibits recruitment of dynamin II (Nabi & Le 2003), was used to inhibit caveolae-mediated

endocytosis (Vercauteren et al. 2010). Cytochalasin D, an inhibitor that destabilizes the cytoskeletal structure of cells by inducing actin network depolymerization (Gottlieb et al. 1993), was used to inhibit macropinocytosis. Hypertonic sucrose, which inhibits clathrin and HA2 adapters from forming into mature vesicles (Hansen et al. 1993; Heuser & Anderson 1989), was also used to inhibit clathrin-mediated endocytosis. It was hypothesized that these phage clones are internalized through an active transport mechanism and inhibition of cellular processes involved in specific endocytosis pathways would result in a significantly reduced phage titer following a phage capture assay. As expected from phage binding and uptake results, a significant difference (Dunnett's test; $p < 0.0001$) in phage uptake for all treatments following incubation with different endocytosis inhibitors compared to untreated control cells was observed (Figure 14). The greatest difference was observed in ANGRPSMT phage recovery following chlorpromazine (27.6 ± 2.8%, two-tailed t-test vs. control cells; $p < 3.67\times10^{-4}$) or genistein (27.8 ± 0.4%, two-tailed t-test vs. control cells; $p < 5.27\times10^{-5}$) treatment. Similarly, the greatest difference in recovery of VNGRAEAP phage was observed following treatment with genistein (42.5 ± 0.50%, two-tailed t-test vs. control cells; $p < 2.17\times10^{-5}$) or cytochalasin D (41.75 ± 2.62%, two-tailed t-test vs. control cells; $p < 8.82\times10^{-5}$) suggesting fundamentally different primary mechanisms in how these intact phage particles are taken up into mammalian cells. These data show that phage ANGRPSMT is internalized primarily by clathrin-mediated or caveolae-mediated endocytosis, suggesting a receptor-mediated intracellular transport mechanism to occur following a specific interaction between ANGRPSMT phage particles and a currently unknown receptor. In contrast, phage VNGRAEAP is internalized primarily by caveolae-mediated endocytosis or macropinocytosis, suggesting this phage is internalized primarily by fluid phase transport mechanisms or different receptor-mediated transport mechanisms.

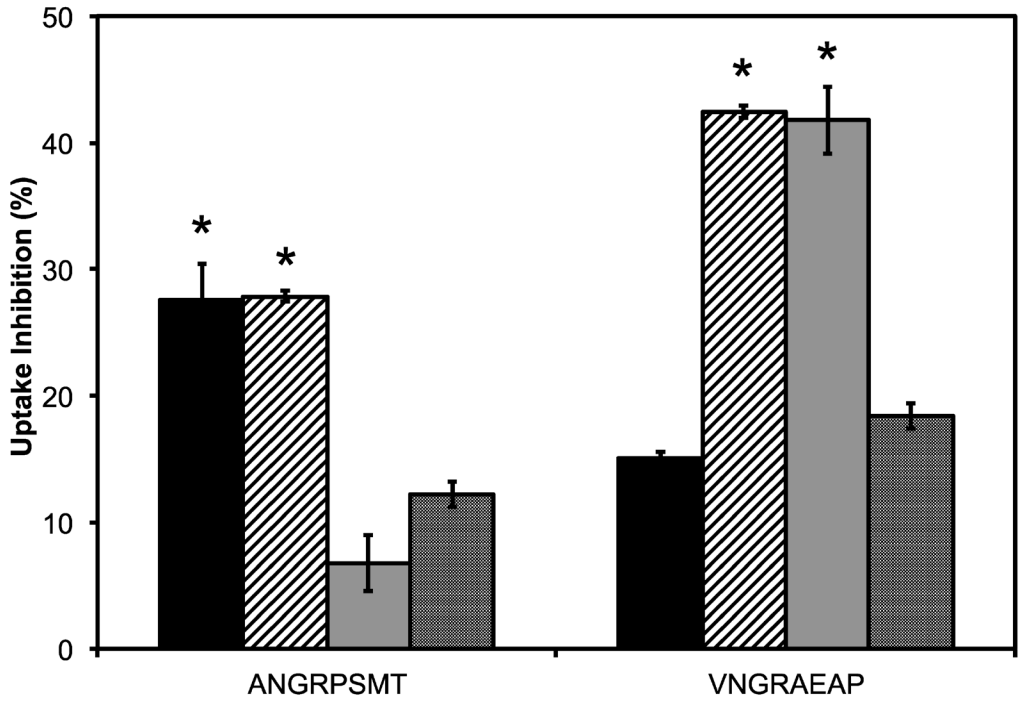

Figure 14: Decrease of phage endocytosis in Calu-3 cells by chemical inhibition. Calu-3 cells were incubated with different endocytosis inhibitors for 1 hour prior to the addition of isolated phage clones ANGRPSMT and VNGRAEAP. Cells were washed, lysed and the remaining cell-associated phage were counted by titering in K91BluKan *E. coli*. The percent uptake inhibition was calculated as the number of phage particles taken up by Calu-3 cells in the presence of endocytosis inhibitor per number of phage particles taken up by Calu-3 cells without an inhibitor. Significantly different changes in phage uptake in the presence of different inhibitors were marked (two-tailed t-test vs. control; * $p < 0.0001$). Treatments from left to right: Chlorpromazine (black bars), Genistein (striped bars), Cytochalasin D (gray bars), and Sucrose (hashed bars).

Confocal microscopy was used to confirm the observed difference in uptake mechanisms between the two NGR phages, ANGRPSMT and VNGRAEAP. A significant difference in phage labeling between the two different NGR phages in Calu-3 cells was observed prior to treatment with any endocytosis inhibitor. ANGRPSMT phage (Figure 15A) showed an accumulation of phage primarily within the cytoplasm and is suspected to be found within endosomes as suggested by the orange overlay found in the cytoplasm. However, VNGRAEAP phage (Figure 15C) showed large changes in cell morphology and phage distribution compared to ANGRPSMT phage in representative micrographs as shown. These cells appeared to have a large protrusion extending from the cytoplasmic membrane

engulfing a large number of phage particles. A redistribution of phages was apparent following treatment of Calu-3 cells with genistein for both ANGRPSMT (Figure 15B) and VNGRAEAP (Figure 15D) phage as expected from the phage capture assay following endocytosis inhibition. Inhibition of caveolae-mediated endocytosis in Calu-3 cells followed by treatment with phage shows predominant clustering of both phage clones to be restricted to the cell surface, resulting in minimal phage uptake. Restriction of phage to the cell surface did not result in co-localization of phage particles with the cell membrane labeled with wheat germ agglutinin. Combined results of the phage capture assay and microscopy show that ANGRPSMT and VNGRAEAP phage interact with the same target cells, but with different primary mechanisms of endocytosis leading to differences in subcellular distribution.

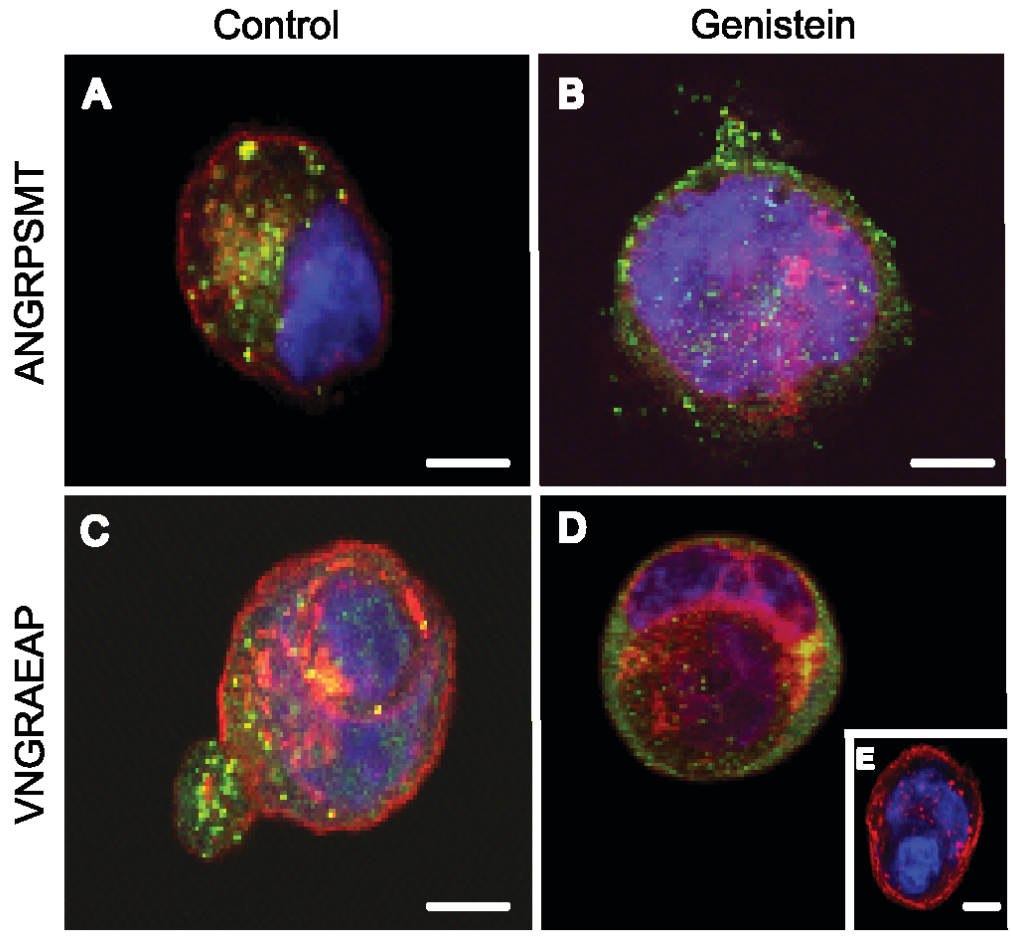

Figure 15: Confocal microscopy of phage associated with Calu-3 cells. Calu-3 cells were incubated with two different phage clones, ANGRPSMT (A and B) and VNGRAEAP (C and D), at the same concentration in the presence (B and D) or absence (A and C) of genistein, an inhibitor of caveolin-mediated endocytosis. Cells were washed, fixed, and permeabilized prior to treatment

with a rabbit anti-fd phage antibody followed by a goat anti-rabbit antibody conjugated with Alexa fluor 488 (green). Cell membranes were identified by incubation with WGA-Alexa fluor 555 (red) and cell nuclei were identified by staining with TOPO-3 (blue). Control cells that were untreated with phage are shown (E). Images were obtained on a Nikon Eclipse TE 2000-E under the same magnification (60X) and image acquisition settings. Scale bar = 10 μm.

4.4. *In vitro* activity of phage protein-modified liposomal doxorubicin

The application of two of the top binding phage clones (ANGRPSMT and VNGRAEAP), containing a conserved NGR motif, in a previously developed liposomal doxorubicin platform was demonstrated (Petrenko & Jayanna 2014). It was hypothesized that the peptide VNGRAEAP would significantly increase the toxicity of unmodified liposomal doxorubicin due to the large accumulation of phage in the post-elution wash (cytoplasm). As shown in Figure 16, there was a significant decrease in cell viability following treatment with VNGRAEAP-modified Lipodox at high concentrations ($P < 0.05$), however we also observed a significant decrease in viability with ANGRPSMT-modified Lipodox ($P < 0.05$). As hypothesized previously, active targeting of nanomedicines is expected to increase the intracellular concentration of cytotoxic drugs. The increase in toxicity was, in part, due to the increased cellular accumulation of VNGRAEAP-modified Lipodox compared to unmodified Lipodox ($P < 0.05$) as shown in Figure 17.

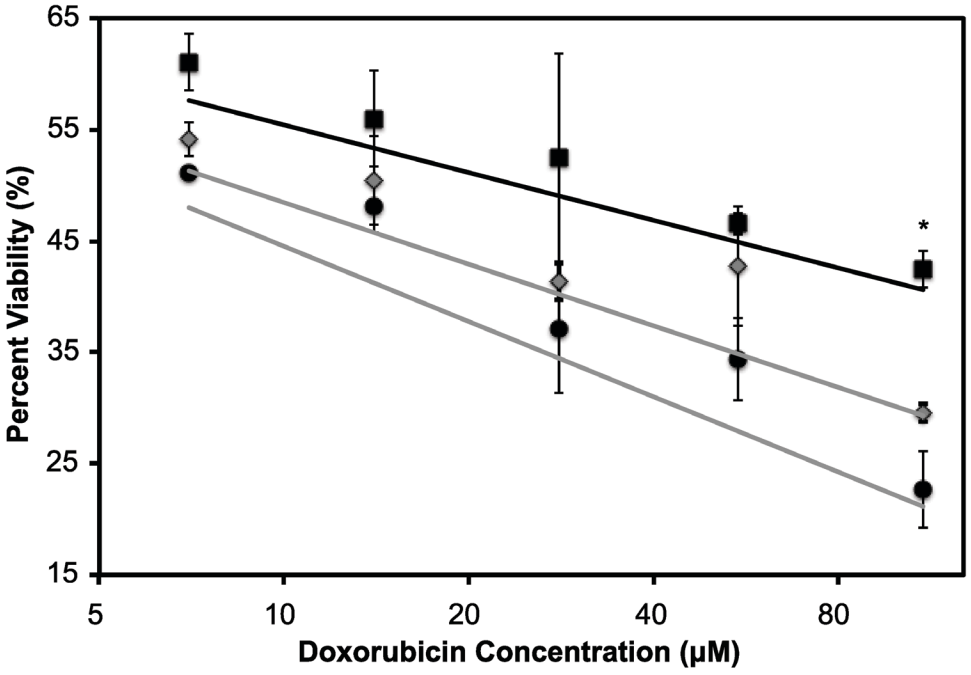

Figure 16: Cell viability of Calu-3 cells after treatment with Lipodox (squares), ANGRPSMT-modified Lipodox (diamonds), and VNGRAEAP-modified Lipodox (circles) for 36 hours. Cell viability was estimated by MTT assay. Data are presented as the mean ± standard deviation where N = 3. T-test was performed between modified and unmodified samples and * $P < 0.05$ was considered statistically significant.

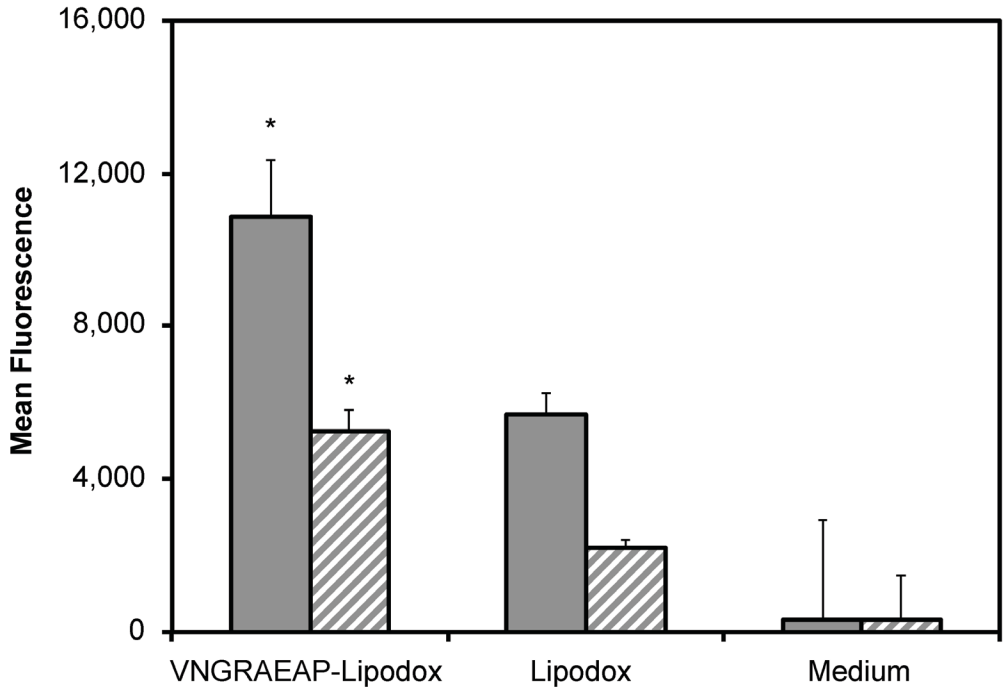

Figure 17: Doxorubicin cell-associated uptake after 4 hours of treatment of 20 μg/mL (grey) or 5 μg/mL (striped) doses of doxorubicin in Calu-3 cells. Doxorubicin was extracted by acidified isopropanol and quantified by fluorescence (ex 470/em 590). Data are presented as the mean ± standard deviation where N = 3. T-test was performed between modified and unmodified samples and * $P < 0.05$ was considered statistically significant.

5. Discussion

Phage display libraries containing a rich collection of highly diverse molecular probes are commonly used in biopanning/selection screens to identify protein sequences with high affinity to a desired target. Neoplastic cells, including lung cancer cells, often result in cells with different molecular phenotypes leading to different cell surface receptors being expressed across the cellular landscape. This cellular landscape can also be affected by differences in local tumor microenvironment following chemotherapy and/or radiotherapy treatments leading to a more complex landscape. Due to the dynamic nature of the cellular landscape, identification of a suitable selection scheme and cellular targets is important for the improvement of tumor-specific therapeutics or diagnostics.

Here, a subtractive selection scheme was used to identify a collection of peptides with specificity towards a lung cancer adenocarcinoma cell line previously receiving chemotherapy before isolation from a metastatic site.

Identification of cancerous cells that may have received previous chemotherapy and/or also may have metastasized away from the primary lesion remains a challenge. The identified peptides would be ideal candidates for detection and targeted cancer chemotherapy applications. Lung cancer specific peptides have been isolated by other groups from pIII phage display libraries displaying 12-mer (Zang et al. 2009) or 20-mer (Tsuksa Oyama et al. 2003; Tsukasa Oyama et al. 2006) peptide sequences within the five copies of the mature pIII protein. The pVIII landscape phage display library format, rather than modification of the pIII protein commonly used with other phage display libraries, provides a unique protein landscape across the length of the surface of each phage based on the selected fusion peptide sequence. A comparison of affinity between selected phage from both types of libraries has been described elsewhere (Knez et al. 2013), with phage identified from landscape libraries often displaying higher affinities in the sub-nanomolar Kd range due, in part, to the density of ligands within each phage. It was shown recently that a landscape phage clone, displaying a breast cancer specific ligand (DMPGTVLP) had an affinity in the picomolar range ($Kd = 1.3x10^{-12}$ M) to its target MCF-7 breast cancer cells suggesting the utility of landscape phage in generating high affinity targeting probes (Fagbohun et al. 2012).

Using a previously developed phage capture assay, recovered phage clones were screened in their target cell line to determine how they interact with the cells. One noted limitation of our phage capture assay is the ability to only identify intact, infective phage particles. This could slightly alter the elution profiles of each phage due to phage degradation by proteases at physiological temperatures or collapse of phage structure intracellularly. This limitation is unlikely given the highly stable structure of phage particles and the short incubation time of phage with mammalian cell targets. Using the information content generated from the RELIC analysis, it was hypothesized that phage with high relative information content would bind specifically with our target cells. This information content statistic could allow for identification of phage likely to interact with a given target compared to the unselected library and provide an ideal starting point for selectivity experiments following a final round of selection that may result in a large number of highly diverse structural families. However, using this statistic to replace selectivity experiments is not recommended, as the degree of selectivity or specificity towards a given target is not included in the calculation. For example, from the f8/9 clones presented, DESISYIDQ showed to be highly selective producing a specificity ratio of 14.01 from an information content of 25.029, however EVNVEEINL was less selective with a specificity ratio of only 3.31 from a higher relative information content of 28.245 (Table IV).

Neighboring peptides surrounding a shared structural motif can modulate the binding or activity of the RGD motif with surface integrins as proposed previously (Koivunen et al. 1995), as was shown with the RGD motif. It was shown here that a similar effect was observed with an NGR motif. Structurally, the NGR motif was located in the same position on each of the studied phages (A**NGR**PSMT and V**NGR**AEAP), however the selectivity and subcellular distribution were consistently different between the two phages. One clone, VNGRAEAP, showed dramatic cell specificity and was commonly found within the cytoplasm of Calu-3 cells. Alternatively, ANGRPSMT, showed more broad reactivity with cancer cells and found predominately in membrane bound organelles or endosomes. Thus, the results show that these neighboring residues can increase the affinity or specificity of the parent motif as well as modulate cell signaling and other regulatory events within the cell after binding (Maheshwari et al. 2000). Phage recovered in higher percentages from the post-elution wash fraction, such as VNGRAEAP phage, can significantly increase the toxicity of liposomal doxorubicin. Therefore, targeting ligands that internalize into the target cell rather than bind to surface restricted receptors should be used for delivery of cytotoxic drugs as shown previously with antibody-targeted liposomes (Sapra & Allen 2002).

Optimization of the subcellular delivery of nanomedicines should proceed through specific pathways that lead to improved deposition of doxorubicin in the nucleus that results in reduction of off-target toxicities and decreased resistance phenotypes. Here, phage VNGRAEAP was internalized by caveolae-mediated endocytosis and macropinocytosis while phage ANGRPSMT was internalized by clathrin- and caveolae-mediated endocytosis. It is expected that nanomedicines modified with these phage proteins will modify the primary endocytic pathway of intracellular uptake. Macropinocytosis of the VNGRAEAP-modified Lipodox was suggested to internalize larger volumes of nanomedicines from the environment, however macropinosomes (vesicles formed following uptake by macropinocytosis) mature to lysosomes. Alternatively, VNGRAEAP-modified Lipodox can also be internalized by caveolae-mediated endocytosis, which typically bypasses maturation into lysosomes and can delivered to the nucleus or other subcellular organelles (Sahay et al. 2010). Thus, it can be shown that phage proteins can be selected that allows delivery by a specific subcellular pathway.

6. Supplemental Material

Table V: Cancer-interacting motifs. Lung cancer identified peptides were screened for additional common structural motifs between phage selected against other cancer or cell surface markers using the publically accessible database, MimoDB v4.2. Common motifs between recovered phage and other libraries are shown in bold.

Calu-3 cell interacting peptides	Motif-containing peptides from other selected peptides	Target/Reference
ADTSEASTL	CLS**ASTL**MC	Human colon cancer cell line, HT29 (Kelly & D. A. Jones 2003)
ADYDFMVDN	PYRIDAW**AD**V**D**E**MV**WM	ICAM-1[2] (Bélizaire et al. 2003)
AEYGESVNA	**AEYGESVNA** **AEYGES**G**NA** **AEYGESV**LI **AEYGE**RG**NA**	Human PC[3] cell line, PC-3 (Jayanna, Bedi, DeInnocentes, et al. 2010a)
ALWSDSGA	VNSHQ**ALWS**PAQ TLQSILPPR**LWS**	Human NSCLC[4] cell line, CL1-5 (T.-Y. Lee et al. 2007) Aminopeptidase N (Y. Zhang et al. 2010)
ANDVYLD	RNVPPIF**NDVY**WIAF	Caveolin-1 (Couet et al. 1997)
APGFSGQP	**GFSG**HRLFDLSS PVRY**GFSG**PRLAILW	Aminopeptidase N (Y. Zhang et al. 2010) Caveolin-1 (Couet et al. 1997)
APMFSDHDT	R**SD**L**DT**LLARHQ	Integrin α5/β6 (Kraft et al. 1999)
APYSFDADT	**PY**RI**DA**WADVDEMVWM	ICAM-1[1] (Bélizaire et al. 2003)
ASLPGTSQ	YPHY**SLPGSS**TL VAPFWV**ASLP**AP	Human NSCLC[3] cell line, NCI-H1299 (Zang et al. 2009) Human glioblastoma cell line, U87MG (C. Wu et al. 2008a)
ASPLAAPA	CLL**PLAAP**C FGRIP**SPLA**YTYSFR GLLKYQQW**ASPL**C RGD**LAAP**HRTGA **LAAP**PKA NSLSN**AS**EFR**AP** SLTMM**SP**P**AA**SD	Human colon cancer cell line, HT29 (Kelly & D. A. Jones 2003) Integrin α6/β3 (Murayama et al. 1996) Human epidermoid carcinoma, A431 (Kamada et al. 2007) Integrin α5/β3 (Kraft et al. 1999) FGFR-2[5] (Maruta et al. 2002) Angiopoietin-1 receptor (X. Wu et al. 2008b) Human osteosarcoma cell line, OS732 (Zhu et al. 2003)
ASPMDVNS	CDH**ASPM**HC	VCAM-1[6] (Kelly et al. 2005)
ATLWSLGQ	RGDVW**TLWS**V**VG**DTRS TPGLD**AA**VF**WSLGS**E	Integrin α5/β1 (Healy et al. 1995) Human PC cell line, PC-3 (Newton-Northup et al. 2011)
AYDPDLGGD	CI**DPSLG**LC	Human colon cancer cell line, HT29 (Kelly & D. A. Jones 2003)
DASFMAVDQ	C**ASF**F**AV**QC **MAVD**PLR AYILPRIK**SF**T**A**	Integrin α5/β1 (Koivunen et al. 1994) FGFR-2[4] (Maruta et al. 2002) Human heptatocellular carcinoma cell line, HepG2 (Zhao et al. 2013)
DESISYIDQ	VTRG**DSISY**L RGDWY**ESVSY**WGVIDW	Integrin α5/β5 (R. Li et al. 2003) ICAM-1[1] (Bélizaire et al. 2003)
DGRFDSETS	RQ**GRG**D**S**R**TS** **AL**G**RGDSD**LI VQ**GRG**D**S**HPAI	Integrin α5/β3 (R. Li et al. 2003) Integrin α5/β3 (R. Li et al. 2003) Integrin α5/β3 (Hufton et al. 2000)
DGRSYTGED	**DGRSYS**TKYWFM	Integrin α5/β3 (Kraft et al. 1999)
DIPWYGDES	**IPWY**PY LWS**PWYG**GSW	Con A[7] (Scott et al. 1992) P-glycoprotein, Pgp (Popkov et al. 1998)
DPLAEVTTL	**DP**R**A**TT**TT** **EVTT**EHVEAN C**VTTL**NLTC	Human PC[2] cell line, LNCaP (Romanov et al. 2001) Anti-HER-2 Polyclonal Antibody (Denisova et al. 2009) Human colon cancer cell line, HT29 (Kelly and Jones, 2003)
DPRVESMSG	**DPRI**AT**MS**	Human PC[2] cell line, LNCaP (Romanov et al. 2001)

[2] Intercellular adhesion molecule 1
[3] Prostate Carcinoma
[4] Non-small Cell Lung Cancer
[5] Fibroblast growth factor receptor 2
[6] Vascular cell adhesion protein 1
[7] Concanavalin-A

DPTGTSAP	IYSN**TSAP**HLII	Human PC[2] cell line, LNCaP (Qin et al. 2011)
DSSLSYIDQ	MWVFSRG**DSSL**FCCG	Integrin α5/β3 (Healy et al. 1995)
DYPNEYSSA	AHGESSLLAWLLSG**EYSSA** DDTR**YSSA**	Estrogen receptor (Chang et al. 1999) Rat glioma cell line, RG2 (Samoylova et al. 2003)
EDARTAAMA	**DPRTAAMA** CSL**RTAA**AC	Human PC[2] cell line, LNCaP (Romanov et al. 2001) Human colon cancer cell line, HT29 (Kelly & D. A. Jones 2003)
EFYAESTSL	WPR**YAEST**LQLR	Human nasopharyngeal carcinoma cell line, CEN-1 (SUN et al. 2007)
EGMNYHIDQ	**EGM**H**YH**T	EFGR[8] (Hamzeh-Mivehroud et al. 2012)
EHVYDEGSN	VVF**YD**Y**GS**	Con A[6] (Oldenburg et al. 1992)
EIDPEASTL	CGTRCVRCQNG**PEAS**CEQPL CLS**ASTL**MC	Human breast cancer tumor (Krag et al. 2006) Human colon cancer cell line, HT29 (Kelly & D. A. Jones 2003)
EMSYNADA	IT**MS**S**NAE**HSRI	Human NSCLC[3] cell line, NCI-H1299 (Zang et al. 2009)
EPFEPGLAS	FRS**FE**SC**LA**KSH PVG**EPGL**LWRLLSAPVWRE	Interlukin-10 receptor α, IL-10R (Naiyer et al. 2013) Estrogen Receptor (Chang et al. 1999)
EPRGDSLDL	**EVRGDSL**P	Rat glioma cell line, RG2 (Samoylova et al. 2003)
ETMMPYGT	L**PYGT**SNRHAPV	Human glioma cell line (Ho et al. 2004)
EVNVEEINL	C**VNVE**YR**N**C ISSLL**EEIN**TILMDIIEYL	Integrin α5/β1 (Koivunen et al. 1994) Interlukin-6, IL-6 (Kobayashi et al. 2011)
EYSPYAGDT	**SP**AR**GD**LFRFMGAVH ASGAL**SP**SRL**DT**	Integrin α5/β1 (Healy et al. 1995) Human osteosarcoma cell line, 143B (Sun et al. 2010)
GEYVELVNA	A**EYG**E**SVNA** A**EYG**E**RGNA** A**EYG**E**SGNA** AKYYCE**ELVN**HCTSAQ CRFDK**EY**RT**LV**C	Human PC[2] cell line, PC-3 (Jayanna, Bedi, DeInnocentes, et al. 2010a) Human PC[2] cell line, PC-3 (Newton-Northup et al. 2011) PSA[9] (P. Wu et al. 2000)
GLNGRGDPD	GS**GRGD**A**D**LH	Integrin α5/β3 (R. Li et al. 2003)
GMVMEPGLD	P**VGEPGL**LWRLLSAPVWRE T**PGLD**AAVFWSLGSE	Estrogen Receptor (Chang et al. 1999) Human PC[2] cells, PC-3 (Newton-Northup et al. 2011)
GNATLSSME	TRDLH**TLSS**TRH	Integrin α5/β6 (Kraft et al. 1999)
GSLEESSNL	YPHY**SL**PG**SST**L	Human NSCLC[3] cell line, NCI-H1299 (Zang et al. 2009; Tu et al. 2009)
GSLEEVSTL	IK**A**PNPPS**VSTL**PPR YPHY**SL**PGS**STL** CTC**VSTL**SC	Human PC[2] cell line, PC-3 (Newton-Northup et al. 2011) Human NSCLC[3] cell line, NCI-H1299 (Zang et al. 2009; Tu et al. 2009) Human breast cancer xenograft, MDA-MB-435 (Arap, Pasqualini & Ruoslahti 1998b)
GTPLLSPE	SHWE**TPLLS**WFF **SPLLS**TRAVQLS	VEGFR-1[10] (An et al. 2004) Human NSCLC[3] cell line, CL1-5 (T.-Y. Lee et al. 2007)
GVDSEIVSL	VDV**SE**QM**SL**	Human PC[2] cell line, PC-3 (Jayanna, Bedi, DeInnocentes, et al. 2010a)
GVSYVDMDQ	**VS**RG**DM**PPMW	Integrin α5/β3 (R. Li et al. 2003)
VDGRTGTDS	E**VDGR**WWIVETFLAKWDHMA	IGFBP-1[11] (Lowman et al. 1998)
VDIAEQSTA	**VDVSEQ**MSL MG**IAEQ**LMH RG**DI**PSM**ST**LPR	Human PC[2] cell line, PC-3 (Jayanna, Bedi, DeInnocentes, et al. 2010a) Undifferentiated embryonic carcinoma stem cell line, P19 (Morita et al. 2006)

[8] Epidermal growth factor receptor
[9] Prostate specific antigen
[10] Vascular endothelial growth factor receptor 1
[11] Insulin-like growth factor binding protein 1

	A**QSTA**FQKPLIM CGWVDV**IA**SGD**TA**TLAC	Integrin α5/β6 (Kraft et al. 1999) Human NSCLC[3] cell line, CL1-5 (T.-Y. Lee et al. 2007) P-selectin (Molenaar et al. 2002)
VEEGGYIAA	**GGSIAA**SELEYY	VPAC1 receptor (Tang et al. 2013)
VGDYDVVDS	**VGDYDVVDS**	Human PC[2] cell line, PC-3 (Jayanna, Bedi, DeInnocentes, et al. 2010a)
VTDPSAST	QHTLIIDA**TMPSAS**P	Human PC[2] cell line, PC-3 (Newton-Northup et al. 2011)

CHAPTER 3

COMBINATORIAL SYNTHESIS AND SCREENING OF CANCER CELL-SPECIFIC NANOMEDICINES TARGETED VIA PHAGE FUSION PROTEINS

1. Abstract

Active tumor targeting of nanomedicines has recently shown significant improvements in the therapeutic activity of currently existing drug delivery systems, such as liposomal doxorubicin (Doxil/Caelyx/Lipodox). Previously, we have shown that isolated pVIII major coat proteins of the fd-tet filamentous phage vector, containing cancer cell-specific peptide fusions at their N-terminus, can be used as active targeting ligands in a liposomal doxorubicin delivery system *in vitro* and *in vivo*. Here, we show a novel major coat protein isolation procedure in 2-propanol that allows spontaneous incorporation of the hydrophobic protein core into preformed liposomal doxorubicin with minimal damage or drug loss while still retaining the targeting ligand exposed for cell-specific targeting. Using a panel of 12 structurally unique ligands with specificity towards breast, lung, and/or pancreatic cancer, we showed the feasibility of pVIII major coat proteins to significantly increase the throughput of targeting ligand screening in a common nanomedicine core. Phage protein-modified Lipodox samples showed an average doxorubicin recovery of 82.8% across all samples with 100% of protein incorporation in the correct orientation (N-terminus exposed). Following cytotoxicity screening in a doxorubicin-sensitive breast cancer line (MCF-7), three major groups of ligands were identified. Ligands showing the most improved cytotoxicity included: DMPGTVLP, ANGRPSMT, VNGRAEAP, and ANDVYLD showing a 25-fold improvement ($p < 0.05$) in toxicity. Similarly DGQYLGSQ, ETYNQPYL, and GSSEQLYL ligands with specificity towards a doxorubicin-insensitive pancreatic cancer line (PANC-1) showed significant increases in toxicity (2-fold; $p < 0.05$). Thus, we demonstrated proof-of-concept that pVIII major coat proteins can be screened in significantly higher throughput to identify novel ligands displaying improved therapeutic activity in a desired cancer phenotype.

2. Introduction

Cancer remains the second leading cause of death in the United States across all age groups for both genders and continues to produce a significant burden on the healthcare system for improved patient outcomes with an improved quality of life in cancer survivors (Siegel et al. 2015). Treatment options include surgery, chemotherapy, radiation therapy or a combination of the three and are dependent on the tumor stage at initial

diagnosis and the overall health/age of the patient. For example, breast cancer is commonly treated with surgery and radiation therapy (60%) in early stages (I or II) with the addition of chemotherapy in some cases (39%). However in later stages (III or IV), chemotherapy is used significantly more often (74%) in a patient's treatment strategy (DeSantis et al. 2014). Tumor management with chemotherapy has shown to prevent tumor recurrence and prolong a patient's overall survival, but can also decrease the quality of life due to non-specific side effects associated with the high toxicity profile of many chemotherapy treatments.(Early Breast Cancer Trialists' Collaborative Group (EBCTCG) 2005; Riihimäki et al. 2012)

Pegylated liposomal doxorubicin (Doxil, Caelyx, or Lipodox) was introduced as the first FDA-approved nanomedicine composed of the commonly used anticancer drug doxorubicin encapsulated within the core of liposomes. Liposomal doxorubicin is the first nanomedicine approved for use in the clinic for a variety of cancer types. It showed significant improvements in circulation and bioavailability, and leads to overall reduction of tumor volume while significantly increasing the long-term survival of patients (Gabizon et al. 2003). Nanomedicines provide an increase in therapeutic activity by passively targeting their therapeutic payloads and using the leaky vasculature commonly associated with many tumors, a pathophysiological phenotype known as the enhanced permeability and retention (EPR) effect (J. Fang et al. 2011). It has been suggested extensively from pre-clinical models that active targeting of nanomedicines can provide an additional improvement in the therapeutic activity compared to solely relying on the EPR effect and other passive targeting strategies. Active targeting commonly involves attachment of a homing molecule onto either the therapeutic drug molecule, such as a doxorubicin-conjugate (Florent & Monneret 2008), or onto a drug delivery system, such as doxorubicin-loaded liposomes (Shroff & Kokkoli 2012; Petrenko & Jayanna 2014). The homing molecule would then provide cell-specific accumulation of the therapeutic molecule specifically to the desired cells, thereby reducing major side effects and also reducing dose-limiting toxicities commonly seen with highly active molecules like doxorubicin.

Two broad mechanisms are commonly used to conjugate a targeting ligand into a liposomal drug delivery system: "pre-insertion" modifications and post-insertion modifications. "Pre-insertion" modifications consist of a covalent conjugation of the targeting ligand to one of the subcomponents of the drug delivery system before assembly of the nanoparticle. Attachment of a peptide/protein is commonly achieved by covalent modification of an activated lipid or polyethylene glycol (PEG)-lipid through either an amide conjugation or a disulfide/thioether conjugation (Rongrong Wang et al. 2012b). Following conjugation, the protein-lipid conjugates can then be used as

one of the many assembly blocks used in a self-assembly mechanism to produce larger drug delivery systems, such as observed with liposomes (D.-H. Lee et al. 2014). There are several advantages of attaching a ligand prior to nanoparticle assembly including: 1) highly controlled reaction conditions of ligand to a specific lipid, 2) more commonly available characterization methods available for quality control, and 3) a highly stable conjugation of the ligand to the lipid molecule. However, "pre-insertion" modifications often require a trained chemist to optimize reaction conditions/analyze products, result in moderate yields of the desired final product which then require purification, and can also degrade the functional activity of the targeting molecule depending on reaction conditions. Alternatively, post-insertion methods of nanomedicine modification involve attachment of a targeting ligand after assembly and drug loading. It has been reported that some liposomal nanomedicines are stable enough to perform an amide conjugation to an activated lipid exposed from the nanomedicine surface, however this still requires purification of final product before testing (Kung & Redemann 1986). Another common method of post-insertion modification includes the use of a biotinylated lipid embedded in a lipid bilayer, which will then react almost irreversibly with a streptavidin-peptide conjugate or streptavidin-biotin-peptide conjugate (Loughrey et al. 1987). Another method of post-insertion modification includes the use of pVIII major coat proteins isolated from filamentous bacteriophage, such as M13 or fd, that display a targeting motif fused at the N-terminus of the protein (Petrenko & Jayanna 2014). Post-insertion methods offer several advantages including rapid/simple modification reactions, milder reaction conditions that keep nanomedicines and ligands functionally intact, and stable non-covalent interactions between nanomedicines and the attached ligands. However, post-insertion methods can also cause nanomedicine instability or drug loss during modification that requires the optimization of reaction conditions to prevent undesired effects.

Filamentous bacteriophage of class Ff, including phage vectors such as M13, fd, and f1, are long cylindrical virions (~1 μm × 6.5 nm) structurally composed of a single-stranded DNA genome (<10 kbp) and 5 structural proteins (pIII, pVI, pVII, pVIII, and pIX) (Marvin et al. 2014). Each of the wild-type phage particles consist of 2,700 copies of the pVIII major coat protein, which accounts for ~90% of the mass of each virion. The remaining 10% is derived from the phage's DNA genome and also a minor contribution from the four remaining structural proteins (<1%). Landscape phage display libraries of type f8, introduce a random peptide fusion into each of ~4,000 domains of the pVIII major coat protein of the fd-tet vector to create a unique landscape across the surface of each phage clone (G. P. Smith 1993; Petrenko et al. 1996; Kuzmicheva, Jayanna, Sorokulova, et al. 2009b).

Landscape phage libraries have been used extensively to generate ligands with specificity towards various cancer phenotypes (Bedi et al. 2014; Fagbohun et al. 2012; Jayanna, Bedi, DeInnocentes, et al. 2010a). The pVIII major coat proteins produced from these phage vectors have an 8- or 9-mer peptide fusion at the N-terminus and also contain an intrinsic membrane-spanning domain between residues 21-39 of the wild-type vector. This highly hydrophobic core serves to accumulate the pre-coat protein in the bacterial membrane during phage morphogenesis and also participates in formation of a highly stable phage particle to protect the genome from degradation. Filamentous phage particles and their isolated proteins show superior thermal stability while also maintaining the desired binding capacity compared to antibodies and also retain functional activity after exposure to harsh environments including relatively high temperatures (Brigati & Petrenko 2005), acidic or alkaline solutions, moderate percentages of organic solvents (Olofsson et al. 1998), and protealytic enzyme treatment (Schwind et al. 1992) making filamentous phage and their pVIII major coat proteins ideal candidates for substitute antibodies in the targeted drug development (Petrenko & G. P. Smith 2000; Petrenko 2008). The intrinsic membrane domain of the pVIII major coat protein has provided an ideal platform to develop targeted nanomedicines by isolating the major coat protein and introducing the solubilized proteins into preformed, drug-loaded liposomes through spontaneous interactions of the hydrophobic core with the liposome bilayer (Tao Wang, D'Souza, et al. 2010a; Jayanna, Bedi, Gillespie, et al. 2010b; Petrenko & Jayanna 2014). Several methods for solubilization and isolation of phage major coat protein have been studied including phenol extraction, several classes of detergents and a number of organic solvents. However, two critical factors that significantly effect the functional activity of the isolated protein include: 1) rapid aggregation rates of the protein due to the highly hydrophobic nature of the protein, and 2) an irreversible conformation change in secondary structure from α-helical to a β-sheet (Spruijt et al. 1989; W. Li et al. 2007b). Identification of a solvation procedure that allows high recovery of phage major coat protein in an α-helical conformation that would also limit damage to the membrane of pre-formed liposomes is ideal.

One of the major limitations in ligand screening of targeted nanomedicines is due to highly complex reactions and optimizations required to prepare and purify a single targeted nanomedicine. In this study, we have developed a rapid protein isolation method to solubilize the pVIII major coat protein in high concentration, yield, and purity that also retains the desired functional activity. (Figure 18) We show this isolated protein is then suitable to prepare targeted nanomedicines following a post-insertion modification strategy of preformed, drug-loaded liposomes. We hypothesized that optimization of ligand solubilization and insertion strategies would allow

identification of cancer cell-specific ligands that increase the desired specific cytotoxic effect of liposomal nanomedicines in much higher throughput. We demonstrate the application of this technique for identifying ligands in a single combinatorial experiment combining novel cancer cell-specific ligands with a preformed liposomal doxorubicin core generating 12 nanomedicines targeted with structurally unique ligands and subsequently screening for their anticancer activity *in vitro*. From this screening experiment, we were able to identify 8 novel targeting ligands able to significantly increase the therapeutic response of untargeted liposomal doxorubicin across two different cancer types.

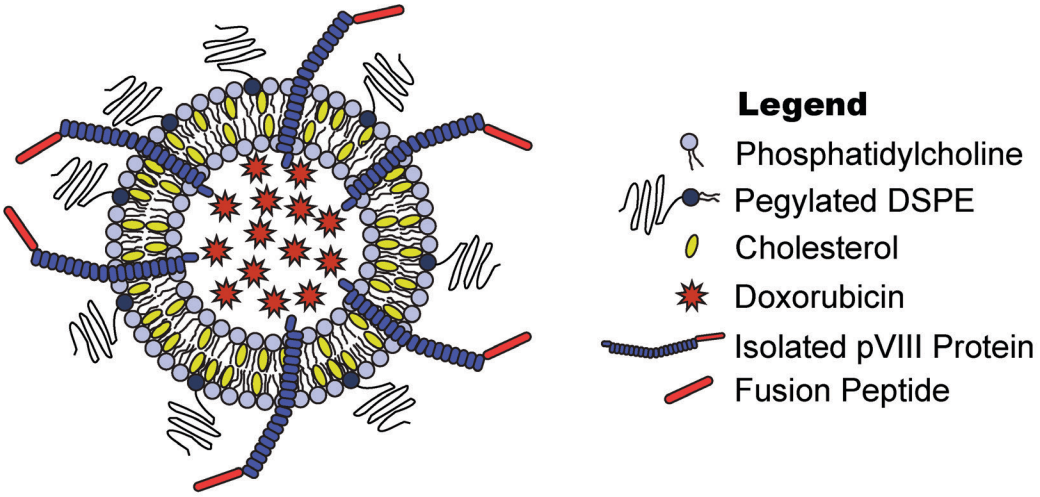

Figure 18: Phage fusion protein-targeted nanoparticles. Target-specific phage fusion protein selected from phage libraries can be introduced into drug-loaded PEGylated liposomes exploiting their intrinsic properties to spontaneously integrate into lipid bilayers.

3. Materials and Methods

3.1. Reagents

Reagent grade or higher calcium chloride, chloroform, hydrochloric acid (HCl), 3-(4,5-dimethylthiazol-2-yl)-2,5-diphenyltetrazolium bromide (MTT), phenylmethylsulfonyl fluoride (PMSF), 2-propanol, proteinase K, and sodium dodecyl sulfate (SDS) were obtained from Sigma Aldrich (St. Louis, MO). Lipodox (PEGylated liposomal doxorubicin, composed of 1,2-distearoyl-sn-glycero-3-phosphocholine, cholesterol, 1,2-distearoyl-sn-glycero-3-phosphoethanolamine-N-[amino(polyethylene glycol)-2000] (ammonium salt) (DSPE- PEG2000) in molar ratio 56 : 39 : 5 containing ~2 mg/mL encapsulated doxorubicin) was obtained from SUN Pharmaceutical Ind. Ltd. (Gujaat, India).

3.2. Cell Culture

An established breast adenocarcinoma cell line, MCF-7 (ATCC, HTB-22™), and an established pancreatic adenocarcinoma cells line, PANC-1 (ATCC, CRL-1469™), were used throughout this study. All cell lines were purchased from the American Type Culture Collection (ATCC, Manassas, VA) as a frozen vial and maintained as described in the technical bulletins in a 37ºC cell culture incubator with 5% CO_2. Cells were maintained in the recommended basal medium supplemented with 10% defined fetal bovine serum (FBS) and 1% v/v 100X antibiotics/antimycotics (Ab/Am). Cells were tested for mycoplasma contamination using a commercial mycoplasma PCR detection kit (ATCC) and confirmed to be free of mycoplasma contamination following all experimental procedures. Eagle's Minimum Essential Medium (EMEM) and Dulbecco's Modified Eagle's Medium (DMEM) were obtained from ATCC. Hyclone defined FBS and Gibco 100X Ab/Am, a cocktail of 10,000 U/mL penicillin, 10,000 µg/mL streptomycin, and 25 µg/mL amphotericin B, were obtained from Thermo Fisher Scientific (Waltham, MA).

3.3. Phage Propagation & Protein Isolation in 2-propanol

All general phage handling, propagation, purification, titering, and DNA sequencing procedures have been described previously (Brigati et al. 2008). Phage clones isolated from landscape phage display libraries f8/8 and f8/9 were designated by the sequences of the foreign fusion peptides. Phage clones DMPGTVLP or VPTDTDYS were isolated from an *in vitro* biopanning of the f8/8 library over MCF-7 breast cancer cells; similarly, the phage clone VEEGGYIAA was isolated from an *in vitro* biopanning of the f8/9 library over MCF-7 breast cancer cells as described previously (Fagbohun et al. 2012). Phage clones ANDVYLD, ANGRPSMT, GLNGRGDPD, or VNGRAEAP were isolated from the f8/8 library through *in vitro* biopanning with Calu-3 non-small cell lung cancer (NSCLC) cells, and phages DGQYLGSQ, DVRGDGLQ, EPSQSWSM, ETYNQPYL, or GSSEQLYL were isolated from the f8/8 library by *in vitro* biopanning with the PANC-1 pancreatic cancer cells, as described previously (Bedi et al. 2014).

Approximately 3×10^{13} phage particles dissolved in 1X TBS were transferred to a sterile 1.7 mL microcentrifuge tube followed by addition of 3 volumes of 100% 2-propanol and 30 µL of chloroform. Phage samples were vortexed vigorously to mix and shear intact phage particles into its primary components. Phage DNA was removed from the mixture by centrifuging at 13,000 × g for 5 minute at room temperature. The upper phase containing phage protein was transferred to a new sterile 1.7 mL microcentrifuge tube and stored at 4ºC. Phage

protein concentration was determined by measuring the UV/Vis absorbance of the solution at 280 nm with a NanoDrop. Absorbance values were converted to protein concentration, in mg/mL, using the appropriate 1 A(280) conversion factor as listed in Table VI.

Table VI: Phage Major Coat Protein (pVIII) Properties. Phage major coat protein (pVIII) properties were calculated following sequence analysis of the full length (55 amino acid) pVIII protein sequence using DNAStar Protean version 10.0.1. Phage are identified by their 8- or 9-mer fusion peptide sequence within the full length protein sequence of NH_2-A**XXXXXXXX[D/X]**PAKAAFDSLQASATEYIGYAWAMVVVIVGATIGIKLFKKFTSK AS-COOH, where X can be any amino acid. Proteins with an 8-mer peptide fusion will contain a D in the 10^{th} position of the pVIII fusion protein, while proteins with a 9-mer peptide fusion will have a random amino acid.

Phage	MW (g/mol)	1 A(280) = X mg/mL
ANDVYLD	5612.49	0.59
ANGRPSMT	5751.67	0.70
DGQYLGSQ	5786.62	0.58
DMPGTVLP	5747.72	0.70
DVRGDGLQ	5777.65	0.70
EPSQSWSM	5869.76	0.42
ETYNQPYL	5946.84	0.52
GLNGRGDPD	5703.57	0.69
GSSEQLYL	5815.70	0.58
VEEGGYIAA	5711.63	0.60
VNGRAEAP	5731.62	0.69
VPTDTDYS	5815.64	0.61

3.4. Characterization of Isolated Phage Protein by SDS-PAGE

Two-fold serial dilutions of isolated phage protein in 1X Laemmli sample buffer were heated at 95ºC for 1 hour. A 10-fold dilution of the Precision Plus Protein WesternC Standards (Bio-Rad, Hercules, CA) was diluted in 1X Laemmli sample buffer and heated at 95ºC for 10 minutes. Prepared samples were separated on a 4-20% Mini-PROTEAN TGX polyacrylamide gel (Bio-Rad, Hercules, CA) at a constant voltage of 100 V for 45 minutes. Following separation, the gel was fixed for 10 minutes in a methanol/acetic acid/water (v/v/v 50:10:40) fixing solution. Protein bands were labeled with a Colloidal Blue Staining Kit (Thermo Fisher Scientific, Waltham, MA) as described in the manufacturer's instructions. Briefly, the fixed gel was incubated in the prepared staining solution (stainer A/stainer B/methanol/water v/v/v/v 20:5:20:55) for 3 hours at room temperature with gentle shaking. The

staining solution was replaced with distilled water and destained for 11 hours at room temperature with gentle shaking. Following destaining, bands were visualized using an EDAS Imaging Station (Eastman Kodak Co., Rochester, NY) equipped with a DC290 digital camera and a white light box. Images were captured and analyzed using Molecular Imaging Software (v. 4.0.3; Eastman Kodak Co., Rochester, NY).

3.5. Insertion of Phage Protein into Liposomal Doxorubicin (Lipodox)

Phage protein-modified Lipodox was prepared at room temperature (20ºC) by rapidly introducing isolated DMPGTVLP major coat protein into a preparation of Lipodox at a protein-to-lipid weight ratio of 1:200 as described previously (Tao Wang et al. 2011b). Samples were mixed vigorously by vortexing and diluted with 1 volume of 1X TBS, pH 7.4 before incubating at 37ºC overnight with gentle rotation.

3.6. Theoretical Calculation of Ligands per Liposome

The number of lipids per liposomes was calculated based on the surface area of a unilamellar liposome with a bilayer thickness, h, of 5 nm; an average diameter, d, of 83 nm; and an average lipid headgroup area, a, of 0.5775 nm^2 for the mixed lipid population according to previous reports (Pidgeon & Hunt 1981) as discussed briefly below:

$$N_{Lipids} = \frac{4\pi}{a}\left[\left(\frac{d}{2}\right)^2 + \left(\frac{d}{2} - h\right)^2\right] \quad (5)$$

The concentration of liposomes was subsequently calculated as follows, where the molar concentration of lipid in Lipodox, M, was 0.0216 M; and N_A is Avagadro's Number:

$$C_{Lipos}\ (Liposomes/mL) = \frac{M \times N_A}{N_{Lipids} \times 1000} \quad (6)$$

The number of ligands per liposome was calculated as follows, where N_{ligand} is the number of phage proteins calculated from the molar mass:

$$N_{Ligands/Liposome} = \frac{N_{Ligands}}{N_{Liposomes}} \quad (7)$$

3.7. Purification of Phage Protein-Modified Lipodox by Size Exclusion Chromatography

Protein modified Lipodox was purified by size exclusion chromatography (SEC) on a column (30 cm × 1 cm) packed with Superose 6 prep grade resin (GE Healthcare, Little Chalfont, UK) as described previously (Jayanna et al. 2009). Liposomes were eluted with 10 mM Tris-HCl, pH 8.0 containing 0.2 mM EDTA at a flow rate of 0.25 mL/min. The elution profile was monitored by an Econo UV monitor (Bio-Rad, Hercules, CA) at an AUFS of 0.5 with fractions collected every 10 minutes (2.5 mL fractions). Fractions were stored at 4ºC until further analysis.

3.8. Quantification of Doxorubicin

Encapsulated doxorubicin was quantified by monitoring the absorbance at 492 nm following incubation with Triton X-100 (1% v/v final concentration) and comparing to a standard curve with known doxorubicin concentrations as described previously (Jayanna, Bedi, Gillespie, et al. 2010b).

3.9. Size Distribution and Zeta Potential of Liposomes

Liposome size distribution was determined using dynamic light scattering. Briefly, samples were diluted 100-fold with 1X PBS, pH 7.4 in a plastic sizing cuvette and analyzed on a ZetaSizer Nano ZS90 (Malvern Instruments Inc., Worcestershire, UK) maintained at 25ºC with a scattering angle of 90º in triplicate. All liposome samples were found to be unimodal distributions, however samples were reanalyzed if multiple populations were identified. Size distributions are presented as the mean of triplicate Z-averages (nm) ± sample standard deviation.

Liposome zeta potential was determined by particle electrophoretic mobility as measured using laser Doppler electrophoresis and phase analysis light scattering. Briefly, samples were diluted 100-fold in 10 mM Tris-HCl, pH 8.0 with 0.2 mM EDTA in a plastic sizing cuvette and analyzed on a ZetaSizer Nano ZS90 with a Zeta Dip cell (Malvern Instruments Inc., Worcestershire, UK). Samples were maintained at 25ºC during measurement and performed in triplicate. All recorded samples were equal in conductivity (± 0.01 of mean). Zeta potentials are presented as the mean of triplicate zeta potentials (mV) ± sample standard deviation.

3.10. SDS-PAGE and Western Blot of Modified Liposomes

Aliquots of each fraction following SEC were diluted with an equal volume of 2X Laemmli sample buffer and heated at 95ºC for 1 hour. Prepared samples were analyzed using a 4-20% Mini-PROTEAN TGX polyacrylamide gel at a constant voltage of 100 V for 45 minutes. Proteins separated by the SDS-PAGE were then transferred to a polyvinylidene fluoride (PVDF) membrane and blocked overnight with 1X protein-free PBS/0.05% Tween 20 blocking buffer. Membranes were probed with a rabbit polyclonal anti-fd IgG (1:5,500 dilution, ~9 μg IgG) described previously (G. P. Smith et al. 1998), incubated with a biotin-SP-conjugated Affinipure goat anti-rabbit secondary IgG (1:30,000 dilution, ~1.3 μg IgG; Jackson ImmunoResearch Laboratories, Inc., West Grove, PA Cat # 111-065-003 RRID: AB_2337959) and with NeutraAvadin-Horseradish Peroxidase (HRP) (1:30,000 dilution) and visualized with West Pico substrate solution (Pierce, Rockford, IL). Membranes were imaged on a C-DiGit blot scanner (LI-COR, Inc., Lincoln, NE) and analyzed by densitometry with Image Studio Lite (v. 4.0; LI-COR, Inc.).

To ensure the N-terminus was exposed to the exterior environment of the liposome following phage protein modification, a proteinase K digestion assay was performed on modified Lipodox as described previously (Jayanna, Bedi, Gillespie, et al. 2010b). Briefly, an aliquot of protein-modified liposomes were treated with 1.25 µg of proteinase K containing 0.25 mM $CaCl_2$ for 1 hour at room temperature. The reaction was inhibited by the addition of PMSF to a final concentration 5 mM followed by incubation at room temperature for 5 minutes. Samples were analyzed by SDS-PAGE and Western blot as described above.

3.11. Phage Protein Orientation Assay of Modified Liposomes by Dot Blot Analysis

Samples were prepared as described above, except proteinase K reactions were performed overnight with gentle rotation at 37ºC. Samples were then diluted 2-fold with distilled water and 1.0 µL of each sample were dotted onto a 0.2 µm nitrocellulose membrane (Bio-Rad Laboratories, Hercules, CA). Dots were allowed to dry overnight at room temperature. The resulting dots were probed with rabbit anti-Fd IgGs with specificity towards either the pVIII N-terminus (1:5000 dilution, ~9.24 µg rabbit anti-Fd IgG) or C-terminus (1:100 dilution, ~126 µg rabbit anti-Fd C-terminus IgG affinity purified). Membranes were then treated as above with a biotinylated-SP-conjugated goat anti-rabbit secondary IgG, NeutraAvadin-HRP and West Pico substrate before imaging with a C-DiGit blot scanner and quantified using Image Studio Lite.

3.12. Concentration of Modified Liposomes

Liposomes were concentrated by Amicon 100k Molecular Weight Cut Off (MWCO) centrifugal concentration devices (EMD Millipore, Billerica, MA) as follows. Briefly, a 100k MWCO concentrator was washed with 2 mL of 10 mM Tris-HCl, pH 8.0/0.2 mM EDTA running buffer. Samples were applied and centrifuged at 5,000 × g in 15 minute increments at 4ºC until all samples were concentrated to a final volume of 0.5 mL. Doxorubicin liposomes found in the retentate were recovered and analyzed as above.

3.13. Characterization of Liposome Modification by Flow Cytometry

Phage displaying the fusion peptide DMPGTVLP was propagated as above, however phage was dissolved in 1X PBS, pH 7.2 at the final recovery step. Phage proteins were labeled with an Alexa 488 Protein Labeling kit (Invitrogen, Waltham, MA) as described previously (Fagbohun et al. 2012) and according to the manufacturer's instructions. Briefly, phage were added to a vial of reactive dye at room temperature and mixed for 1 hour at room temperature. Unreacted dye was inactivated by addition of 1X TBS, 7.4 and removed by an overnight PEG precipitation of phage and solubilization in 1X TBS, pH 7.4. Phage protein was isolated in 2-propanol as described

above and the degree of protein labeling was determined according to the manufacturer's instructions. Lipodox was modified with labeled protein as described above. Liposomes were analyzed on an Accuri C6 flow cytometer (BD Biosciences, Franklin Lakes, NJ) with an excitation wavelength of 488 nm and emission collected on three different channels (533/30, 585/40 and 670LP). The collection threshold was set to collect events greater than 10,000 on the forward scatter height (FSC-H) channel. After collection, a threshold to collect events greater than 1,000 RFU on the 670LP height (FL3-H) channel was applied to reduce the background noise. A minimum of 100,000 events was collected per sample for analysis. Channels were compensated for channel spillover using single labeled controls. Labeled phage protein was monitored with the 533 nm emission filter channel and Lipodox was monitored on both 585 and 670 nm emission filter channels. Flow cytometry data were captured and analyzed using the Accuri C6 Software (ver. 1.0.264.21; BD Biosciences). All flow cytometry data files were annotated and deposited into the publically available flow cytometry data repository FlowRepository (Repository ID: FR-FCM-ZZJY) (Spidlen et al. 2012).

3.14. Cell Viability of Cancer Cells Treated with Phage Protein-Modified Liposomes

Cell viability was determined by MTT assay as described previously (Bedi et al. 2014). Briefly, MCF-7 breast cancer cells were seeded at an initial density of 5×10^5 cells per well in a 96-well cell culture-treated array plate and incubated at 37ºC for 24 hours. Lipodox samples (modified and unmodified) were diluted in EMEM containing 10% FBS and added to the cells for 24 hours. Following treatment, the medium was replaced with phenol red-free MEM containing 0.45 mg/mL MTT and incubated for 4 hours at 37ºC. After 4 hours, 100 µL of 10% SDS in 0.01 N HCl was added to each of the wells and incubated at 37ºC for an additional 4 hours. The absorbance of the wells was measured at 570 nm using a Synergy H1 plate reader (BioTek, Winooski, VT). Blank wells containing only culture medium and MTT were subtracted from each sample. The percent viability was expressed as a ratio between the absorbance of treated cells by the average absorbance for a set of untreated cells.

3.15. Quantification of Cell-Associated Doxorubicin

Cell-associated doxorubicin was quantified as previously described (Bedi et al. 2014) with minor modifications. Briefly, cells were plated at 5,000 cells per well in a 96-well culture plate and incubated overnight in a 5% CO_2 cell culture incubator at 37ºC. Cells were then treated with 2 µg of doxorubicin of either 1) unmodified Lipodox or 2) DMPGTVLP-Lipodox for 4 different time periods (4, 8, 12, and 24 hours). Cells were washed twice with 1X PBS, pH 7.2 before extracting cell-associated doxorubicin with 0.075 N HCl in 90% 2-propanol and

incubating at 4ºC overnight. Doxorubicin was determined by measuring the fluorescence (470 ex/590 em) with a Synergy H1 plate reader (BioTek, Winooski, VT) using untreated cells as a blank.

3.16. Screening of Phage Protein-Modified Liposomes

3.16.1. Insertion of Isolated Phage Protein in Lipodox

Phage protein was isolated in 2-propanol as described above. Isolated phage protein (2 µL) was added to 45 µL aliquots of Lipodox (90 µg doxorubicin) and mixed vigorously before addition of 1 volume of 1X TBS, pH 7.4 to the sample. Samples were incubated at 37ºC overnight with gentle rotation. Buffer was exchanged to dilute any residual 2-propanol by washing the liposomes in a 100K NanoSep centrifugal filter device (Pall Co., Port Washington, NY) with 5 volumes of 1X PBS, pH 7.2 for 5 minutes. Samples were centrifuged at 14,000 × g for 10 minutes and the flow through was removed. Liposomes were recovered from the retentate and analyzed as above.

3.16.2. Cytotoxicity of Modified Liposomes

Cells were seeded at 5,000 cells/well in a 96-well cell culture treated assay plate and incubated in a 37ºC cell culture incubator with 5% CO_2 overnight. Dilutions of phage protein-modified Lipodox were prepared in complete culture medium containing 10% FBS and added to the appropriate wells and incubated for 24 hours at 37ºC. Medium containing Lipodox was removed from the cells and replaced with an equal volume of fresh culture medium containing 10% FBS and incubated at 37ºC for an additional 48 hours. Cell viability was measured as above using an MTT viability assay and calculations performed as above.

3.17. Statistics

Data from all experiments are expressed as the mean ± sample standard deviation (SD). Differences between samples were determined using the Student's independent *t*-test or and alternative appropriately identified test listed in the text with a $P < 0.05$ as being statistically significant.

4. Results

4.1. Isolation of pVIII Major Coat Protein in 2-propanol

To prepare solubilized phage major coat protein in 2-propanol, we added 3 volumes of 2-propanol to ~2.3×10^{13} virions of intact DMPGTVLP phage particles, which displays the full length, 55 amino acid pVIII major coat protein sequence of NH_2-A**DMPGTVLP**DPAKAAFDSLQASATEYIGYAWAMVVVIVGATIGIKLFKKFTSKAS-COOH (designated shortly by the sequence of peptide fusion at the N-terminus; DMPGTVLP) and a small volume of chloroform to

perturb the hydrophobic interactions between neighboring pVIII monomers (Manning et al. 1981). After exposing intact phage to increased shear force by vortexing, phage ssDNA was released from the phage particles and precipitated in 75% 2-propanol. UV/Vis spectroscopy of the phage protein supernatant (Figure 19) revealed a spectrum commonly observed for a pure protein sample with a corresponding 260/280 ratio of 0.559, which is close to the theoretical 260/280 ratio of 0.5 expected for pure pVIII major coat protein. Conversion of A280 into a corresponding mass revealed a quantitative recovery of the protein mass (~1 mg).

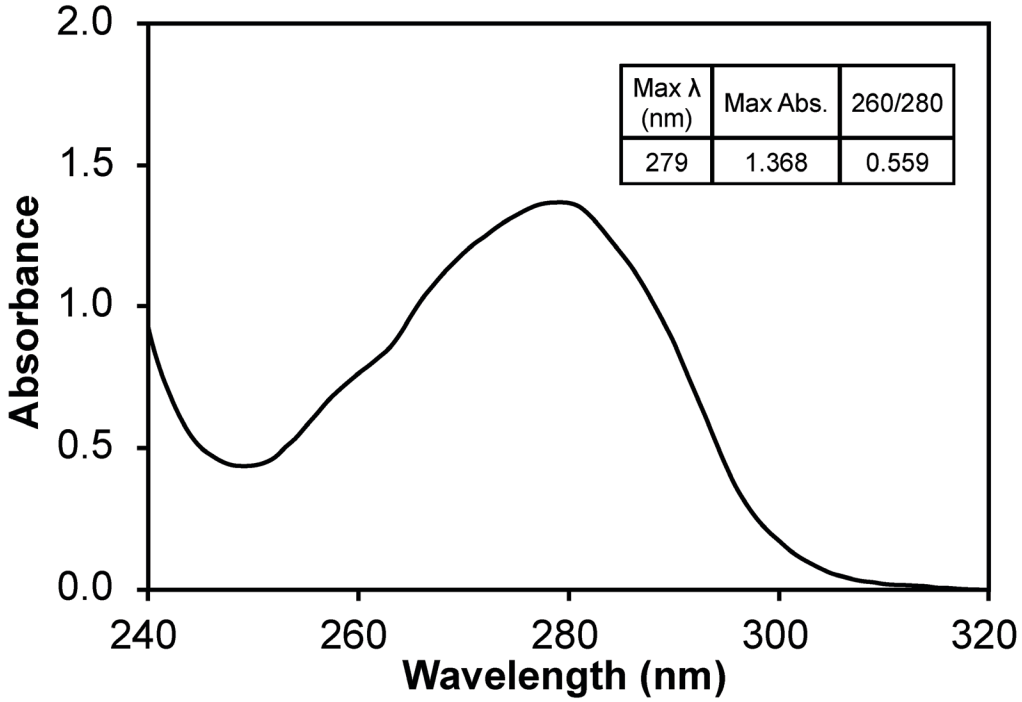

Figure 19: UV/Vis spectrum (1 nm scan) of pVIII major coat protein solubilized in 75% v/v 2-propanol/1X TBS, pH 7.4 blanked with solution of 75% v/v 2-propanol/1X TBS, pH 7.4.

To test the purity of isolated phage major coat protein, serially diluted samples of phage protein were separated on a 4-20% polyacrylamide gel and stained with a colloidal Coomassie blue staining solution. The stained protein gel (Figure 20) reveals a single, low molecular weight protein band at an apparent molecular weight of ~7.5 kDa, which corresponds to the monomeric-form of phage major coat protein (calculated molecular weight of 5.75 kDa, DNAStar Protean v. 10.0.1). Major coat protein, pVIII, was detectible down to ~200 ng of protein under these conditions with colloidal blue staining. It is interesting to note that minor coat proteins pII, pVI, pVII and pIX, which account for ~1.4% of the total protein mass, were not identified under these conditions and may indicate that

2-propanol extraction allows not only separation of DNA from coat protein, but also prepare pure major coat protein pVIII.

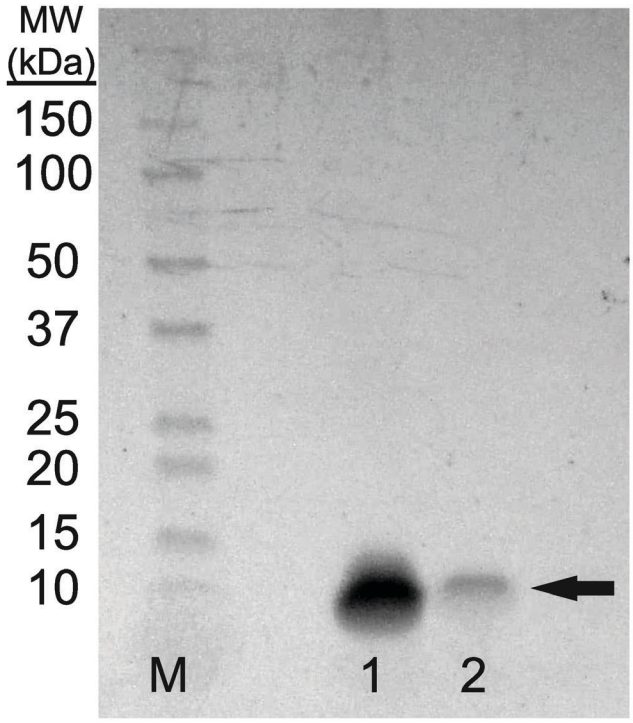

Figure 20: SDS-PAGE of pVIII major coat protein solubilized in 75% 2-propanol/1X TBS, pH 7.4 separated on a 4-20% polyacrylamide gel. Bands were identified by staining with a colloidal blue staining kit (Invitrogen) to reveal a single, low molecular weight band of approximately 7.5 kDa (as noted by the arrow) in samples 1 and 2. M (Marker) – 1:10 dilution of Precision Plus Protein WesternC Standards (Bio-Rad), Sample 1 – 1.36 µg DMPGTVLP phage protein, Sample 2 – 0.27 µg DMPGTVLP phage protein.

4.2. Preparation and Physicochemical Characterization of Phage Protein-Modified Lipodox

To prepare targeted Lipodox (pegylated liposomal doxorubicin, 2 mg/mL doxorubicin) preparations, 23.6 µg of isolated DMPGTVLP phage major coat protein was rapidly added to liposomes, composed of 4.73 mg of lipid and 0.9 mg of doxorubicin, in small aliquots to prevent dissolution of the liposomes. The residual 2-propanol and chloroform were diluted to a final concentration of 2.0% and 0.076% respectively, was shown previously to not cause an increased dissolution of liposomes (data not shown). Following incubation at 37ºC overnight, samples were eluted through a size exclusion chromatography column packed with Superose 6 and the elution profile was

monitored by relative absorbance with a UV/Vis monitor. The elution profile for DMPGTVLP-modified Lipodox (Figure 21) showed a single broad peak with 2 minor peaks at either side of the main peak (fractions 4 & 9). The broad peaks observed were also present in unmodified liposomes and is hypothesized to be due to the heterogeneous composition of the liposomes, however both minor peaks were excluded from further analysis.

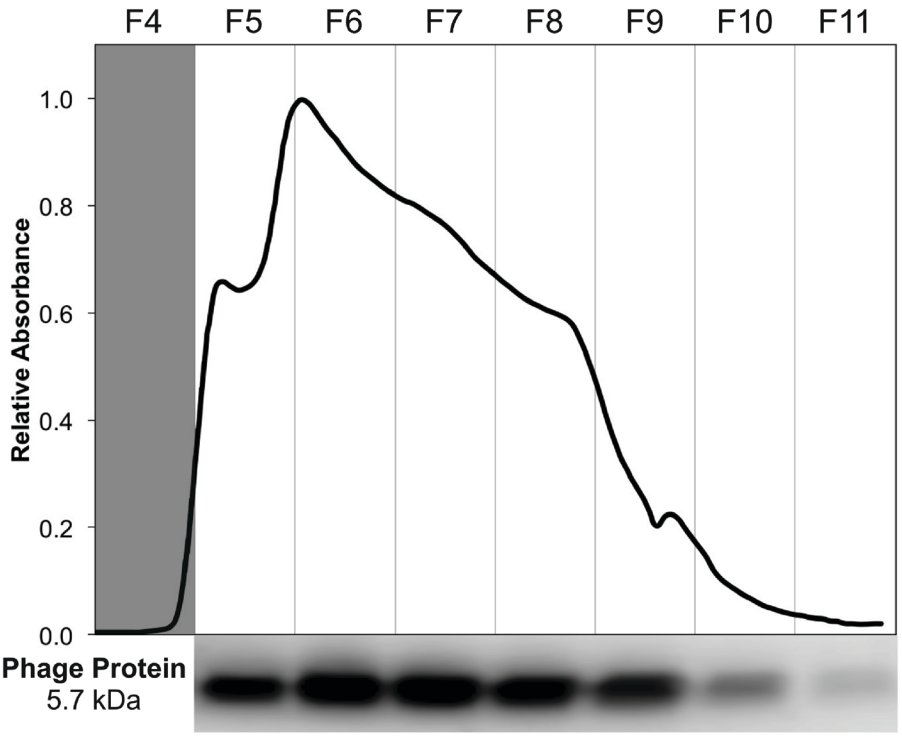

Size (d.nm)	81.2	78.6	79.2	86.0	88.5	NM	NM
Zeta Potential (mV)	-23.7	-25.9	-26.2	-45.2	-50.9	NM	NM
Doxorubicin (µg)	161	435	665	862	ND	ND	ND
Yield (%)	17.9	30.4	25.6	21.9	ND	ND	ND

Figure 21: Purification and characterization of DMPGTVLP-modified Lipodox. Size exclusion chromatography of modified Lipodox on a Superose 6 column, fractions 4-11 of the elution profile are shown. Western blot of recovered fractions probed with a polyclonal anti-fd rabbit primary IgG, followed by a biotinylated goat anti-rabbit secondary IgG and detected with NeutrAvadin-HRP and Pico West luminol substrate. Physicochemical characterization of recovered fractions for size distribution (d.nm), zeta potential (mV), doxorubicin recovery (µg) and percent doxorubicin recovery (%).

To ensure phage protein was associated with the liposomes, a Western blot of each fraction (fractions 5-11) was performed with an anti-fd phage IgG that demonstrates specificity towards the N-terminus of the major coat protein. The blot revealed a single ~5.7 kDa molecular weight band with most of the phage protein associated with

the liposomes found in fractions 6 and 7, however phage protein was also recovered in fractions 5-10 (Figure 21). Phage protein was not observed as free protein in the absence of liposomes. Fractions 5 through 8 were further characterized for recovery of doxorubicin and physical properties (size distribution and zeta potential) of the recovered liposomes. As shown in the summary table (Figure 21), 862 μg of doxorubicin (95.79% yield, 900 μg doxorubicin input) was recovered in the 4 fractions, which was significantly higher than previous post-insertion methods using cholate, which commonly resulted in 50-80% doxorubicin recovery. The size distribution of the resulting fractions showed a mean diameter of 81.25 ± 3.36 nm with an average PDI of 0.127 ± 0.029, which corresponds to a monodisperse population of liposomes with a low tendency for particle aggregation. The zeta potential of the fractions showed a mean zeta potential of -30.25 ± 10.0 mV with a mean conductivity of 0.020 ± 0.005 mS/cm, which suggests a generally negative surface charge of the liposomes in a solution of constant ionic strength and composition.

Since fractions 5 through 8 displayed similar composition and physical properties, they were concentrated with 100K MWCO centrifugal concentration devices and analyzed again for final characterization properties. After concentration, 589 μg of doxorubicin (68.4% recovery, 862 μg doxorubicin input) was recovered; suggesting a large portion of doxorubicin was lost during concentration most likely due to doxorubicin sticking or passing through the membrane. Following concentration, DMPGTVLP-modified liposomes showed a mean diameter of 80.27 ± 1.30 with an average PDI of 0.104 ± 0.015, which shows no statistically significant change in size or aggregation due to concentration effects (two-tailed t-test, $P = 0.605$ and $P = 0.196$ respectively). DMPGTVLP-modified liposomes showed a significant 11.3% increase in size compared to unmodified Lipodox (72.07 nm; two-tailed t-test, $P = 8.06\times10^{-3}$), however this increase is negligible in the biological systems to be tested and is hypothesized to be due to swelling associated with major coat protein incorporation. After concentration, DMPGTVLP-modified liposomes showed a mean zeta potential of -19.87 ± 0.50, which again shows no statistically significant difference in zeta potential due to concentration effects (two-tailed t-test, $P = 0.08$). Modified liposomes showed a significant 11.4% decrease in zeta potential compared to unmodified Lipodox (-17.83 mV; two-tailed t-test, $P = 4.2\times10^{-2}$). We hypothesize that observed decrease might be due to the introduction of the fusion pVIII major coat protein, which contains a negatively charged N-terminus that is exposed to the environment following liposome modification and can influence the observed charge at the liposome surface.

We next sought to determine if the N-terminus of the fusion protein, which contains the cancer cell-specific targeting domain, was exposed outside of the liposomal environment following concentration as previously shown (Jayanna, Bedi, Gillespie, et al. 2010b). As illustrated in Figure 22, treatment of modified liposomes with proteinase K causes protein not protected by the liposome membrane to be hydrolyzed. To show that the N-terminus is exposed, a portion of modified liposomes was treated with proteinase K followed by SDS-PAGE and detection of the N-terminus of major coat protein with an anti-fd antibody. The resulting blot and densitometry of bands shows that isolated major coat protein can be detected as a single 5.7 kDa molecular weight band at the same protein mass used in a matched liposome modification (~500 ng of protein analyzed) and subsequently degraded to completion when treated with proteinase K under these conditions as expected (Figure 23, lanes 1 and 2 respectively). After insertion into Lipodox, phage protein is detected in untreated samples and is absent following treatment with proteinase K (Figure 23, lanes 3 and 4 respectively), suggesting that the N-terminus is exposed following modification and liposome concentration as expected.

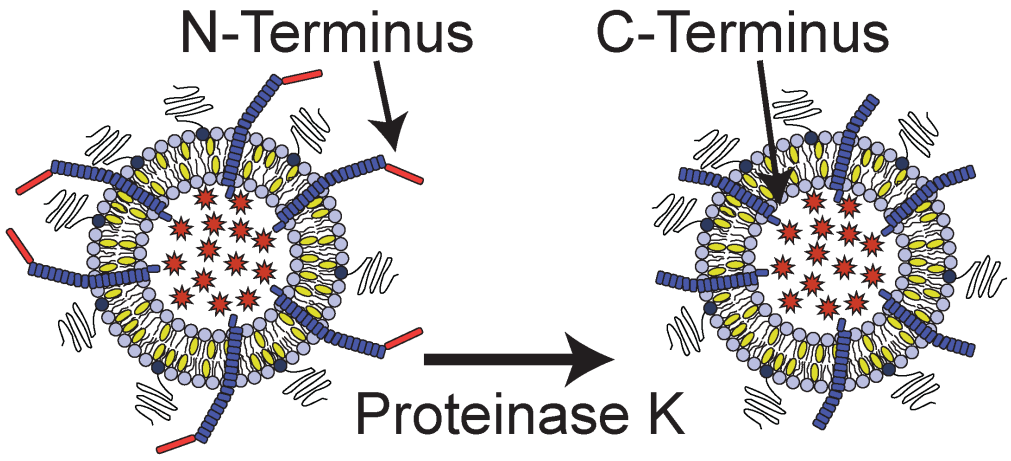

Figure 22: Schematic of phage protein orientation assay, where it is expected that the N-terminus of the protein is exposed to proteinase K degradation while the C-terminus of the protein is protected from degradation by the lipid bilayer.

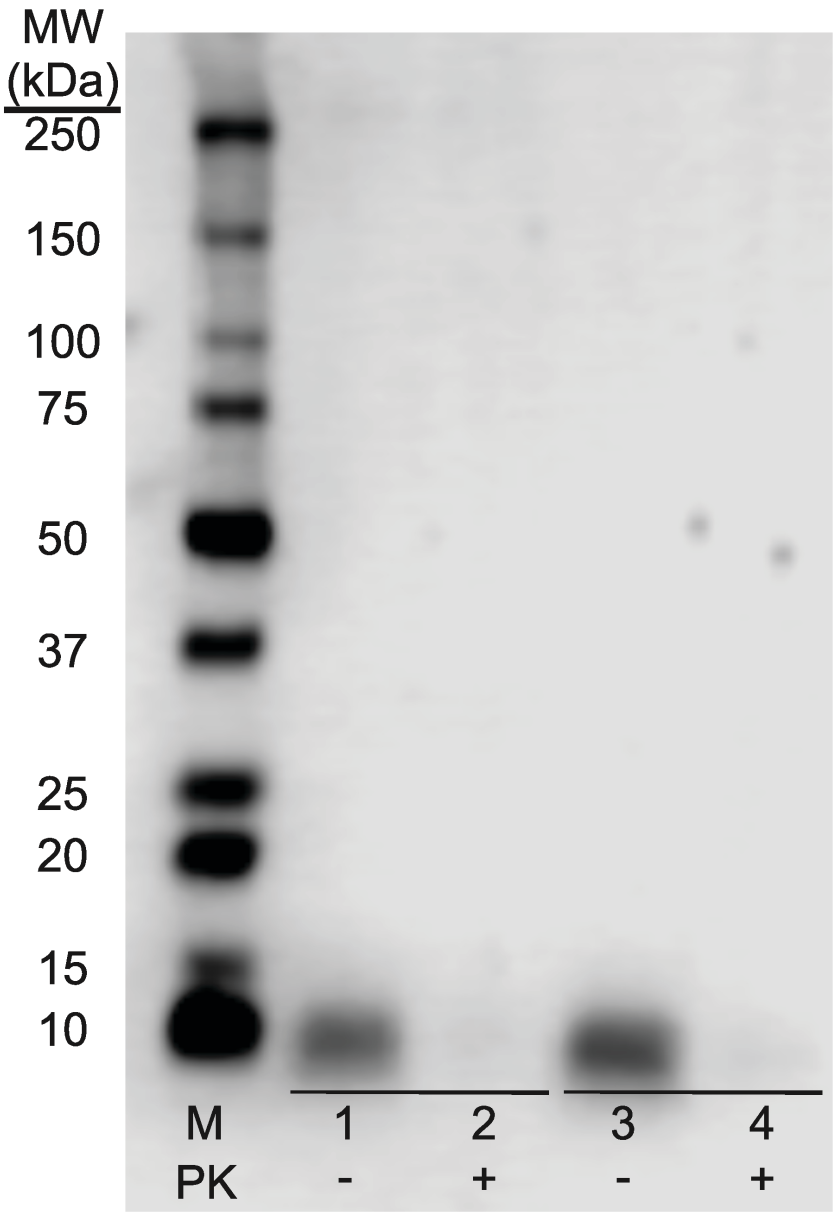

Figure 23: N-terminal orientation assay in DMPGTVLP-modified Lipodox. SDS-PAGE of concentrated DMPGTVLP-modified Lipodox followed by assay by Western Blot. M (Marker) – 1:10 dilution of Precision Plus WesternC Standards, Samples 1 & 2 – 500 ng DMPGTVLP isolated protein, Samples 3 & 4 – DMPGTVLP-modified Lipodox (~500 ng DMPGTVLP protein). Samples 1 & 3 – untreated controls, Samples 2 & 4 – Proteinase K (PK) treated samples.

As previously suggested, we hypothesized that the C-terminus of the phage major coat protein would be embedded in the hydrophobic membrane and protected from degradation by proteases. We therefore sought to

determine the orientation of the C-terminus by a semi-quantiative dot blot assay. It was shown previously that degradation of the N-terminus produces a highly hydrophobic protein fragment that results in irreversible aggregation of monomers, causing visible smearing of bands in Western blots probed with a C-terminus specific antibody. To overcome this limitation and produce semi-quantitative estimates of the amount of each terminus following degradation, we optimized a dot blot assay and probed the resulting membranes with anti-fd IgGs with specificity to either the N- or C-terminus of the major coat protein (Figure 24). Treatment of a 1X phage protein sample (~375 ng) with proteinase K resulted in complete degradation of the protein and was undetectable with both N-terminal (two-tailed t-test, $P = 1.09\times10^{-3}$) and C-terminal (two-tailed t-test, $P = 1.77\times10^{-2}$) antibodies. To ensure reaction conditions were optimal for excess phage protein, a 2X phage protein sample (~750 ng) was digested under the same reaction conditions to again reveal complete degradation of the both N-terminus (two-tailed t-test, $P = 3.18\times10^{-3}$) and C-terminus (two-tailed t-test, $P = 5.35\times10^{-6}$) of the phage protein. Modified Lipodox (containing 375 ng phage protein) was digested with proteinase K using the same reaction conditions and probed with N-terminal and C-terminal specific antibodies. Probing the proteinase K treated Lipodox sample with the N-terminal antibody revealed complete degradation (two-tailed t-test, $P = 5.58\times10^{-5}$), confirming previously observed results obtained by Western blot (Figure 23). Similarly, probing the same proteinase K treated Lipodox sample with a C-terminal specific antibody revealed no degradation of protein (two-tailed t-test, $P = 0.169$).

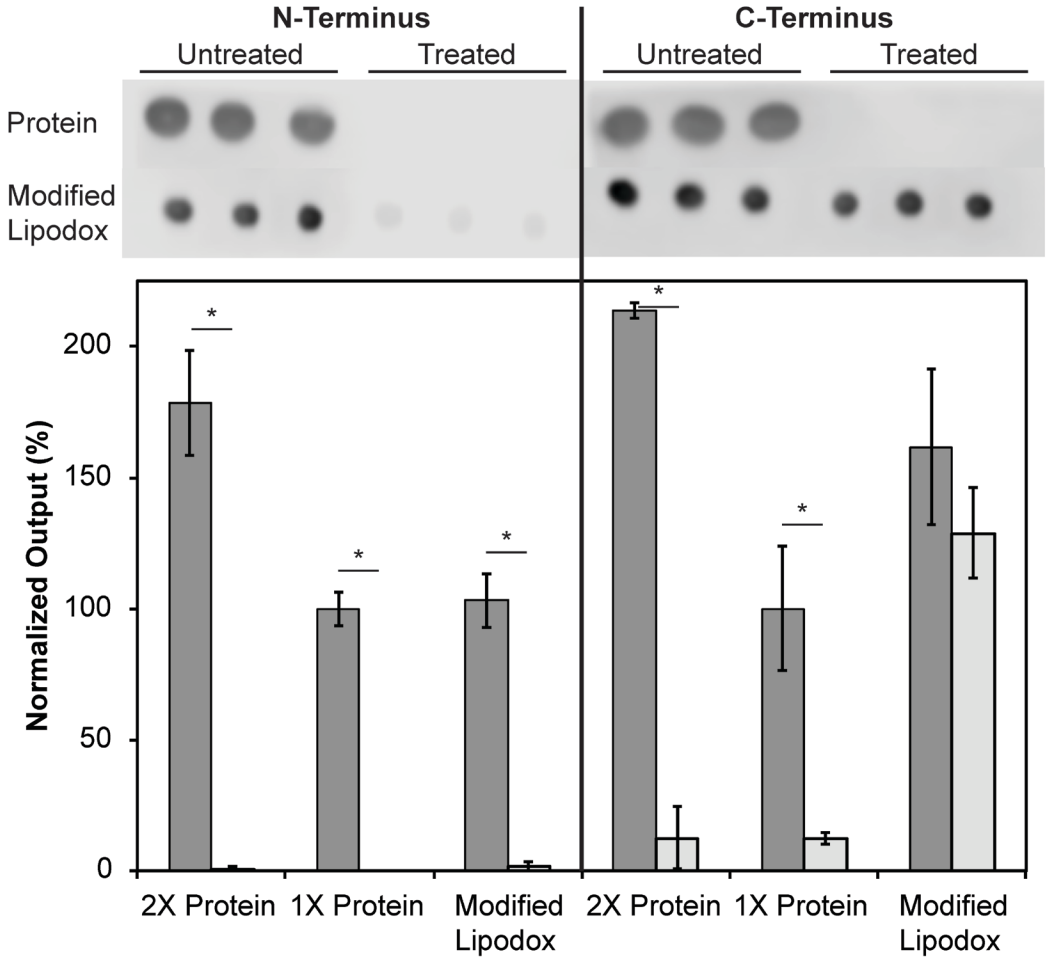

Figure 24: Phage protein orientation assay by dot blot analysis with data quantified by densitometry and presented as the mean ± standard deviation of output signal normalized to 1X untreated protein (~375 ng protein). Untreated samples (dark bars) are compared to proteinase K treated samples (light bars) N = 3; $*P < 0.05$, paired, two-tailed Student's t-test vs. proteinase K treated sample.

4.3. Analysis of Alexa-488-Labeled Phage Protein-Modified Liposomes by Flow Cytometry

We further sought to determine an approximate degree of liposome modification by monitoring individual liposomes with flow cytometry. To estimate the modification efficiency of modified liposome, we fluorescently labeled intact phage particles with Alexa Fluor-488 and isolated the labeled protein as above. We have shown previously that intact phage can be modified with an amine-reactive Alexa Fluor-488 *N*-hydroxysuccinimide (NHS)-ester that reacts with the N-terminal amine and the exposed ε-amine of Lys-13 on pVIII major coat protein

(Fagbohun et al. 2012). The resulting degree of fluorescence labeling was calculated to be ~10% of the total phage protein mass, which is routinely achieved for phage after amine modification. Following isolation of pVIII protein, 25 μL of Lipodox (50 μg of doxorubicin) was modified with 14.4 μg of protein in which 10% of protein (1.4 μg) was labeled with Alexa Fluor-488.

We hypothesized that these particles could then be quantified by flow cytometry with individual particles containing doxorubicin being identified by a relative fluorescence threshold of 1,000 RFU set on the 670LP emission filter to reduce background noise. Unmodified Lipodox liposomes were analyzed across two channels (Em 585/40 and 670LP filters) to accurately identify liposomes from random background events. The Lipodox positive gates were identified on each channel from the samples displaying a linear correlation across both channels, identifying 95.6% of the sample population. Due to the broad emission spectrum of doxorubicin, the fluorescently labeled protein positive gate was identified at the maximum emission fluorescence of unmodified Lipodox using a 533/30-emission filter. The resulting gate also identified free-protein aggregates displaying high particle fluorescence. Analysis of unmodified Lipodox shows that 96.5% of the total population is found in the doxorubicin positive/protein negative quadrant (lower-right) with a minimal percentage in the doxorubicin/protein positive quadrant (upper-right) (Figure 25A). After liposome modification, there was a significant increase to 6.5% of the total population found in the doxorubicin/protein positive quadrant (upper-right) and a significant increase to 4.5% of the total population found in the doxorubicin negative/protein positive quadrant (upper-left) (Figure 25B). Since free protein was found to have high channel fluorescence, we suggest that the observed increase in the doxorubicin negative/protein positive quadrant (upper-left) is due to minor loss of encapsulated doxorubicin in modified liposomes below our doxorubicin positive gate. We therefore show a total detectible protein positive population of 11%.

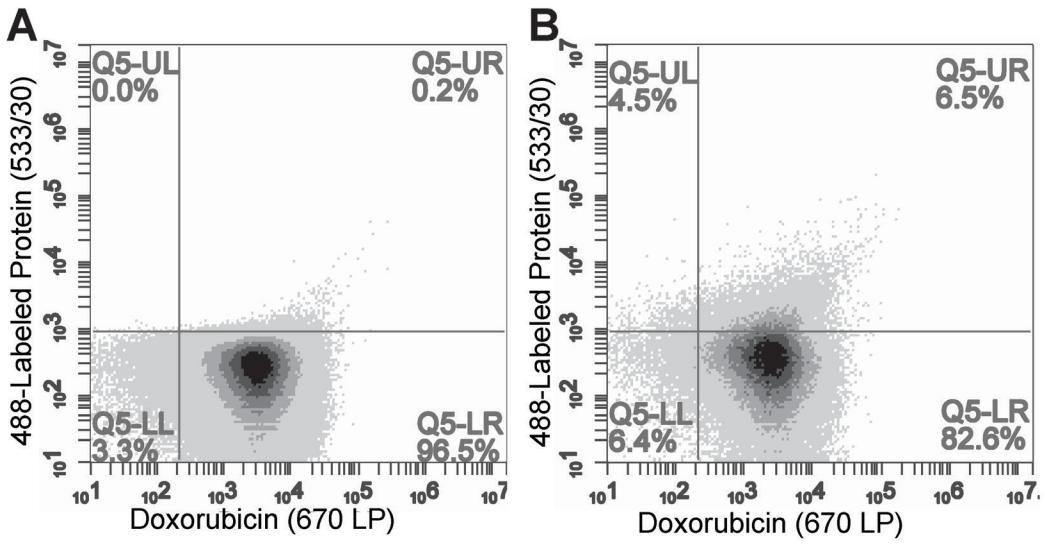

Figure 25: Flow cytometry analysis of (A) unmodified Lipodox and (B) 488-labeled-DMPGTVLP-modified Lipodox. Doxorubicin quantified on 670LP emission channel and 488-labeled phage protein quantified on 533/30 emission channel. Samples were excited using a 488 nm laser.

4.4. Cytotoxicity and Uptake of DMPGTVLP-modified Lipodox in Breast Cancer Cells

It was shown previously that DMPGTVLP-modified Lipodox, with modification by cholate solubilized phage protein, would significantly increase the toxicity in MCF-7 breast cancer cells *in vitro* and also *in vivo* (Tao Wang, D'Souza, et al. 2010a; Tao Wang, S. Yang, et al. 2010c; Tao Wang et al. 2014). We therefore sought to determine if liposome modification by phage protein solubilized in 2-propanol would produce similar results. MCF-7 cells were incubated with DMPGTVLP-modified Lipodox or unmodified Lipodox dilutions for 24 hours before quantification of viable cells by MTT assay. DMPGTVLP-modified Lipodox produced a significant decrease in the number of viable cells compared to unmodified Lipodox samples under the same conditions in a dose dependent manner at higher doxorubicin concentrations of 30 μg/mL (62.7 ± 2.5% vs. 80.6 ± 3.7% viable; two tailed t-test, $P = 8.11\times10^{-4}$) and 60 μg/mL (32.3 ± 1.3% vs. 50.8 ± 2.5% viable; two tailed t-test, $P = 4.97\times10^{-3}$) as expected (Figure 26).

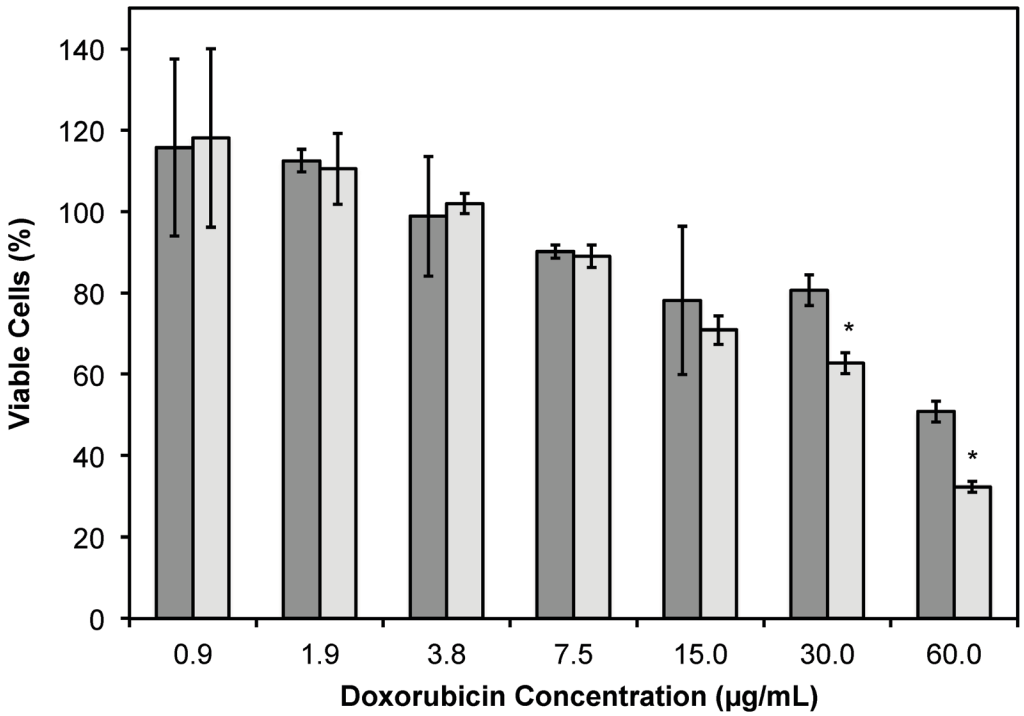

Figure 26: MTT viability assay of MCF-7 cells treated with dilutions of Lipodox (dark bars) or DMPGTVLP-modified Lipodox (light bars) after 24 hours of incubation. Data are presented as the mean ± sample standard deviation of the percent viable fraction compared to untreated control cells, which were taken as 100% viable. N = 3; *$P < 0.05$, paired, two-tailed Student's t-test vs. unmodified Lipodox.

As shown previously, the increased cytotoxicity observed with DMPGTVLP-modified Lipodox is due to an increased uptake of targeted Lipodox in target cells compared to untargeted Lipodox. We therefore hypothesized that there would be a significant increase in intracellular doxorubicin over time in DMPGTVLP-modified Lipodox compared to unmodified Lipodox. We show over a 24-hour time period, there is a significant increase in cell-associated doxorubicin in DMPGTVLP-modified Lipodox compared to the unmodified control Lipodox (Figure 27). After 12 hours of incubation, there is a significant increase in fluorescence of ~710 RFU (two-tailed t-test, $P = 1.82\times10^{-4}$) corresponding to an increase of approximately 1.6 µg of total doxorubicin compared to unmodified (328.8 pg of increased doxorubicin/cell). Similarly, after 24 hours of incubation, there is a significant increase in fluorescence of ~640 RFU (two-tailed t-test, $P = 3.99\times10^{-3}$) corresponding to an increase of approximately 1.5 µg of total doxorubicin compared to unmodified (294.9 pg of increased doxorubicin/cell). We therefore can confirm that

modification of Lipodox by phage major coat protein in 2-propanol retains the previously observed increased cytotoxicity of targeted Lipodox via an increased delivery of doxorubicin to breast cancer cells.

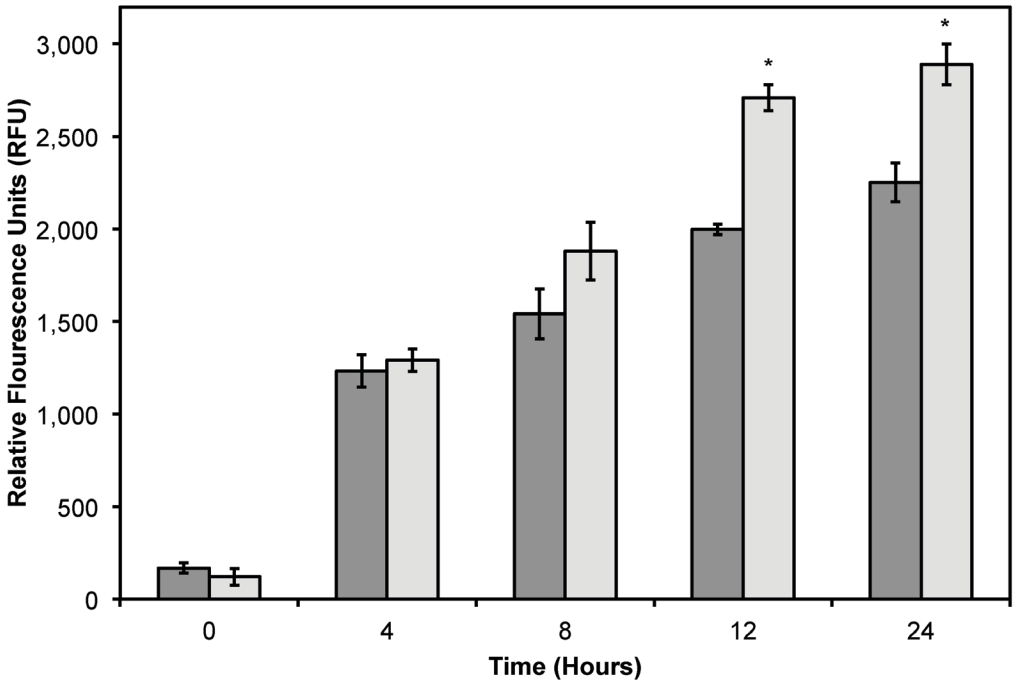

Figure 27: Doxorubicin uptake assay in MCF-7 cells treated with 2 μg of Lipodox (dark bars) or 2 μg DMPGTVLP-modified Lipodox (light bars) over 24 hours. Data are presented as the mean ± sample standard deviation of the relative fluorescence of doxorubicin at an excitation wavelength of 470 nm and emission wavelength of 590 nm. N = 3; *$P < 0.05$, paired, two-tailed Student's t-test vs. unmodified Lipodox.

4.5. Screening of Phage Protein-Modified Lipodox

We next sought to screen a number of cancer cell-specific phage proteins isolated in 2-propanol to identify a panel of phage proteins that may enhance the specific toxicity of Lipodox towards cancer cells. We hypothesized that screening ligands in this manner would significantly increase the throughput of ligand identification for targeted drug delivery using a common Lipodox platform and varying the targeting ligand while retaining a common incorporation method. We initially screened 9 different ligands in MCF-7 breast cancer cells, which are commonly sensitive to doxorubicin. Next we screened an additional 5 ligands in PANC-1 pancreatic cancer cells, which are commonly reported to express a multiple drug resistance (MDR) phenotype and become resistant to doxorubicin treatment. Phage protein-modified Lipodox samples were prepared and characterized as above and summarized in

Table VII to identify preparation parameters for potential bias in the observed toxicity. As shown previously, all modified samples demonstrated a significant increase in mean size distribution (two-tailed t-test, $P < 0.05$). Five of the prepared samples (ANDVYLD, EPQSQWSM, VEEGGYIAA, DGQYLGSQ, and DVRGDGLQ) demonstrated a statistically significant change in zeta potential (two-tailed t-test, $P < 0.05$), however they were all within a biologically acceptable range. On average, most insertions produced high doxorubicin recovery rates (mean recovery 82.8 ± 20.4%) with no significant loss of doxorubicin following modification (mean loss 3.34 ± 2.02%). Modification with the protein ligand ANDVYLD caused significant loss of recovered doxorubicin (33.8%), however there was still sufficient material to complete the assay and all other parameters were similar to the other preparations.

Following Lipodox modification and characterization, we hypothesized that targeting ligands specific for a certain cell type would increase the toxicity of Lipodox as suggested previously. MCF-7 breast cancer cells were treated with the 9 different phage protein-modified Lipodox and cell viability was measured 72 hours after initial treatment. As shown in Figure 28 and from the calculated IC_{50} values in Table VII, there were a number of protein-modified Lipodox samples that significantly increased the toxicity profile of unmodified Lipodox, including DMPGTVLP as shown previously. The ligands screened stratified into three different groups covering a 100-fold change in IC_{50}: 1) ligands showing no improvement from unmodified Lipodox (Figure 28, squares), 2) ligands showing moderate improvement (Figure 28, diamonds), and 3) ligands showing large improvements (Figure 28, circles). As expected ligands with similar structural motifs grouped together, such as ANGRPSMT and VNGRAEAP, and produced similar IC_{50} values. Correlations between all factors in Table VII compared to the IC_{50} were performed to identify parameters that might have influenced the toxicity profile apart from the targeting ligand and all parameters had a low to weak Pearson's R correlation ($R < 0.3$) suggesting the observed increase in toxicity was due to the cell-specific targeting ligands.

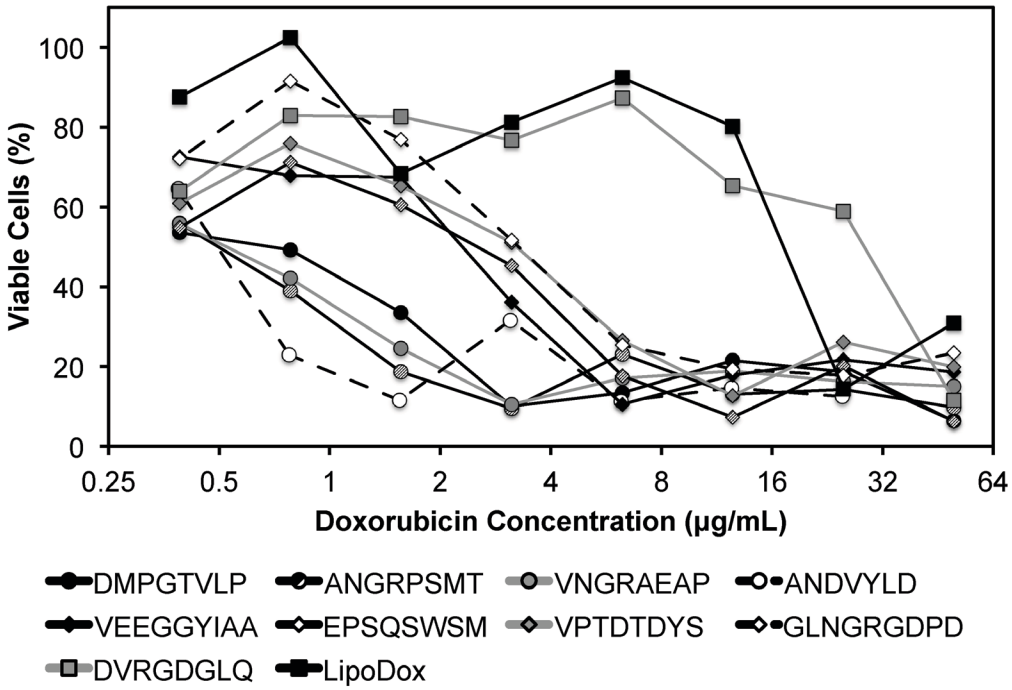

Figure 28: MTT viability assay of MCF-7 cells treated with dilutions of phage protein-modified Lipodox after 24 hours of drug incubation followed by 48 hours of drug washout. Modified samples are identified by their displayed 8- or 9-mer fusion peptide sequence in the legend above.

Table VII: Phage Protein-Modified Lipodox Characterization.

Phage	Protein Added (µg)	Recovered Doxorubicin (%)	Free Doxorubicin (%)	Size Distribution (d.nm)	Zeta Potential (mV)	IC_{50} (µg/mL)
Round 1 – MCF-7 Breast Cancer Cells						
ANDVYLD	0.41	33.84	1.61	81.75 ± 0.31*	-19.9 ± 0.1*	0.6
ANGRPSMT	0.86	109.02	1.72	80.53 ± 0.62*	-18.4 ± 1.4	0.5
DMPGTVLP	0.60	105.38	6.59	79.50 ± 1.44*	-18.3 ± 0.7	1.3
DVRGDGLQ	1.49	85.19	1.62	82.00 ± 0.66*	-19.0 ± 0.7	30.0
EPSQSWSM	1.24	104.46	2.83	80.47 ± 0.54*	-19.7 ± 0.3*	2.8
GLNGRGDPD	0.53	110.92	2.71	80.39 ± 1.40*	-18.7 ± 0.6	3.2
VEEGGYIAA	0.53	73.91	1.72	81.36 ± 1.28*	-21.3 ± 0.7*	2.6
VNGRAEAP	0.97	59.18	1.42	80.80 ± 1.49*	-18.4 ± 1.3	0.6
VPTDTDYS	1.38	77.99	1.61	80.74 ± 1.30*	-18.5 ± 0.4	3.3
No Protein	N/A	98.51	1.18	73.46 ± 0.49	-18.6 ± 0.4	13.5
Round 2 – PANC-1 Pancreatic Cancer Cells						
DGQYLGSQ	1.58	75.75	4.88	89.11 ± 1.70*	-16.7 ± 0.5*	NC[a]
DVRGDGLQ	2.48	81.20	5.91	88.98 ± 0.50*	-16.7 ± 0.5*	NC[a]
EPSQSWSM	0.93	82.34	5.10	89.06 ± 0.91*	-17.7 ± 0.5	NC[a]
ETYNQPYL	0.50	80.37	6.37	90.72 ± 1.21*	-19.7 ± 0.8	NC[a]
GSSEQLYL	1.22	79.71	4.80	89.66 ± 1.07*	-17.4 ± 0.5	NC[a]

[a] NC = Not calculated *$P < 0.05$, paired, two-tailed Student's t-test vs. unmodified Lipodox (control).

PANC-1 pancreatic cancer cells are shown to be resistant to doxorubicin by a MDR phenotype caused by overexpression of P-glycoprotein (Pgp) efflux pumps that prevent doxorubicin from accumulating within the cancer cells (Figure 29, black square). It was hypothesized that the inclusion of a cell-specific targeting ligand into the surface of Lipodox would allow the MDR phenotype to be overcome by delivering a lethal dose of doxorubicin intracellularly before it is inactivated or removed from the cell. The ability of an actively targeted nanomedicine to overcome drug resistance was shown previously by the addition of the ligand EPSQSWSM to Lipodox (Bedi et al. 2014). We therefore sought to identify other ligands with specificity towards pancreatic cancer that would also significantly increase the toxicity of unmodified Lipodox in PANC-1 pancreatic cancer cells. Five ligands with specificity towards PANC-1 pancreatic cancer cells were inserted and screened as above with liposome characterization parameters identified in Table II. As shown in Figure 29, all ligands significantly increased the toxicity of unmodified Lipodox at high concentrations (two-tailed t-test, $P < 0.001$) and a subset of ligands [DGQYLGSQ, ETYNQPYL, and GSSEQLYL] showed a statistically significant increase in toxicity at doxorubicin concentrations of 12 and 24 μg/mL as well (two-tailed t-test, $P < 0.05$).

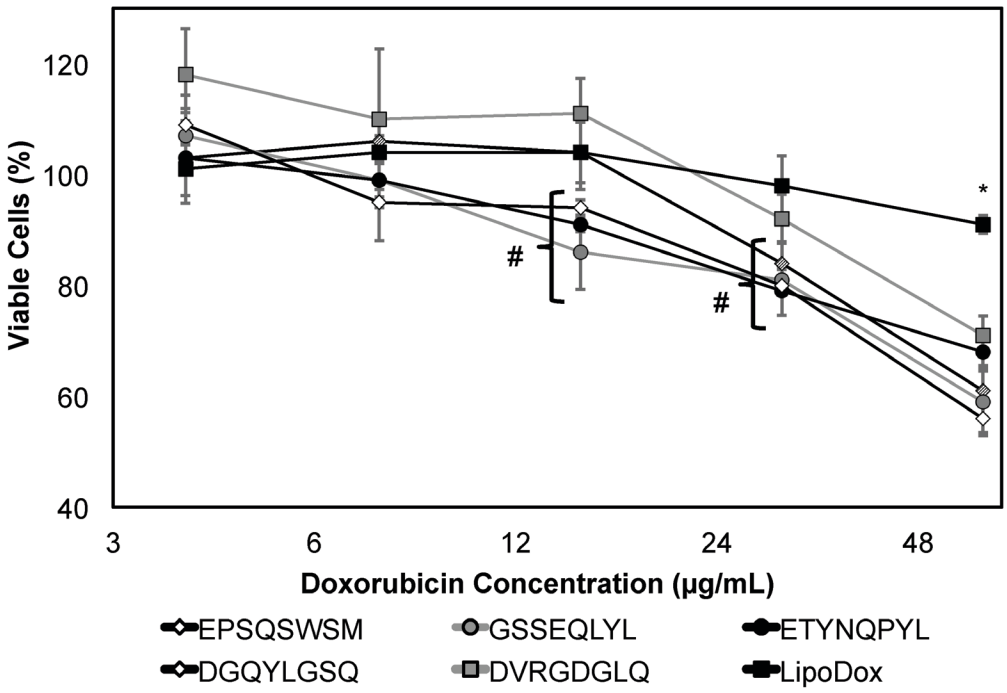

Figure 29: MTT viability assay of PANC-1 cells treated with dilutions of phage protein-modified Lipodox after 24 hours of drug incubation followed by 48 hours of drug washout. Modified samples are identified by their displayed 8-mer fusion peptide sequence in the legend above. Data

are presented as the mean ± sample standard deviation of the percent viable fraction compared to untreated control cells, which were taken as 100% viable. N = 3; *$P < 0.001$, paired, two-tailed Student's t-test vs. unmodified Lipodox; #$P < 0.05$, paired, two-tailed Student's t-test vs. unmodified Lipodox.

5. Discussion

Although targeted nanomedicine delivery has demonstrated its efficiency in systemic cancer treatment in animal models and recently shown success in an ongoing Phase II clinical trial (Hrkach et al. 2012), identification of ideal targeting ligands for active tumor targeting remains a significant challenge. Many methods require multiple conjugation or purification steps before testing the functional activity of a ligand in a given nanomedicine scaffold. A number of these strategies are expensive, time consuming, require large batch volumes due to reactions that produce products with a low overall yield, or require modification of an identified ligand before conjugation. These limitations effectively reduce the ability to screen large numbers of ligands even within the same nanomedicine scaffold. Phage display has been commonly used as a source of novel ligands for various cancer related diagnostic or therapeutic markers. The most commonly used phage display libraries are performed with Ff class of filamentous bacteriophage vectors (including M13, fd, and f1) that displays a random peptide on the pIII minor coat protein, which supports a peptide insert of many different sizes (G. P. Smith & Petrenko 1997). However, the pIII minor coat protein is only expressed in 5 copies at the infectious head of each phage particle, making it necessary to synthesize the identified cell-specific ligands separately from the phage and conjugate it to the nanoparticle carrier that may compromise the specific binding properties of the selected peptides. Previously, we have generated another type of display system—landscape phage in which the N-terminus of every copy of the pVIII major coat protein is modified with a randomized peptide fusion of 8 or 9 amino acids and have been used extensively to identify a number of cancer-specific ligands targeting a number of different cancer phenotypes (Romanov et al. 2001; Jayanna, Bedi, DeInnocentes, et al. 2010a; Fagbohun et al. 2012; Bedi et al. 2014; Samoylova et al. 2003). Since the pVIII major coat protein is expressed in 4,000 copies per phage in these fd-tet-type vectors (Zacher et al. 1980), scaling of phage propagations up to 1 L scale can routinely produce protein yields up to 20 mg that can subsequently be purified from the bacteriophage genomic DNA using a number of standard techniques. Unlike the pIII minor coat protein, the recovered pVIII major coat protein can then be used directly in a number of drug delivery systems via a post-insertion modification of the nanomedicine scaffold using the inherent peptide domains designed naturally into the

full-length coat protein as shown previously (Petrenko & Jayanna 2014). Here we show a novel combinatorial extension of the phage display technology that allows testing for specific tumor cytotoxicity in a common nanomedicine core modified with different phage protein ligands in much higher screening throughput than traditional technologies to identify candidate ligands for further optimization.

In this study, we showed that the pVIII major coat protein could be isolated in 2-propanol to yield highly pure protein that was free from phage DNA. We hypothesize that the protein retains the α-helical secondary structure as suggested by the interaction of protein with liposomes and the solubility of the isolated protein. Under certain conditions and long storage conditions, the phage pVIII protein commonly adopts an irreversible β-sheet conformation, which causes the solubility of the isolated protein to decrease due to aggregation of large protein multimers (Spruijt et al. 1989). We do notice that extended storage of isolated phage protein in 2-propanol at room temperature will result in precipitated protein aggregates that remain insoluble in agreement with previous studies showing freshly prepared samples lose α-helical structure with time. Thus, freshly prepared phage proteins are recommended for all applications requiring α-helical protein structure, including modification of liposomes. The ability to retain the desired α-helical secondary structure following insertion into drug-loaded liposomes remains to be studied, however modified liposomes have been reported to maintain their targeting ability at least a month after preparation (Tao Wang et al. 2014).

Following a similar insertion scheme as described previously using sodium cholate to solubilize pVIII proteins (Jayanna et al. 2009), we prepared a model drug delivery system consisting of isolated DMPGTVLP protein in 2-propanol inserted into preformed Lipodox liposomes. We then showed that liposomes were successfully modified with protein with significantly less loss of doxorubicin during modification while still retaining functional activity. As shown from a mock insertion of isolated DMPGTVLP phage protein into buffer, the complete loss of phage protein can be suggested to be due to the highly hydrophobic nature of the pVIII major coat protein causing any free protein to precipitate or adsorb to other hydrophobic materials. Similarly, as suggested by the partition coefficient of major coat protein for POPC (1-palmitoyl-2-oleoyl-sn-glycero-e-phosphocholine) lipid membranes reported to be 1.0×10^5 M^{-1}, it is hypothesized that 100% of the isolated protein will partition into the lipid bilayer primarily by hydrophobic interactions (Soekarjo et al. 1996).

In an attempt to identify the degree of protein labeling per liposome, we used semi-quantitative dot blotting and flow cytometry of intact liposomes to characterize protein-loading properties following Lipodox modification.

From theoretical calculations based on mass of lipid/liposome and calculated molecular weights of phage proteins, it is estimated that there are approximately 50-100 ligands per liposome depending on the diameter of the liposomes used for modification. The data we obtained from dot blotting suggests there is no free protein in solution after liposome modification and we maintain a correct orientation of targeting protein with N-terminus exposed from the liposome and the C-terminus protected within the liposome core. Following degradation of phage protein-modified liposomes with Proteinase K, there was complete degradation of the N-terminus and no degradation of C-terminus. These data suggest that Proteinase K is sufficient to degrade all exposed proteins and 100% of the N-terminus is exposed from the liposome surface. We also estimate that 100% of the C-terminus is protected from degradation suggesting that the insertion of protein was complete and that no free phage protein is found in solution. We therefore show that the C-terminus of the pVIII major coat protein was able to translocate through the liposome membrane with high orientation specificity. We also show that following insertion of Alexa 488-labeled DMPGTVLP major coat protein into Lipodox, there was a significant shift of the liposome population towards the Alexa 488-positive gate. Only 11% of the liposome population showed a detectible increase in Alexa 488-positive labeling. Due to the low labeling efficiency (~10%) of the phage protein prior to insertion, we are unable to detect all ligand incorporations into the liposomes and can only resolve the most fluorescently intense liposomes receiving large numbers of Alexa 488-labeled phage proteins. Based on an estimate of 50 ligands/liposome, it can be expected that insertion of labeled proteins will follow a normal distribution with a mean of 5 labeled ligands/liposome. However, because of the poor resolution between the two populations, we can only observe the (11%) upper-tail of the normally distributed population, which are the most bright. Optimization of fluorophore conjugation to the phage ligands or changing to a brighter fluorophore can increase the efficiency of this assay. It was also noted that there was a slight decrease in the doxorubicin mean channel fluorescence following modification (unmodified = 7,929 RFU vs. modified = 5,679 RFU in 670 LP-H channel) consistent with a slight loss in encapsulated doxorubicin. Free DMPGTVLP labeled protein appeared to aggregate heavily and form very bright particles, however in phage protein-modified Lipodox we observed only moderate increases in fluorescence. As we only see moderate increases in fluorescence, this suggests that there is no detectible free protein in solution with the modified Lipodox. This data is in agreement with previous reports on the completeness of insertion using different concentrations of isolate phage protein while maintaining a constant lipid mass up to a protein/lipid ratio of 1:200 (Soekarjo et al. 1996; Tao Wang et al. 2011b). We note that a significant limitation of this assay is the requirement for gating on a fluorescent

population of liposomes. Since we are near the detection limits of the equipment, we found that empty liposomes, when performed with the same parameters, produce unreliable results as there is no precise method to identify liposomes from background noise during the measurement. We have seen that translocation through preformed lipid membranes is spontaneous (not requiring any host proteins), pH and temperature dependent. We propose that insertion of pVIII major coat protein is a two-stage process: 1) attachment of protein to the liposome surface, and 2) translocation of the C-terminus (Figure 30). The association of isolated pVIII major coat protein has been studied in detail previously, however the mechanism of C-terminal translocation has not been fully elucidated. We have previously proposed a mechanism in which the positively charged C-terminus is able to penetrate through a lipid bilayer (Petrenko & Jayanna 2014), however detailed studies on the mechanism of translocation remain to be completed.

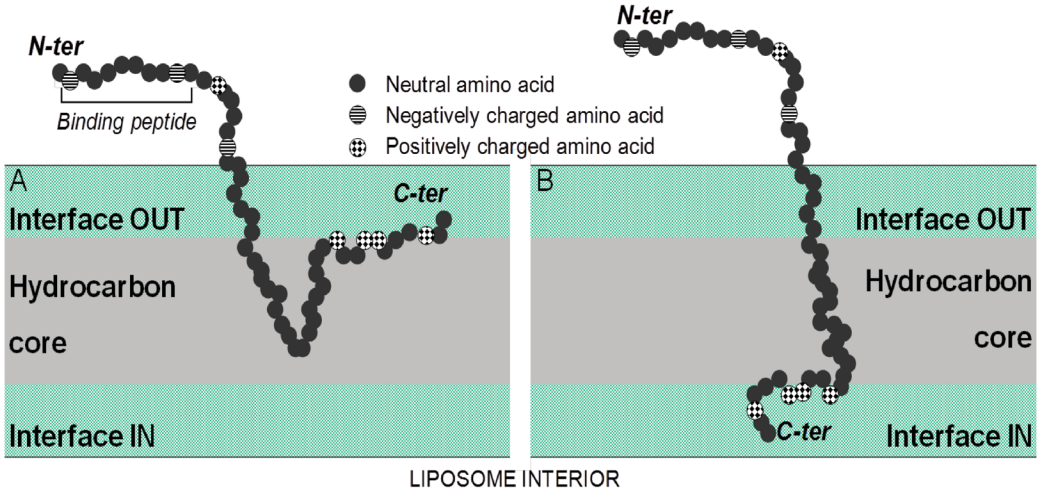

Figure 30: Spontaneous insertion of the major coat protein into lipid membranes. (A) In the first step, the isolated coat protein binds to the lipid membrane using electrostatic interactions of the C-terminus with negatively charged phosphate headgroups of lipids, followed by the insertion of the hydrophobic region of the protein into the hydrocarbon core of the lipid bilayer. (B) In the second step, the hydrophilic tail is released into the *trans* side of lipid bilayer through a process similar to cell-penetrating peptides. From (Petrenko and Jayanna, 2014).

It remains to be seen whether there is a direct correlation between the strength of phage ligand binding to a target cell line and a subsequent increase in functional cytotoxicity activity *in vitro*. From our preliminary data, we find that sometimes weak binding phage clones perform better as targeting ligands in liposomal nanomedicines than

strong binding phages. It has been suggested that low affinity ligands may be ideal for improved tumor penetration, as actively targeted drug delivery systems targeted by high affinity ligands are suggested to remain on the tumor periphery (Gray et al. 2013). For this reason, we used a functional screening assay of the final targeted nanomedicine in which new candidate ligands can be identified based on the desired increase in cytotoxicity rather than building an ideal drug delivery system based on optimization of individual components. For the functional screening assays, the drug exposure time was maintained at 24 hours for all viability experiments to prevent excess drug leakage due to liposome degradation over the total measurement time. We have seen minimal doxorubicin leakage of phage protein-modified doxorubicin liposomes at 37ºC in the presence of serum over the total test period (data not shown), however we sought to optimize screening conditions with alternative encapsulated drugs in mind displaying less carrier stability. We also increased the total incubation time of viability assays to a total of 72 hours consisting of 24 hours with phage protein-modified Lipodox samples plus an additional 48 hours washout period in complete culture medium. The extended assay conditions allowed all cells, irrespective of origin, sufficient time to complete a normal cell cycle and thereby produce an increased toxicity profile in doxorubicin treated cells due to the inability of genomic DNA to replicate, resulting in a stalled cell cycle phenotype in the G_0/G_1 phase commonly observed with doxorubicin toxicity (Lukyanova et al. 2009). Given the broadly defined parameters, this screening assay can therefore be extended to a variety of cell types and also a number of drug classes employing different mechanisms of action. A limitation of this screening assay is the inherent nature of the MTT assay as a measure of mitochondrial succinate dehydrogenase activity in metabolically active cells rather than a cytotoxic event. However as shown in previous work by us and other authors, doxorubicin will cause cell death by activation of caspase cascades leading to apoptosis (Suwei Wang et al. 2004). As we have not changed the properties of the cytotoxic drug and we have shown that phage proteins are non-toxic (Bedi et al. 2014), we don't expect significant changes in the primary mechanism of cell death, only an increase in intracellular delivery of cytotoxic drug. Since we have shown previously that the MTT assay is a good indicator of cell death in this system and death can be confirmed by visual observations, the reduction in cell viability as determined by the MTT assay would be sufficient for identification of ligands in a screening assay.

From our screening experiment in MCF-7 cells, we were able to identify a previously validated breast cancer cell-specific protein DMPGTVLP that interacts with cell surface expressed nucleolin and increases the therapeutic effect of liposomal doxorubicin *in vitro* and in *vivo* by increasing the specific delivery of doxorubicin to

MCF-7 cell nuclei (Fagbohun et al. 2012; Tao Wang et al. 2014; Tao Wang, D'Souza, et al. 2010a). Liposomes modified with a phage fusion protein displaying the peptide ANDVYLD showed the greatest increase in toxicity with a calculated IC_{50} of 0.6 μg/mL in MCF-7 cells. We also identified two peptides containing a positionally constrained **NGR** motif (A**NGR**PSMT and V**NGR**AEAP) that showed similar toxicity profiles (average IC_{50} = 0.55 μg/mL) as expected. Surprisingly, phage VNGRAEAP did not show binding to MCF-7 cells in our previous binding assays, however this limitation may be due to a short binding assay duration (1 hour) compared to the duration of the cytotoxicity assay (24 hours) or due to a difference in primary uptake mechanism between the two phage as shown previously (Gillespie et al. Submitted, Chapter 2). A similar motif containing a positionally different **NGR** motif (GL**NGR**GDPD) showed improvement in toxicity to 3.2 μg/mL, however it was unable to reach the same toxicity of the other motifs. This may be due to a difference in the NGR motif availability to the receptor or an effect of peptide affinity. Inclusion of a pancreatic cancer-specific ligand (DVRGDLQ) resulted in no significant increase in toxicity suggesting the specificity of ligands to increase doxorubicin delivery specifically to the target cells and is not a result of modification. Screening the DVRGDLQ peptide in pancreatic cancer cells produced an increase in cytotoxicity compared to unmodified Lipodox. Interestingly, a subset of ligands with similar motifs (DGQYLGSQ, ETYNQPYL, and GSSEQLYL) grouped together to produce similar cytotoxicity profiles. Comparison of a shared **D**XXXX**G**X**D** motif showed that there was a significant difference between DVRGDGLQ and DGQYLGSQ ligands at higher concentrations (two-tailed t-test, $P < 0.01$) with the DGQYLGSQ ligand producing greater toxicity suggesting minimal involvement of the **D**XXXX**G**X**D** motif. Comparison of the **YL** motif found in different positions of the three ligands showed no statistical differences between the three ligands (two-tailed t-test, $P > 0.05$), however all three showed significant differences compared to unmodified. These data therefore suggest the **YL** motif, irrespective of position, will cause an increase in toxicity. No putative receptor has been suggested for any of the three ligands at this time, however it is interesting to note the number of essential amino acids (Y, L, W, and V) present in the identified ligands that are typically underrepresented in our phage display library (Kuzmicheva, Jayanna, Sorokulova, et al. 2009b). The presented data demonstrate the use of phage display technology along with a combinatorial screening strategy to significantly enhance the screening throughput of targeted nanomedicines that may considerably accelerate progress in actively targeted drug development.

CHAPTER 4

CONCLUSIONS

The development of precision medicines that provide their action specifically at the site of disease has been a long sought goal for many decades. With the development of nanomedicines, significant leaps towards this goal have been reached. Active targeting has been proposed to significantly enhance the therapeutic activity and decrease non-related side effects, however it has been shown that the tumor microenvironment is much more complex than previously believed and active targeting has shown minimal improvements. As identification of new barriers that prevent delivery are understood, nanomedicine systems can be developed to overcome those barriers using appropriate targeting ligands or physical properties of the nanomedicines. Alternatively, an actively targeted nanomedicine system was developed that allows identification of functional ligands in a combinatorial design scheme that is based on the desired outcome, for example, decreased cell viability.

Here, two landscape phage display libraries were used to identify a number of NSCLC ligands that can be used for therapeutic, diagnostic or theranostic nanomedicine systems. Of the identified ligands, two ligands containing a structurally conserved NGR motif were studied in more detail and shown to improve therapeutic activity of a liposomal nanomedicine in a drug-resistant NSCLC cell line *in vitro*. Results of the study show that the amino acids surrounding a common NGR motif has implications for modulating the activation of cell penetration mechanisms/endocytosis that can be exploited for drug delivery applications. This results in improved intracellular delivery of therapeutic molecules and demonstrates the requirement for ligand internalization for optimal drug delivery. The targeting system was then extended to include a larger panel of ligands, which could be studied in a common nanomedicine core with a common insertion mechanism using the intrinsic transmembrane domain of the pVIII major coat protein to anchor the ligands to the nanomedicine. Previously, most active targeting systems only study a single targeting ligand. However, targeting ligands can be screened in much higher throughput (10+ ligands per group), which improves the non-rational development and screening of nanomedicines that are functionally active. It can be hypothesized that a number of novel cell surface targets can be subsequently identified using this type of functional screening assay.

APPENDIX I

TECHNIQUES IN PHAGE PROTEIN-BASED NANOMEDICINES

1. Phage Propagation Protocols

1.1. Preparation of K91BluKan *E. coli* Glycerol Stocks

E. coli bacterial stocks are typically stored in 50% glycerol for long-term storage at -80ºC.

Reagents:

- Glycerol, 50%
- NZY Medium

Materials:

- K91BluKan *E. coli* Cells
- Microcentrifuge Tubes, (0.65 mL)

Equipment:

- Balance: (Mettler Toledo #B2002-S)
- Macroman Pipetter: (Gilson, Model F110752)

Procedures:

Day 1

1) Prepare a starter culture of K91BluKan strain *E. coli* in 20 mL NZY medium in a 125 mL flask.
2) Incubate in a shaker-incubator at 200 rpm overnight at 37ºC.

Day 2

3) Pipette 50 µL of 50% glycerol into 40 sterile 0.65 mL microcentrifuge tubes.
4) Pipette 50 µL portions of the overnight K91BluKan *E. coli* culture into the glycerol-containing microcentrifuge tubes.
5) Vortex the tubes to mix completely.
6) Label the microcentrifuge tubes.
7) Store the tubes in a racked box at -80ºC.

1.2. Preparation of K91BluKan *E. coli* Starved Cells

K19BluKan *E. coli* cells are the commonly used strain of gram-negative bacteria used as a host to propagate fd-tet bacteriophage clones.

Reagents:

- NZY Medium
- K91BluKan *E. coli* Glycerol Stock
- Kanamycin (100 mg/mL)
- NaCl (80 mM)
- NAP Buffer

Materials:

- Snap-cap Culture Tubes, 13 mL: (Sarstedt #62.515.006)
- Sidearm Flask, 300 mL: (Bellco)
- Pipettes, 10 mL: (Costar #4488)
- Oak Ridge tubes, 50 mL
- Culture Flask, 125 mL: (Kimble #25615)

Equipment:

- I2500/C25 Shaker-Incubator: (New Brunswick)
- Genesys 20 Spectrophotometer: (Thermo Scientific)

Procedures:

Day 1

1) Remove a tube of glycerol stock K91BluKan cells from the freezer and allow to warm to room temperature.
2) Label a snap-cap tube as “K91BK” and include date and medium used. Label a second snap-cap tube as “Blank”.
3) Pipette 2 mL NZY medium into each of the snap-cap tubes.
4) Pipette 2 µL of 100 mg/mL kanamycin into each of the snap-cap tubes (Final concentration of 100 µg/mL kanamycin).
5) Pipette 2 µL of K91BluKan cells into the snap-cap tube labeled “K91BK”.

6) Incubate both tubes in shaker-incubator overnight at 37ºC/200 rpm.

Day 2

7) Visually check both tubes for growth. Snap-cap tube labeled "K91BK" should be turbid from bacterial growth. Snap-cap tube labeled "Blank" should be clear from no growth. If blank tube shows growth, repeat overnight culture with fresh medium/antibiotics stocks if needed.
8) Transfer 20 mL NZY medium into a 300 mL sidearm flask.
9) Pipette 300 µL of overnight K91BK cells into the sidearm flask.
10) Incubate the flask in shaker-incubator at 37ºC/200 rpm.
11) Measure the turbidity by the side-arm cuvette until the optical density at 600 nm (OD_{600}) reaches 0.45. Blank the spectrophotometer with a sterile solution of NZY medium.
12) Incubate the flask with gentle shaking at 37ºC/50 rpm for 7 minutes to allow sheared F pili to regenerate.
13) Gently transfer the solution with a 10 mL pipette from the sidearm flask to a sterile 50 mL Oak Ridge tube labeled as "K91KB starved cells" with your initials and date of propagation.
14) Align the Oak Ridge tube so the label faces out from the center of the rotor. Centrifuge tube at 550 × g (Beckman Roter JA-17; 2,000 rpm or Beckman Roter JA-20; 2,100 rpm) for 10 minutes at 4ºC. Be sure to include a balance also.
15) Pour off the supernatant into a waste container (Pour away from the pellet). Gently pipette 20 mL of 80 mM NaCl onto the cells and gently invert to mix. Do not vortex cells to dissolve pellet.
16) Gently pour the cells into a sterile 125 mL culture flask and transfer the label from the Oak Ridge tube to the flask. Incubate the flask with gentle shaking at 37ºC/50 rpm for 45 minutes in a shaker-incubator.
17) Gently pour the solution to a new, sterile 50 mL Oak Ridge tube and transfer the label to the Oak Ridge tube.
18) Again, align the Oak Ridge tube so the label faces out from the center of the rotor. Centrifuge tube at 550 × g (Beckman Roter JA-17; 2,000 rpm or Beckman Roter JA-20; 2,100 rpm) for 10 minutes at 4ºC.

19) Pour off the supernatant into a waste container (Pour away from the pellet). Gently pipet 1 mL of cold NAP buffer onto the cells.

20) Store cells at 4ºC. Cells remain infective to fd-tet bacteriophage for 3-5 days, but show best infectivity if used within a few hours. Concentration of viable cells is ~5×10^9 cells/mL.

1.3. Assay of Starved Cell Infectivity by Titering of Control Phage Vector (f8-5)

Reagents:

- Starved K91BluKan *E. coli* cells
- Control Phage, f8-5: ($2x10^{12}$ vir/mL)
- TBS, pH 7.4 (1X)

Materials:

- 0.65 mL Microcentrifuge tubes

Equipment:

- Incubator, 37ºC

Procedures:

Day 1

1) Prepare serial dilutions ($10^{-2} \sim 10^{-8}$) of wild type phage f8-5:
2) Add 10 µL of starved cells to a 0.65 mL microcentrifuge tubes. Gently add 10 µL of phage dilutions from tube 4 & 5 and gently mix.
3) As a control, add 10 µL of starved cells in a microcentrifuge tube. Gently add 10 µL of 1X TBS and mix gently.
4) Incubate at room temperature for 15 minutes for infection to occur.
5) Add 180 µL NZY/0.2 µg/mL Tetracycline to each tube.
6) Incubate in 37ºC incubator for 45 minutes to develop TetR.
7) Spread 200 µL suspensions from microcentrifuge tubes onto NZY/20 µg/mL Tetracycline plates.
8) Incubate plates overnight in 37ºC incubator.

Day 2

9) Count the number of colony forming units (CFU) on each plate.
10) Calculate the tier according to the following formula, where N is the number of CFU on a plate:

$$\text{Titer (CFU/mL)} = \frac{\text{N (CFU)}}{10\ \mu\text{L}} \times \frac{1000\ \mu\text{L}}{1\ \text{mL}} \times \text{Dilution Factor} \quad (8)$$

1.4. Propagation of fd-tet Phage Vectors and Derivatives

1.4.1. 2 mL Scale Propagation

Reagents:

- PEG/NaCl (16.7%/3.3 M), 600 mL
- TBS, pH 7.4 (1X), 500 mL: (Teknova #T9867)
- NZY Medium, 500 mL
- Tetracycline (20 mg/mL), 100 mL

Materials:

- Oak Ridge Tubes, 50 mL
- Snap-cap Culture Tubes, 13 mL: (Sarstedt #62.515.006)
- 1.7 mL Microcentrifuge Tubes

Equipment:

- I2500 Series Shaker-Incubator: (New Brunswick)
- Microfuge 18 Centrifuge: (Beckman Coulter)

Procedures:

Day 1

1) Prepare labeled snap-cap tubes for each clone to be propagated. Place 2 mL NZY/20 µg/mL Tetracycline medium into each of the snap-cap tubes.
2) Using forceps and toothpicks, pick an individual colony from a NZY/Tet plate. Place the sample (including the toothpick) into the snap-cap tube.
3) Incubate the tubes in a shaker-incubator at 200 rpm overnight at 37ºC.

Day 2

4) Transfer 1.5 mL of the overnight culture into a labeled 1.7 mL microcentrifuge tube.
5) Microcentrifuge (Beckman Microfuge) at 13,000 rpm for 5 minutes to pellet cells.
6) Pipette 1 mL of the supernatant into a new 1.7 mL microcentrifuge tube containing 150 µL of 16.7% PEG-8000/3.3 M NaCl. Invert approximately 100 times to mix the contents. Incubate the tubes at 4ºC overnight.

Day 3

7) Microcentrifuge (Beckman Microfuge) the tubes at 13,000 rpm for 15 minutes. Remove the supernatant and remove supernatant from the pellet, recentrifuge for 5 minutes at the same speed/orientation and remove the residual supernatant.
8) Dissolve the pellet in 200 µL 1X TBS. Store at 4ºC.
9) Estimate the concentration by measuring the absorbance of each sample at 269 nm (Blank with 1X TBS) with the NanoDrop. Calculate the concentration of phage according to the following formula:

$$\text{Concentration Phage (vir/mL)} = \text{Abs}_{269} \times 6.5 \times 10^{12} \quad (9)$$

1.4.2. 20 mL Scale Propagation

Reagents:

- PEG/NaCl (16.7%/3.3 M), 600 mL
- TBS, pH 7.4 (1X), 500 mL: (Teknova #T9867)
- NZY Medium, 500 mL
- Tetracycline (20 mg/mL), 100 mL

Materials:

- Oak Ridge Tubes, 50 mL
- Snap-cap Culture Tubes, 13 mL: (Sarstedt #62.515.006)
- Pipets, 25 mL
- Culture Flask, 125 mL: (Kimble #25615)
- 1.7 mL Microcentrifuge Tubes

Equipment:

- Avanti J-26 XP Centrifuge: (Beckman Coulter)
- I2500 Series Shaker-Incubator: (New Brunswick)
- Microfuge 18 Centrifuge: (Beckman Coulter)

Procedures:

Day 1

1) Label snap-cap culture tubes with each of the phage clones to be propagated and 1 snap-cap culture tube as a blank control.

2) Transfer 2 mL of NZY/Tetracyline (20 μg/mL) to each of the labeled culture tube.
3) Using forceps and a toothpick, for each phage clone pick an isolated colony of E. coli infected with phage and place the toothpick into the labeled 15 mL culture tube.
4) Incubate the tubes in shaker-incubator overnight at 37ºC/200 rpm.

Day 2

5) Label 125 mL culture flasks with each of the phage clones to be propagated.
6) Place 20 mL of NZY medium into each of the flasks. To each of the flasks labeled for tetracycline, add 20 μL of 20 mg/mL tetracycline.
7) Pipet 20 μL of each overnight culture into the appropriately labeled flask for each phage clone.
8) Incubate all flasks in the same shaker-incubator overnight at 37ºC/200 rpm.

Day 3

9) Pour each culture into a 50 mL Oak Ridge tube and balance tubes as needed. Transfer the label from each flask to the appropriate Oak Ridge tube.
10) Centrifuge balanced tubes at 3,500 x g (Beckman Rotor JA-20; 5,379 rpm or Beckman Rotor JA-17; 5,040 rpm) for 10 minutes at 4ºC.
11) Pour the supernatants into new 50 mL Oak Ridge tubes and transfer the label to the new tube.
12) Centrifuge the tubes at 12,000 x g (Beckman Rotor JA-20; 9,960 rpm or Beckman Rotor JA-17; 9,333 rpm) for 10 minutes at 4ºC.
13) Pour the supernatants into new 50 mL Oak Ridge tubes with 3 mL PEG/NaCl in each tube. Transfer the label to the new tube and invert the tubes 100 times to mix. Incubate the tubes at 4ºC overnight.

Day 4

14) Centrifuge the tubes at 20,000 x g (Beckman Roter JA-20; 12,859 rpm or Beckman Rotor JA-17; 12,049 rpm) for 30 minutes at 4ºC. Pour off the supernatant into a waste container. Remove the supernatant and remove supernatant from the pellet, recentrifuge for 5 minutes at the same speed/orientation and remove the residual supernatant for each sample.
15) Add 1 mL 1X TBS to dissolve each pellet. Dissolve each pellet by vortexing vigorously.
16) Transfer the solution into a new, labeled 1.7 mL microcentrifuge tube.

17) Centrifuge the tubes at 15,000 x g (Beckman Microfuge 18; 13,000 rpm) for 2 minutes at room temperature.
18) Transfer the supernatants to a new, labeled 1.7 mL microcentrifuge tube containing 150 µL PEG/NaCl. Invert the tubes 100 times to mix. Incubate the tubes at 4ºC overnight.

Day 5

19) Centrifuge the tubes at 15,000 x g (Beckman Microfuge 18; 13,000 rpm) for 10 minutes. Discard the supernatant into the waste and remove the supernatant and remove supernatant from the pellet, recentrifuge for 5 minutes at the same speed/orientation and remove the residual supernatant for each sample.
20) Add 100 µL 1X TBS to each pellet and vortex vigorously to dissolve.
21) Centrifuge each sample at 2,000 x g (Beckman Microfuge 18; 5,000 rpm) for 1 minute.
22) Transfer the supernatant to a new, labeled 1.7 mL microcentrifuge tube and incubate the tubes at 4ºC for storage.
23) Estimate the concentration by measuring the absorbance of each sample at 269 nm (Blank with 1X TBS) with the NanoDrop. Calculate the concentration of phage according to the following formula:

$$\text{Concentration Phage (vir/mL)} = \text{Abs}_{269} \times 6.5\times10^{12} \quad (10)$$

1.4.3. 1 L Scale Propagation

Reagents:

- PEG/NaCl (16.7%/3.3 M), 600 mL
- TBS, pH 7.4 (1X), 500 mL: (Teknova #T9867)
- NZY Medium, 1000 mL
- Tetracycline (20 mg/mL), 100 mL

Materials:

- 500 mL Centrifuge Bottles
- Oak Ridge Tubes, 50 mL
- Snap-cap Culture Tubes, 13 mL: (Sarstedt #62.515.006)
- Pipets, 25 mL
- 1.7 mL Microcentrifuge Tubes

- 3 L Culture Flasks

Equipment:

- Avanti J-26 XP Centrifuge: (Beckman Coulter)
- I2500 Series Shaker-Incubator: (New Brunswick)
- Microfuge 18 Centrifuge: (Beckman Coulter)

Procedures:

Day 1

1) To each liter of NZY medium, add 1 mL 20mg/mL tetracycline stock and mix thoroughly.
2) Using a toothpick, inoculate a single colony of infected K91BK cells into a 3 L flask containing 1 L of NZY/20 µg/mL tetracycline.
3) Incubate in a shaker-incubator at 200 rpm overnight at 37ºC.

Day 2

4) Divide the overnight culture into three 500 mL centrifuge bottles of ~ 330 mL.
5) Centrifuge the bottles at 5,000 rpm (Beckman Avanti) for 10 minutes at 4ºC.
6) Pour the supernatant into new 500 mL centrifuge bottles and centrifuge at 8,000 rpm (Beckman Avanti) for 10 minutes at 4ºC.
7) Pour the final cleared supernatant into new 500 mL centrifuge bottles and note the net volume. Volume should be less than 350 mL.
8) Add 50 mL (0.15X volume) of 16.7% PEG/3.3 M NaCl solution to each of the bottles. Invert approximately 100 times. Incubate bottles at 4ºC overnight.

Day 3

9) Centrifuge PEG precipitated phage at 8,000 rpm (Beckman Avanti) for 40 minutes at 4ºC.
10) Pour off the supernatant. Remove the supernatant and remove supernatant from the pellet, recentrifuge for 5 minutes at the same speed/orientation and remove the residual supernatant.
11) Add 10 mL 1X TBS to each bottle and dissolve the pellet. Bottles cam be shaken in shaker-incubator at 200 rpm for 30 minutes to dissolve pellet.
12) Transfer the solutions from all three 500 mL bottles to a single 50 mL Oak Ridge tube. Centrifuge at 15,000 rpm (Beckman Avanti) for 10 minutes at 4ºC.

13) Pour the supernatant into a new 50 mL Oak Ridge tube with 4.5 mL (0.15X volume) 16.7% PEG/3.3 M NaCl solution. Invert approximately 100 times and allow phage to precipitate at 4ºC overnight.

Day 4

14) Collect the precipitated phage by centrifuging at 15,000 rpm (Beckman Avanti) for 15 minutes at 4ºC.
15) Pour off the supernatant and remove the supernatant and remove supernatant from the pellet, recentrifuge for 5 minutes at the same speed/orientation and remove the residual supernatant for each sample.
16) Add 1 mL 1X TBS to dissolve the pellet and allow the pellet to soften for 1 hour at room temperature. Tubes may be shaken at 200 rpm in shaker-incubator for 1 hour. Vortex to dissolve and homogenize the solution.
17) Centrifuge at 15,000 rpm (Beckman Avanti) for 10 minutes at 4ºC.
18) Transfer the supernatant to a sterile 1.5 mL microcentrifuge tube and store at 4ºC.
19) Estimate the concentration by measuring the absorbance of each sample at 269 nm (Blank with 1X TBS) with the NanoDrop. Calculate the concentration of phage according to the following formula:

$$\text{Concentration Phage (vir/mL)} = \text{Abs}_{269} \times 6.5 \times 10^{12} \quad (11)$$

1.5. Endotoxin Removal from Phage Vectors

Reagents:

- Phage to be purified
- Triton X-114: (Acros Organics #42365000)
- Endotoxin-free 1X TBS: (Teknova #T9867)
- PEG/NaCl (16.7%/3.3 M), 600 mL

Materials:

- 15 mL Centrifuge Tubes: (Corning #430052)
- Oak Ridge Tubes, 50 mL
- 1.7 mL Microcentrifuge Tubes

Equipment:

- Avanti J-26 XP Centrifuge: (Beckman Coulter)
- Allegra R21 Centrifuge: (Beckman Coulter)

Procedures:

Day 1

1) Dilute phage (~10^{11} vir/mL final) in 10 mL Endotoxin-free 1X TBS in a 15 mL centrifuge tube.
2) Add 1% Triton X-114 (100 µL) and vortex vigorously.
3) Place in an ice bath for 5 minutes to create a homogeneous solution.
4) Vortex and warm at 37ºC for 15 minutes for two phases to form.
5) Centrifuge (Beckman Allegra) at maximum speed for 7 seconds.
6) Equilibrate in an incubator at 37ºC for 1 hour.
7) Centrifuge (Beckman Allegra) at maximum speed for 30 seconds.
8) Remove the upper aqueous phase carefully and transfer to a new 15 mL centrifuge tube.
9) Repeat for a total of three separations.
10) Transfer into a single 50 mL Oak Ridge tube.
11) Centrifuge at 15,000 rpm (Beckman Avanti) for 10 minutes at 4ºC.
12) Pour supernatant into a new 50 mL Oak Ridge tube.
13) Add 1/6 volume (3.35 mL) of 16.7% PEG/3.3 M NaCl to each of the tubes to precipitate the phage. Incubate at 4ºC overnight.

Day 2

14) Collect the precipitated phage by centrifuging at 15,000 rpm (Beckman Avanti) for 10 minutes at 4ºC.
15) Pour off the supernatant and do RRR .
16) Add 0.5 mL endotoxin-free 1X TBS to dissolve the pellet.
17) Transfer to a 1.7 mL microcentrifuge tube and heat at 70ºC for 7 minutes to heat inactivate the sample.
18) Centrifuge at 13,000 rpm (Beckman Microfuge) for 2 minutes.
19) Transfer the supernatant to a new 1.7 mL microcentrifuge tube. Store at 4ºC.
20) Estimate the concentration by measuring the absorbance of each sample at 269 nm (Blank with 1X TBS) with the NanoDrop. Calculate the concentration of phage according to the following formula:

$$\text{Concentration Phage (vir/mL)} = \text{Abs}_{269} \times 6.5\times10^{12} \quad (12)$$

2. Selection and Screening of Landscape Phage Display Library Protocols

2.1. First Round Selection of Landscape Phage Against Mammalian Cells *in vitro*

Reagents:

- Phage Library: f8/8 or f8/9 (From Dr. Petrenko)
- Control Phage: f8-5 (2x1012 vir/mL)
- K91BlueKan *E. coli* Starved Cells
- Minimum Essential Medium (MEM) w/ Earle's Balanced Salts, Nonessential Amino Acids & Sodium Pyruvate, 500mL: (ATCC #302003)
- NZY/Tetracycline (20 µg/mL) Plates, 60
- 1M Tris-HCl, pH 9.1: (100 mL)
- Elution Buffer: (100 mL)
    - Dissolve 1.5 g glycine in 90 mL of distilled water.
    - Adjust the pH to 2.2 with 2 N HCl.
    - Add 100 mg BSA (Sigma #A2153-100G) and 10 mg phenol red (Sigma #P-2417-5G).
    - Add water to bring the solution to 100 mL.
    - Filter sterilize and store at 4ºC.
- Lysis Buffer (2% w/v Sodium Desoxycholate/10 mM Tris-HCl/2 mM EDTA): (50 mL)
    - Dissolve 1 g sodium desoxycholate (Fisher #S285-100) and 0.06 g Tris base into 40 mL of distilled water.
    - Add 200 µL 0.5 M EDTA and mix.
    - Adjust the pH to 8.0 with 2 N HCl .
    - Add water to bring the solution to 50 mL.
    - Filter sterilize and store at 4ºC.
- Washing Buffer (0.1% Tween 20/0.5% BSA/MEM Medium): (100 mL)
    - Add 500 µL 20% Tween 20 and 10 mL 5% BSA to 90 mL of MEM medium.
    - Mix thoroughly, filter sterilize and store at 4ºC.
- Blocking Buffer (0.5% BSA/MEM medium): (100 mL)
    - Add 10 mL 5% BSA to 90 mL MEM medium.

- Mix thoroughly, filter sterilize and store at 4ºC.

Materials:

- 25 cm^2 Cell Culture Flasks: (Corning #430168)
- Amicon Ultra-4 100K MWCO Centrifugal Filters: (Fisher #UFC810024)
- 15 mL Centrifuge Tubes: (Corning)
- 1.7 mL Microcentrifuge Tubes:

Equipment:

- Avanti J-26 XP Centrifuge: (Beckman Coulter)
- I2500 Series Shaker-Incubator: (New Brunswick)
- Microfuge 18 Centrifuge: (Beckman Coulter)

Procedures:

Day 1

1) Prepare Mammalian Cell Lines for Selection
   a. Prepare a culture of target cells and normal cells (e.g. Calu-3 and Small Airway Epithelial Cells) in a 25 cm^2 cell culture flask as described in the lab manual.
   b. Continue to grow cells until they have reached 90% confluence.

Day 2

2) Prepare Starved Cells and Check Starved Cells
   a. Prepare 3 flasks of starved K91BlueKan E. coli cells as described in the lab manual. Resuspend in 1 mL of NAP buffer.
   b. Check starved cells and titer control phage f8-5 as described in the lab manual.
   c. Incubate two 25 cm^2 cell culture flasks with medium supplemented with 10% FBS (MEM medium + 10% FBS) overnight in a 37ºC CO_2 incubator.

Day 3

3) Depletion of Phage Binding Plastic
   a. Add 30 µL of phage library f8/8 or f8/9 into 2 mL of blocking buffer in a sterile cell culture flask. Rock gently to cover the entire surface of the culture flask.
   b. Incubate at room temperature for 1 hour.

c. Collect the supernatant.

4) Depletion of Phage Binding Serum (MEM w/ 10% FBS)

a. Remove the medium from the flask.

b. Wash the flask with 4 mL of MEM medium with 10% FBS.

c. Add depleted library to the cell culture flask. Incubate at room temperature for 1 hour.

d. Collect the supernatant.

5) Repeat steps for an additional step of depletion of phage that bind serum.

6) Depletion of Phage Binding Phenotypically Normal Cells (SAE)

a. Remove medium from cell culture flask with 90% confluent SAE cells. Wash the cells with 2 mL MEM medium with serum at room temperature.

b. Incubate cells with 5 mL of MEM medium at room temperature for 1 hour. Remove immediately before application of phage library.

c. Remove the MEM medium and add the depleted library to the flask with the normal cells (SAE). Incubate at room temperature for 1 hour.

d. Remove the supernatant that contains unbound phage. Place into a labeled 15 mL centrifuge tube (Input Phage). Remove a 10 μL aliquot of input phage into a 0.65 mL microcentrifuge tube for titering.

7) Selection of Phage Binding Target Cells (Calu-3 at room temperature with serum)

a. Replace medium in cell culture flask with 90% confluent cells with 5 mL MEM medium supplemented with 10% FBS. Incubate at room temperature for 1 hour. Remove immediately before application of phage.

b. Add sublibrary to the cell culture flask with target (Calu-3) cells. Incubate at room temperature for 1 hour.

c. Remove the supernatant with non-bound phage. Place into a labeled 15 mL centrifuge tube (Unbound Phage) and store at 4ºC.

d. Wash cells with 4 mL of cold washing buffer for 5 minutes.

e. Remove all of the washing buffer and store in a labeled 15 mL centrifuge tube for titering.

f. Repeat for a total of 10 washes.

g. To elute surface bound phage, incubate cells for 10 minutes on ice with 2 mL of elution buffer. Pipette the eluate into a sterile 15 mL centrifuge tube containing 376 µL of 1M Tris-HCl, pH 9.1 (neutralizing buffer). Remove 20 µL of elute phage and place in a 0.65 mL microcentrifuge tube for titering.

h. Wash cells two times with 4 mL of cold washing buffer for 5 minutes. Remove and collect all of the washing buffer and store in a labeled 15 mL centrifuge tube. Remove 20 µL of each Post Elution Wash (PEW) in a 0.65 mL microcentrifuge tube for titering.

8) Recovery of Cell Penetrating Phage

a. Scrape the cell monolayer from the bottom of the flask with a sterile cell scraper in 5 mL of MEM medium. Collect the cells with a pipette and transfer to a 15 mL centrifuge tube.

b. Centrifuge the cell suspension at 2,000 rpm (Beckman Allegra) for 10 minutes.

c. Remove the supernatant and add 200 µL of lysis buffer to the pellet.

d. Mix the solution thoroughly with a pipette tip to ensure complete destruction of the cell membrane. Allow the solution to incubate at room temperature for approximately 10 minutes.

9) Washing and Concentration of Eluted Phage

a. Pipette 2 mL of 1X TBS into a labeled 100K MWCO Amicon Ultra-4 Concentrator. Centrifuge at 2,000 rpm (Beckman Allegra) for 10 minutes.

b. Apply the mixture of eluate and post elution washes (PEW1 & PEW2) to the concentrator. Centrifuge at 3,000 rpm (Beckman Allegra) for 10 minutes.

c. Add 1 mL of 1X TBS to the concentrators and centrifuge at 3,000 rpm (Beckman Allegra) for 10 minutes. Repeat for a total of three washes. Centrifuge until a volume of <100 µL remains.

d. Collect the concentrated phage by washing 50 µL of 1X TBS down each side of the concentrator. Pipette the entire volume into a 1.7 mL microcentrifuge tube.

10) Amplification of Selected Phage Eluate and Lysate

a. Add an equal volume of starved cells (200 µL) to 200 µL of concentrated phage. Incubate at room temperature for 15 minutes for infection to occur.

b. Add mixture into a 125 mL conical flask with 20 mL NZY/0.2 µg/mL tetracycline. Incubate at 200 rpm, 37ºC in a shaking-incubator for 45 minutes to allow TetR to develop.

c. Add 1 mL of starved cells to the cell lysate. Mix gently and incubate at room temperature for 15 minutes.

d. Add mixture into a 125 mL conical flask with 20 mL NZY/0.2 µg/mL tetracycline. Incubate at 200 rpm, 37ºC in a shaking-incubator for 45 minutes to allow TetR to develop.

e. After 45 minutes of incubation, take 20 µL and 200 µL aliquots from each of the two cultures (step J2 and J4) for titering. Add 20 µL of 20 mg/mL tetracycline to each of the flasks and continue to shake at 200 rpm, 37ºC overnight.

11) Phage Titering

a. To each of the 20 µL aliquots, add 180 µL of NZY/0.2 µg/mL tetracycline and mix.

b. Spread the cell suspensions onto NZY/20 µg/mL tetracycline plates.

c. Incubate plates in incubator at 37ºC overnight.

d. Make the following dilutions in 1X TBS/0.1% Gelatin for titering:

i. Input

Tube #	Dilution	Volume Phage (µL)	TBS/Gelatin (µL)	Total (µL)
1	10^{-1}	10 from stock	90	100
2	10^{-2}	50 from tube 1	450	500
3	10^{-3}	50 from tube 2	450	500
4	10^{-4}	50 from tube 3	450	500
5	10^{-5}	50 from tube 4	450	500

ii. Unbound

Tube #	Dilution	Volume Phage (µL)	TBS/Gelatin (µL)	Total (µL)
1	10^{-1}	10 from stock	90	100
2	10^{-2}	50 from tube 1	450	500
3	10^{-3}	50 from tube 2	450	500
4	10^{-4}	50 from tube 3	450	500
5	10^{-5}	50 from tube 4	450	500

iii. Wash 1 & 2

Tube #	Dilution	Volume Phage (µL)	TBS/Gelatin (µL)	Total (µL)
1	10^{-1}	10 from stock	90	100
2	10^{-2}	50 from tube 1	450	500
3	10^{-3}	50 from tube 2	450	500

iv. Wash 3-10

Tube #	Dilution	Volume Phage (µL)	TBS/Gelatin (µL)	Total (µL)
1	0	10	0	10
2	10^{-1}	50 from tube 1	450	500

v. Post Elution Washes 1 & 2

Tube #	Dilution	Volume Phage (μL)	TBS/Gelatin (μL)	Total (μL)
1	0	10	0	10
2	10^{-1}	10 from tube 1	90	100

e. Mix 10 μL of phage from each dilution with 10 μL of starved cells. Incubate at room temperature for 15 minutes for infection.

f. Add 180 μL of NZY/0.2 μg/mL tetracycline. Incubate in 37ºC incubator for 45 minutes to develop TetR.

g. Spread cell suspension onto NZY/Tetracycline plates. Incubate plates in 37ºC incubator overnight.

12) Purification of Amplified Phage Sublibraries

a. Pour each of the overnight cultures into a 50 mL Oak Ridge tube. Centrifuge at 4,600 rpm (2,915xg; JA-17; Beckman Avanti) for 10 minutes at 4ºC.

b. Pour the supernatants into new 50 mL Oak Ridge tubes. Centrifuge at 9,300 rpm (11,915xg; JA-17; Beckman Avanti) for 10 minutes at 4ºC.

c. Pour the cleared supernatants into new 50 mL Oak Ridge tubes. Add 3 mL of 16.7% PEG/3.3 M NaCl to each of the tubes. Invert ~100 times and store at 4ºC overnight.

d. Centrifuge the tubes at 15,000 rpm (30,996xg; JA-17; Beckman Avanti) for 30 minutes. Do RRR .

e. Add 1 mL 1X TBS to each tube and dissolve the pellet.

f. Transfer the solution into a new 1.7 mL microcentrifuge tube and centrifuge at 13,000 rpm (Beckman Microfuge 18) for 2 minutes.

g. Transfer the supernatant into a new labeled 1.7 mL microcentrifuge tube with 150 μL 16.7% PEG/3.3 M NaCl. Invert the tubes 100 times and store at 4ºC overnight.

h. Centrifuge the tubes at 13,000 rpm (Beckman Microfuge 18) for 10 minutes. Remove the supernatant and do RRR.

i. Dissolve the pellet in 200 μL 1X TBS.

j. Centrifuge at 5,000 rpm (Beckman Microfuge 18) for 1 minute.

k. Transfer the supernatant to a new 1.7 mL microcentrifuge tube. Store at 4ºC.

13) Physical Titer Estimation Using NanoDrop

a. Estimate the concentration by measuring the absorbance of each sample at 269 nm (Blank with 1X TBS) with the NanoDrop. Calculate the concentration of phage according to the following formula:

$$\text{Concentration Phage (vir/mL)} = \text{Abs}_{269} \times 6.5\times10^{12} \quad (13)$$

14) Calculation of Phage Titers and Yield

a. Phage titer is calculated according to the following formula: where N is the number of cfu counted per plate, V is the input volume in µL (10 µL in most cases), and DF is the dilution factor.

$$\text{Titer (cfu/mL)} = \frac{\text{N (cfu)}}{\text{V (µL)}} \times \frac{1000\ \mu\text{L}}{1\ \text{mL}} \times \text{DF} \quad (14)$$

b. The total number of cfu is calculated according to the following:

$$\text{Total CFU (cfu)} = \text{Titer (cfu/mL)} \times \text{Total Volume (mL)} \quad (15)$$

c. The eluate and lysate phage output is calculated as follows: where N is the number of cfu counted per plate, V is the input volume in µL (20 or 200 µL)

$$\text{Output (cfu)} = \frac{\text{N (cfu)}}{\text{V (µL)}} \times \frac{1000\ \mu\text{L}}{1\ \text{mL}} \times \text{Total Volume (mL)} \quad (16)$$

d. The total yield is calculated as follows:

$$\text{Yield (\%)} = \frac{\text{Input (cfu)}}{\text{Output (cfu)}} \times 100\% \quad (17)$$

2.2. Additional Rounds of Selection of Landscape Phage Against Mammalian Cells *in vitro*

Reagents:

- Phage Sublibraries: f8/8R1E and f8/8R1L or f8/9R1E and f8/9R1L (from first round)
- Control Phage: f8-5 ($2x10^{12}$ vir/mL)
- K91BlueKan *E. coli* Starved Cells
- Minimum Essential Medium (MEM) w/ Earle's Balanced Salts, Nonessential Amino Acids & Sodium Pyruvate, 500mL: (ATCC #302003)
- NZY/Tetracycline (20 µg/mL) Plates, 60
- 1M Tris-HCl, pH 9.1: (100 mL)
- Elution Buffer: (100 mL)
    - Dissolve 1.5 g glycine in 90 mL of distilled water.
    - Adjust the pH to 2.2 with 2 N HCl.

- Add 100 mg BSA (Sigma #A2153-100G) and 10 mg phenol red (Sigma #P-2417-5G).
- Add water to bring the solution to 100 mL.
- Filter sterilize and store at 4ºC.

- Lysis Buffer (2% w/v Sodium Desoxycholate/10 mM Tris-HCl/2 mM EDTA): (50 mL)
  - Dissolve 1 g sodium desoxycholate (Fisher #S285-100) and 0.06 g Tris base into 40 mL of distilled water.
  - Add 200 µL 0.5 M EDTA and mix.
  - Adjust the pH to 8.0 with 2 N HCl .
  - Add water to bring the solution to 50 mL.
  - Filter sterilize and store at 4ºC.
- Washing Buffer (0.1% Tween 20/0.5% BSA/MEM Medium): (100 mL)
  - Add 500 µL 20% Tween 20 and 10 mL 5% BSA to 90 mL of MEM medium.
  - Mix thoroughly, filter sterilize and store at 4ºC.
- Blocking Buffer (0.5% BSA/MEM medium): (100 mL)
  - Add 10 mL 5% BSA to 90 mL MEM medium.
  - Mix thoroughly, filter sterilize and store at 4ºC.

Materials:

- 25 cm^2 Cell Culture Flasks: (Corning #430168)
- Amicon Ultra-4 100K MWCO Centrifugal Filters: (Fisher #UFC810024)
- 15 mL Centrifuge Tubes: (Corning)
- 1.7 mL Microcentrifuge Tubes:

Equipment:

- Avanti J-26 XP Centrifuge: (Beckman Coulter)
- I2500 Series Shaker-Incubator: (New Brunswick)
- Microfuge 18 Centrifuge: (Beckman Coulter)

Procedures:

Day 1

1) Prepare mammalian cells lines for selection

a. Prepare a culture of target cells and normal cells (e.g. Calu-3 and Small Airway Epithelial Cells) in a 25 cm^2 cell culture flask.

b. Continue to grow cells until they have reached 90% confluence.

Day 2

2) Prepare Starved Cells and Check Starved Cells

a. Prepare 4 flasks of starved K91BlueKan E. coli cells as described in the lab manual. Resuspend in 1 mL of NAP buffer.

b. Check starved cells and titer control phage f8-5 as described in the lab manual.

3) Selection of Phage Binding Target Cells (Calu-3 at 37ºC with serum)

a. Replace medium in cell culture flask with 90% confluent cells with 5 mL MEM medium supplemented with 10% FBS. Incubate at 37ºC in CO2 incubator for 1 hour. Remove immediately before application of phage.

b. Add 2 mL of MEM medium supplemented with 10% FBS to the flask. Add 10^{10} cfu (~10^{11} virions) of each sublibrary from round one to the cell culture flask with target cells. Incubate in 37ºC CO2 incubator for 1 hour.

c. Remove the supernatant with non-bound phage. Place into a labeled 15 mL centrifuge tube (Unbound Phage) and store at 4ºC.

d. Wash cells with 4 mL of cold washing buffer for 5 minutes.

e. Remove all of the washing buffer and store in a labeled 15 mL centrifuge tube for titering.

f. Repeat for a total of 10 washes.

g. To elute surface bound phage, incubate cells for 10 minutes on ice with 2 mL of elution buffer. Pipette the eluate into a sterile 15 mL centrifuge tube containing 376 µL of 1M Tris-HCl, pH 9.1 (neutralizing buffer). Remove 20 µL of elute phage and place in a 0.65 mL microcentrifuge tube for titering.

h. Wash cells two times with 4 mL of cold washing buffer for 5 minutes. Remove and collect all of the washing buffer and store in a labeled 15 mL centrifuge tube. Remove 20 µL of each Post Elution Wash (PEW) in a 0.65 mL microcentrifuge tube for titering.

4) Recovery of Cell Penetrating Phage

a. Scrape the cell monolayer from the bottom of the flask with a sterile cell scraper in 5 mL of MEM medium. Collect the cells with a pipette and transfer to a 15 mL centrifuge tube.

b. Centrifuge the cell suspension at 2,000 rpm (Beckman Allegra) for 10 minutes.

c. Remove the supernatant and add 200 µL of lysis buffer to the pellet.

d. Mix the solution thoroughly with a pipette tip to ensure complete destruction of the cell membrane. Allow the solution to incubate at room temperature for approximately 10 minutes.

5) Washing and Concentration of Eluted Phage

a. Pipette 2 mL of 1X TBS into a labeled 100K MWCO Amicon Ultra-4 Concentrator. Centrifuge at 2,000 rpm (Beckman Allegra) for 10 minutes.

b. Apply the mixture of eluate and post elution washes (PEW1 & PEW2) to the concentrator. Centrifuge at 3,000 rpm (Beckman Allegra) for 10 minutes.

c. Add 1 mL of 1X TBS to the concentrators and centrifuge at 3,000 rpm (Beckman Allegra) for 10 minutes. Repeat for a total of three washes. Centrifuge until a volume of <100 µL remains.

d. Collect the concentrated phage by washing 50 µL of 1X TBS down each side of the concentrator. Pipette the entire volume into a 1.7 mL microcentrifuge tube.

6) Amplification of Selected Phage Eluate and Lysate

a. Add an equal volume of starved cells (200 µL) to 200 µL of concentrated phage. Incubate at room temperature for 15 minutes for infection to occur.

b. Add mixture into a 125 mL conical flask with 20 mL NZY/0.2 µg/mL tetracycline. Incubate at 200 rpm, 37ºC in a shaking-incubator for 45 minutes to allow TetR to develop.

c. Add 1 mL of starved cells to the cell lysate. Mix gently and incubate at room temperature for 15 minutes.

d. Add mixture into a 125 mL conical flask with 20 mL NZY/0.2 µg/mL tetracycline. Incubate at 200 rpm, 37ºC in a shaking-incubator for 45 minutes to allow TetR to develop.

e. After 45 minutes of incubation, take 20 µL and 200 µL aliquots from each of the two cultures for titering. Add 20 µL of 20 mg/mL tetracycline to each of the flasks and continue to shake at 200 rpm, 37ºC overnight.

7) Phage Titering

a. To each of the 20 µL aliquots, add 180 µL of NZY/0.2 µg/mL tetracycline and mix.

b. Spread the cell suspensions onto NZY/20 µg/mL tetracycline plates.

c. Incubate plates in incubator at 37ºC overnight.

d. Make the following dilutions in 1X TBS/0.1% Gelatin for titering:

i. Unbound

Tube #	Dilution	Volume Phage (µL)	TBS/Gelatin (µL)	Total (µL)
1	10^{-1}	10 from stock	90	100
2	10^{-2}	50 from tube 1	450	500
3	10^{-3}	50 from tube 2	450	500
4	10^{-4}	50 from tube 3	450	500
5	10^{-5}	50 from tube 4	450	500

ii. Wash 1 & 2

Tube #	Dilution	Volume Phage (µL)	TBS/Gelatin (µL)	Total (µL)
1	10^{-1}	10 from stock	90	100
2	10^{-2}	50 from tube 1	450	500
3	10^{-3}	50 from tube 2	450	500

iii. Wash 3-10

Tube #	Dilution	Volume Phage (µL)	TBS/Gelatin (µL)	Total (µL)
1	0	10	0	10
2	10^{-1}	50 from tube 1	450	500

iv. Post Elution Washes 1 & 2

Tube #	Dilution	Volume Phage (µL)	TBS/Gelatin (µL)	Total (µL)
1	0	10	0	10
2	10^{-1}	10 from tube 1	90	100

e. Mix 10 µL of phage from each dilution with 10 µL of starved cells. Incubate at room temperature for 15 minutes for infection.

f. Add 180 µL of NZY/0.2 µg/mL tetracycline. Incubate in 37ºC incubator for 45 minutes to develop TetR.

g. Spread cell suspension onto NZY/Tetracycline plates. Incubate plates in 37ºC incubator overnight.

Day 4

8) Grid Individual Colonies for Sequence Analysis

a. Using a toothpick, touch single colonies and transfer to NZY/Tetracycline plates with 100 count grids. Collect clones from each of the eluate, post-elution wash, and lysate fractions.

b. Incubate plates in 37ºC incubator overnight.

9) Purification of Amplified Phage Sublibraries

a. Pour each of the overnight cultures into a 50 mL Oak Ridge tube. Centrifuge at 4,600 rpm (2,915xg; JA-17; Beckman Avanti) for 10 minutes at 4ºC.

b. Pour the supernatants into new 50 mL Oak Ridge tubes. Centrifuge at 9,300 rpm (11,915xg; JA-17; Beckman Avanti) for 10 minutes at 4ºC.

c. Pour the cleared supernatants into new 50 mL Oak Ridge tubes. Add 3 mL of 16.7% PEG/3.3 M NaCl to each of the tubes. Invert ~100 times and store at 4ºC overnight.

Day 5

d. Centrifuge the tubes at 15,000 rpm (30,996xg; JA-17; Beckman Avanti) for 30 minutes. Do RRR .

e. Add 1 mL 1X TBS to each tube and dissolve the pellet.

f. Transfer the solution into a new 1.7 mL microcentrifuge tube and centrifuge at 13,000 rpm (Beckman Microfuge 18) for 2 minutes.

g. Transfer the supernatant into a new labeled 1.7 mL microcentrifuge tube with 150 µL 16.7% PEG/3.3 M NaCl. Invert the tubes 100 times and store at 4ºC overnight.

Day 6

h. Centrifuge the tubes at 13,000 rpm (Beckman Microfuge 18) for 10 minutes. Remove the supernatant and do RRR .

i. Dissolve the pellet in 200 µL 1X TBS.

j. Centrifuge at 5,000 rpm (Beckman Microfuge 18) for 1 minute.

k. Transfer the supernatant to a new 1.7 mL microcentrifuge tube. Store at 4ºC.

10) Physical Titer Estimation Using NanoDrop

a. Estimate the concentration by measuring the absorbance of each sample at 269 nm (Blank with 1X TBS) with the NanoDrop. Calculate the concentration of phage according to the following formula:

$$\text{Concentration Phage (vir/mL)} = \text{Abs}_{269} \times 6.5\times10^{12} \quad (18)$$

11) Calculation of Phage Titers and Yield

a. Phage titer is calculated according to the following formula: where N is the number of cfu counted per plate, V is the input volume in µL (10 µL in most cases), and DF is the dilution factor.

$$\text{Titer (cfu/mL)} = \frac{\text{N (cfu)}}{\text{V (µL)}} \times \frac{1000\ \mu\text{L}}{1\ \text{mL}} \times \text{DF} \quad (19)$$

b. The total number of cfu is calculated according to the following:

$$\text{Total CFU (cfu)} = \text{Titer (cfu/mL)} \times \text{Total Volume (mL)} \quad (20)$$

c. The eluate and lysate phage output is calculated as follows: where N is the number of cfu counted per plate, V is the input volume in µL (20 or 200 µL)

$$\text{Output (cfu)} = \frac{\text{N (cfu)}}{\text{V (µL)}} \times \frac{1000\ \mu\text{L}}{1\ \text{mL}} \times \text{Total Volume (mL)} \quad (21)$$

d. The total yield is calculated as follows:

$$\text{Yield (\%)} = \frac{\text{Input (cfu)}}{\text{Output (cfu)}} \times 100\% \quad (22)$$

2.3. PCR Identification of gpVIII Major Coat Protein Sequence

Reagents:

- Primers: (Integrated DNA Technologies)
  - f8s-20 (10 pmol/µL): 5'-CAAAGCCTCCTAGCCGTTG-3'
    - MW = 6,078 g/mol
    - 60% GC content
    - Tm = 59.5ºC
  - f8as-20 (10 pmol/µL): 5'-CATTCCACAGACAGCCCTCA-3'
    - MW = 5,991 g/mol
    - 55% GC content
    - Tm = 58ºC
  - S20 (50 ng/µL f8s-20 for sequencing)
- DNA Taq Polymerase
- GoGreen Mix
- 100 mM dNTPs
- 25 mM $MgCl_2$
- Agarose

- 1X TBE
- 100 bp DNA Ladder
- 6X Loading Dye
- 10,000X SYBR Green

Materials:

- PCR Plate with Strip Caps
- Parafilm

Equipment:

- Thermal cycler
- Dark Reader/Kodak Imaging System
- Beckman Microfuge 18: (Beckman)

Procedures:

1) Suspend a colony of infected cells into 100 µL DNAse-free water using a toothpick.
2) Thaw 5X Mg-free buffer, primer f8s-20, primer f8as-20, 25 mM MgCl2, and 2.5 mM dNTPs on ice. Mix the following calculated amount of reagents into a 1.7 mL microcentrifuge tube:

Order	Reagent	Volume per Colony (µL)	Final Concentration	Volume per Master Mix (55rxn) (µL)
1	5X Mg-free Buffer	5	1X	275
2	Water	14.36		789.8
3	25 mM $MgCl_2$	2	2 mM	110
4	2.5 mM dNTPs	2	0.2 mM	110
5	10 pmol/µL f8s-20	0.3	0.12 pmol/µL	16.5
6	10 pmol/µL f8as-20	0.3	0.12 pmol/µL	16.5
7	5 U/µL Taq Polymerase	0.04	0.008 U/µL	2.2
	Total Volume (µL)	**24**	**1X**	**1320**

3) Add 24 µL of Master Mix (from step A3) in a 0.2 mL PCR tube. Add 1 µL of diluted phage solution and mix thoroughly.
4) Program the thermocycler with the following program “Phage PCR”:

Temp (ºC)	Time	# Cycles
94	3 min	x1
94	10 sec	x35
46	20 sec	
72	45 sec	
72	4 min	x1
4	∞	x1

5) Store PCR products at -20ºC until analyzed.

6) Prepare a 2% Agarose Gel

   a. Weigh 0.7 g agarose into a 125 mL flask and add 35 mL 1X TBE.

   b. Microwave at power level 3 for 3 minutes.

   c. Let stand until cool to the touch, add 5 µL 10,000X SYBR Green and swirl to mix.

   d. Pour the solution into the gel apparatus and allow the solution to stand for 30 minutes to solidify completely.

7) On a clean piece of parafilm, place 1 µL 5X loading dye, 4 µL of PCR product. Mix the samples thoroughly.

8) Load the DNA samples into the gel. If using multiple rows per gel, load one row and allow the gel to run at 70V for 2 minutes.

9) Run the gel at 70 V/400 mAmps for 45 minutes in 1X TBE buffer.

10) Remove the gel from the gel apparatus and place on the plastic sheet for imaging.

11) Gel is illuminated on the dark reader (Clare Chemical Research) and bands visualized using a Kodak EDAS 290 imaging system (Eastman Kodak).

2.4. Phage Capture Assays

Reagents:

- K91BluKan E. coli Starved Cells
- Control Phage: f8-5 Phage: ($2.0x10^{12}$ vir/mL)
- Select Phage Clones
- EMEM Complete Medium (EMEM w/ 10% FBS & 1% Ab/Am)
- F-12K Complete Medium (F-12K w/ 10% FBS & 1% Ab/Am)
- NZY/Tet plates

- NZY Medium
- Tetracycline Stock (20 mg/mL)
- Kanamycin Stock (100 mg/mL)
- CHAPS Lysis Buffer (2.5% CHAPS/0.5% BSA in EMEM)
- EMEM Blocking Buffer (0.5% BSA in EMEM), 50 mL:
- EMEM Washing Buffer (0.5% BSA/0.1% Tween 20 in EMEM), 250 mL:

Materials:

- Pipette Tips, 1 mL
- Pipette Tips, 0.2 mL
- Pipette Tips, 0.02 mL
- Microcentrifuge tubes, 0.65 mL: (VWR)
- Culture Tubes w/ snap-cap, 13 mL: (Sarstedt #62.515.006)
- Toothpicks, sterile
- Sidearm Flask, 300 mL: (Bellco)
- Oak Ridge Tubes, 50 mL

Equipment:

- I2500/C25 Shaker-Incubator: (New Brunswick)
- Spectrophotometer, Genesys 20: (Thermo Scientific)
- Vortex
- Centrifuge, Avanti J-26 XP: (Beckman Coulter)
- 37ºC Incubator

Procedures:

Day 1

1) Prepare 3 flasks of starved K91BluKan E. coli cells and check infectivity.
2) Subculture cell lines when they reach ~90% confluence and determine the number of viable cells using trypan blue staining and counting with a hemocytometer.
3) Seed $5.0x10^4$ cells into 100 µL of appropriate cell culture medium into each of the wells in a 96-well cell culture treated plate

4) Incubate the plate at 37ºC in a cell culture incubator with 5% CO2 overnight.

Day 2

5) Aspirate the medium from each of the wells using the vacuum on gentle suction.
6) Wash cells with 100 µL of serum-free EMEM in each well and aspirate.
7) Add 100 µL of serum-free EMEM into each of the wells and incubate in a 37ºC incubator with 5% CO_2 for 1 hour. Remove the medium by aspiration before application of phage clones.
8) Calculate and prepare 1.5 mL input solutions containing $1x10^7$ CFU/mL (~$2.0x10^8$ vir/mL) in EMEM blocking buffer for each phage.
9) Add 100 µL of the input solutions prepared above to input $1.0x10^6$ CFU (~$2.0x10^7$ vir) to each well in blocking buffer. Incubate at 37ºC for 1 hour.
10) Carefully remove the blocking buffer containing unbound phage from each of the wells by vacuum aspiration.
11) Wash the cells 8 times with 100 µL of cold EMEM washing buffer for 5 minute intervals. Use a vacuum to carefully aspirate the medium from the wells.
12) Add 25 µL of CHAPS lysis buffer to each well and incubate the plate on a shaker at room temperature for 10 minutes.
13) Add 125 µL of starved cells and incubate at room temperature for 15 minutes.
14) Add 180 µL of NZY/Tet (0.4 µg/mL) to each well and incubate in an incubator at 37ºC for 45 minutes to develop TetR.
15) Spread 200 µL of cell suspensions onto NZY/Tet (20 µg/mL) plates.
16) Incubate in 37ºC incubator overnight.

Day 3

17) Count colonies and calculate phage yield as follows:

$$\text{Yield (\%)} = \left(\frac{\text{Output CFU}}{\text{Input CFU}}\right) \times 100 \qquad (23)$$

3. Phage Protein Techniques

3.1. Isolation of pVIII Major Coat Protein from Intact Phage Particles

Functional phage major coat protein can be solubilized and isolated in either detergent (cholate) or an organic solvent (2-propanol) for a number of downstream applications including insertion into preformed liposomes.

3.1.1. Cholate Solubilization

Reagents:

- Cholate Solubilizing Solution (120 mM cholate/10 mM Tris-HCl/0.2 mM EDTA, pH 8.0)
- Chloroform: (Fisher, BP1145-1)
- Phage for protein isolation: (>10^{13} vir/mL)
- Running Buffer (10 mM cholate/10 mM Tris-HCl/0.2 mM EDTA, pH 8.0)

Materials:

- 1.7 mL Microcentrifuge Tubes
- 5 mL Snap-cap Tubes
- 1 mL Syringe
- 19G Needle

Equipment:

- Sepharose 6B-CL Chromatography Column (30 × 1 cm)
- Bio-Rad Chromatography System

Procedures:

Day 1

1) Dilute phage to a final concentration of 2.7×10^{13} vir/mL (3.0×10^{13} virions in 350 µL in 1X TBS).
2) In a new 1.7 mL microcentrifuge tube, add 350 µL of phage dilution, 700 µL of cholate solubilizing solution, and 27 µL chloroform. Mix by vortexing.
3) Incubate in an incubator at 37ºC overnight with gentle rotation.

Day 2

4) Equilibrate the sepharose chromatography column with running buffer for 1 hour or until a stable baseline has been obtained. Flow rate should be set at 0.5 mL/min and the AUFS should be set at 0.2.

5) Apply 1 mL of the phage sample to the column through the injection port.

6) Collect the fractions. Fractions should be collected every 5 minutes and stored at 4ºC. Allow the sample to completely run off the column and allow running buffer to flow through until a stable baseline has returned.

3.1.2. 2-propanol Solubilization

Reagents:

- Phage (>10^{13} vir/mL)
- TBS, pH 7.4 (1X)
- Isopropanol/2-propanol:
- Chloroform: (Fisher #BP1145-1)

Materials:

- 1.7 mL Microcentrifuge Tubes

Procedures:

1) Transfer (>3x10^{13} virions) to a new 1.7 mL microcentrifuge tube. Add 1X TBS to reach 250 µL, 750 µL of 100% isopropanol and 27 µL of chloroform.
2) Vortex vigorously to mix.
3) Centrifuge at 13,000 rpm (Beckman Microfuge 18) for 5 minutes.
4) Transfer the upper organic phase to a new 1.7 mL microcentrifuge tube.
5) Measure the absorbance at 260 & 280 nm using NanoDrop.

3.2. SDS-PAGE and Western Blot Analysis of fd Phage Proteins

Reagents:

- 1X PBS/0.05% Tween 20 Washing Buffer: 1L
- 1X Protein-free PBS/0.05% Tween 20 Blocking Buffer: 1L
- 3.3mg/mL Polyclonal anti-fd N-terminal Antibody:
- 1.8mg/mL IgG Affinity Purified anti-fd C-terminal Antibody:
- 1.3mg/mL Biotinylated SP-conjugated Affinitipure Goat antirabbit IgG:
- 0.85mg/mL NeutraAvidin-HRP:
- West Pico Luminol/Enhancer Solution: (Pierce #34085)

- West Pico Stable Peroxide Solution: (Pierce #34085)
- 1X Tris/Glycine/SDS Buffer: 1L
    - To a 1L bottle add 100mL of 10X Tris/Glycine/SDS buffer (BioRad #161-0732)
    - Dilute to 1L by adding 900mL of distilled water
    - Mix thoroughly, no need to autoclave
- 2X Laemmli Sample Buffer: 1mL
- Methanol: (Fisher #A454-4L)
- 1X Tris/Glycine Transfer Buffer: 1L
    - Measure 100mL 10X Tris/Glycine Buffer (BioRad #161-0734) into a 1L bottle
    - Add 200mL Methanol and 700mL of distilled water and mix
    - Refrigerate at 4ºC
- Biotinylated SDS-PAGE Broad Range Standards Marker: (BioRad #161-0319)

Materials:

- 0.65mL Microcentrifuge Tubes:
- 0.2µm Immu-Blot PDVF Transfer Membrane: (BioRad #162-0174)
- 4-20% Tris-HCl Ready Gels, 15-well/15µL: (BioRad #161-1123)
- Filter Paper: (BioRad #170-3932)
- Fiber Pads: (BioRad #170-3933)

Equipment:

- Mini Trans-Blot Transfer Cell: (BioRad #170-3930)

Procedures:

Day 1

1) To prepare the biotinylated protein standard marker, dilute 1µL of stock protein standard marker with 9µL of distilled water.
2) To each of the samples (30 µL sample) add 30µL of 2X Lammeli sample buffer. Mix thoroughly and incubate at 95ºC for an hour. After incubation, briefly spin down the sample to ensure that no water has condensed in the top of the microcentrifuge tube and briefly mix.

3) Rinse a 15 well/15µL 4-20% Tris-HCl Ready Gel with distilled water and place into the Mini Gel apparatus. Rinse a 10 well/50µL 4-20% Tris-HCl Ready gel with distilled water and place into the Mini Gel apparatus. Fill the upper and lower chambers with 1X Tris/Glycine/SDS running buffer.
4) Pre-electrophoresis the two gels by running them at 100V (~50mAmp for 2 gels) for 15 min.
5) Load 7µL of the biotinylated protein standard marker prepared into each of the Tris-HCl gels. Load 12µL of each of the protein/modified Doxil samples prepared into the 15 well Tris-HCl gel. Load 40µL of each of the protein/modified Doxil samples into the 50µL Tris-HCl gel.
6) Electrophoresis the gels at 100V (~50mAmp for 2 gels) for 45 min. Ensure the amperage doesn't drop below 11mAmp. If the running conditions reach 11mAmps check the buffer level in the upper buffer chamber. If the buffer is low, fill the upper buffer chamber with 1X Tris/Glycine/SDS buffer to cover the top of the gels.
7) Western Blot with fd-tet N-terminal and C-terminal Specific Antibodies
    a. Soak 4 fiber pads and 4 pieces of filter paper in 1X Tris/Glycine transfer buffer at 4ºC until use.
    b. Soak two 0.2µm PVDF transfer membranes in 100% methanol for 15 sec. Remove the methanol and wash with distilled water for 2 min. Remove the distilled water and wash with 1X Tris/Glycine transfer buffer and store at 4ºC until being used.
    c. After electrophoresis, disassemble the mini gel apparatus. Split the gel cassettes and discard the top plastic portion of the apparatus. Submerge the gel in 1X Tris/Glycine transfer buffer for ~15 min to prevent osmotic changes during protein transfer.
    d. Assemble the transfer cassette as follows building up from the black side of the transfer cartridge: fiber pad, filter paper, SDS-PAGE gel, transfer membrane, filter paper, fiber pad. Before closing the cartridge use a 5mL culture tube to remove any air bubbles trapped between the gel and the transfer membrane. Close the transfer cartridge and place in the transfer apparatus with the black side of the cartridge facing the black face of the transfer apparatus. Place the white ice block into the transfer apparatus. Fill the transfer apparatus with 1X Tris/Glycine transfer buffer to the bottom edge of the ice block.
    e. Place the transfer apparatus into the cold room. Electroblot the gel at 100V (~180mAmp for 2 gels) for 30 min.

f. Disassemble the transfer cassettes and place the transfer membranes into 10-15mL of 1X Protein-free PBS/0.05% Tween 20 blocking buffer. Discard the SDS-PAGE gel and the filter paper. Incubate the 15 well gel at 4ºC overnight in blocking buffer with gentle agitation on a rocker. Incubate the 10 well gel at room temperature for 2 hours in blocking buffer with gentle agitation on a rocker.

g. Prepare a dilution of the 1.8mg/mL IgG affinity purified anti-fd C-terminal antibody by diluting 100µL of stock antibody into 10mL of 1X protein-free PBS/0.05% Tween 20 blocking buffer. Remove the blocking buffer from the 10 well gel and pour the above solution on the membrane. Incubate at 4ºC overnight with gentle agitation on a rocker.

Day 2

h. Prepare a dilution of the 3.3mg/mL polyclonal anti-fd N-terminal antibody by diluting 2.7µL of stock antibody in 15mL of 1X Protein-free PBS/0.05% Tween 20 blocking buffer. Remove the blocking buffer from the 15 well gel and pour the above solution on the membrane. Incubate at room temperature for 1 hour with gentle agitation on a rocker.

i. Wash both membranes five times with ~15mL of 1X PBS/0.05% Tween 20 with 5 min incubations at room temperature with gentle agitation on a rocker.

j. Prepare a dilution of biotinylated-SP-conjugated affinipure goat antirabbit IgG by diluting 1µL of stock antibody in 30mL of 1X Protein-free PBS/0.05% Tween 20 blocking buffer. Remove the washing buffer and pour 15mL of the above solution on each of the membranes. Incubate at room temperature for 1 hour with gentle agitation on a rocker.

k. Wash both membranes five times with ~15mL of 1X PBS/0.05% Tween 20 with 5 min incubations at room temperature with gentle agitation on a rocker.

l. Prepare a dilution of NeutraAvadin-HRP by diluting 0.83µL of AV-HRP with 30mL of 1X Protein-free PBS/0.05% Tween 20 blocking buffer. Remove the washing buffer and pour 15mL of the above solution on each of the membranes. Incubate at room temperature for 1 hour with gentle agitation on a rocker.

m. Wash both membranes five times with ~15mL of 1X PBS/0.05% Tween 20 with 5 min incubations at room temperature with gentle agitation on a rocker.

n. Remove the washing buffer and add 5mL of peroxide solution and 5mL of luminol/enhancer solution to each membrane. Incubate at room temperature for 10 min with gentle agitation on a rocker.

o. Remove the membrane from the developer solution and allow the excess to drip off the membrane.

p. Image membrane with C-DiGit Chemiluminescent reader.

4. Modification and Characterization of Phage-based Nanomedicines

4.1. Insertion of Isolated Major Coat Protein into Liposomes

1) Calculation of Components

a. Calculate the desired percentage of protein to lipid concentration and the subsequent amount of protein to be added based on the following formula. Typical insertions use 0.5% protein, which corresponds to a protein:lipid ratio of 1:200. Using 450µL of 2mg/mL Doxil corresponds to a total lipid mass of 7200µg. The amount of protein can be calculated as follows:

$$\text{Mass of protein } (\mu g) = 7200\ \mu g \text{ lipid} \times \text{percent protein} \tag{24}$$

b. Obtain the 1 A(280) conversion factor calculated in Protean (v 4.03, DNAStar, Inc) using the full length pVIII protein sequence. This conversion factor is specific for each phage coat protein. Measure the absorbance at 280nm of isolated coat protein using the NanoDrop. Use the following formula to determine the concentration of protein:

$$\text{Concentration of protein } (\mu g/mL) = A(280nm) \times \text{conversion factor } (mg/mL) \times \frac{1000\ \mu g}{1\ mg} \tag{25}$$

c. Determine the volume of protein. Note: For an insertion using 0.5% protein, the concentration of phage coat protein must be >72µg/mL

$$\text{Volume protein } (\mu L) = \frac{\text{mass of protein } (\mu g)}{\text{concentration of protein } (\mu g/mL)} \times \frac{1000\ \mu L}{1\ mL} \tag{26}$$

d. Determine the amount of 200mM sodium cholate to add to the solution to obtain a final concentration of 15mM with the following formula:

$$\text{Volume cholate } (\mu L) = \frac{[15\ mM \times \text{Total Volume } (\mu L)] - [\text{Volume Protein } (\mu L) \times \text{Concentration cholate in protein solution } (mM)]}{\text{Stock cholate } (mM)} \tag{27}$$

e. Determine volume of 1X TBS, pH ~7.4 to add to solution to obtain 1mL using the following formula:

Volume TBS (µL)=1000 µL-Volume Doxil (µL)- Volume Protein (µL)- Volume Cholate (µL) (28)

4.1.1. Cholate Dialysis Method

Reagents:

- 2mg/mL Doxil: 450µL (Ortho Biotech
- Isolated pVIII Coat Protein: prepare isolated coat protein as in laboratory manual in 10mM cholate/10mM Tris-HCl, pH 8.0/0.2mM EDTA buffer
- 200mM Sodium cholate: 1L
    - Measure 86.11g of sodium cholate hydrate (Sigma #C6445-500G)
    - Add to 700mL of distilled water
    - Mix well and dilute to 1L with distilled water
    - Mix again and place in a 1L bottle and autoclave/sterile filter as needed
- 1X TBS: 1L

Materials:

- Slide-A-Lyzer Dialysis Cassette (10,000 MWCO): (Pierce #66380)
- 1.7mL Microcentrifuge Tubes
- 20ga Needles
- 5cc Syringes
- 1cc Syringes
- 1L Beaker

Equipment:

- Stir Bar & Magnetic Stir Plate
- 37ºC Incubator

Procedures:

Day 1

1) Add the calculated amounts of the following solutions in this order: Doxil, 1X TBS, cholate, isolated coat protein in a 1.7mL microcentrifuge tube and vortex.
2) Adjust the buffer conditions as needed for the experiment (pH, salt solutions, etc.) Note: This step is commonly omitted as insertions should occur in 1X TBS, pH ~7.4 as a buffer.

a. Hydrate a Slide-A-Lyzer dialysis cassette membrane by immersing it into the buffer adjusted to the correct pH and adding cholate to make the solution buffer 15mM cholate for 1-2 min.
b. Fill a 1mL syringe with the Doxil solution.
c. Insert the needle into one of the syringe ports on the top corner of the dialysis cassette. Be careful not to puncture the membrane and inject the sample into the dialysis cassette.
d. Turn the cassette to allow the sample to be at the bottom of the cassette and retract the plunger on the syringe to remove as much air as possible, while leaving the sample in the cassette. Remove the syringe from the cassette.
e. Place the dialysis cassette into the dialysis buffer containing 15mM cholate. Place the beaker with a stirbar on a stir plate and mix gently for 1 hour at room temperature.
f. Remove the sample from the dialysis cassette. Inject approximately 2mL of air into the dialysis cassette. Turn the cassette to allow the Doxil sample to collect at the end with the needle. Retract the syringe plunger to remove the sample. Remove the needle from the cassette.

3) Place the sample in a 1.7mL microcentrifuge tube. Incubate the sample in a rotator at 37ºC overnight.

Day 2

4) Prepare 1L of 10mM cholate/1X TBS dialysis buffer (950mL 1X TBS, pH 7.4 + 50mL 200mM cholate)
5) Hydrate a dialysis cassette in the 10mM cholate/1X TBS dialysis buffer for 1 min.
6) Fill a syringe with the modified Doxil sample
7) Insert the needle into one of the syringe ports on the top corner of the dialysis cassette. Be careful not to puncture the membrane and inject the sample into the dialysis cassette.
8) Turn the cassette to allow the sample to be at the bottom of the cassette and retract the plunger on the syringe to remove as much air as possible, while leaving the sample in the cassette. Remove the syringe from the cassette.
9) Place the dialysis cassette into the 10mM cholate/1X TBS, pH 7.4 dialysis buffer, place on a stir plate and mix at room temperature with gentle stirring for 1 hour.

10) Prepare 1L of 5mM cholate/1X TBS, pH 7.4 dialysis buffer (975mL 1X TBS, pH 7.4 + 25mL 200mM cholate). Remove the dialysis cassette from the 10mM cholate buffer and place it into the 5mM cholate buffer, incubate at room temperature with gentle stirring for 1 hour.

11) Prepare 1L of 1X TBS, pH 7.4 dialysis buffer. Remove the dialysis cassette from the 5mM cholate dialysis buffer and place it into the 1X TBS buffer, incubate at room temperature with gentle stirring for 1 hour. Change the 1X TBS buffer and incubate at room temperature with gentle stirring for 1 hour. Change the 1X TBS buffer again and incubate at 4ºC with gentle stirring overnight.

Day 3

12) Remove the sample from the dialysis cassette. Inject approximately 2mL of air into the dialysis cassette. Turn the cassette to allow the Doxil sample to collect at the end with the needle. Retract the syringe plunger to remove the sample. Remove the needle from the cassette.

13) Place the sample into a 1.7mL microcentrifuge tube.

4.1.2. 2-Propanol Insertion Method

Reagents:

- Phage protein isolated in 75% 2-propanol/25% 1X TBS
- Lipodox
- 1X TBS, pH 7.4

Materials:

- 0.65 mL microcentrifuge tubes

Equipment:

- Vortex
- 37ºC Incubator

Procedures:

1) To each of the labeled 0.65 mL microcentrifuge tubes, add 45 µL of 2 mg/mL Lipodox.
2) Add 2.8 µL of phage protein isolated in 2-propanol and pipette vigorously to mix.
3) Vortex vigorously upon addition.
4) Add 55 µL 1X TBS to each sample and vortex.
5) Incubate the samples at 37ºC with gentle rotation for at least 7 hours and purify as needed.

4.2. Purification of Phage Protein-Modified Liposomes

4.2.1. Size Exclusion Chromatography

Reagents:

- Running Buffer (10 mM Tris-HCl/0.2 mM EDTA, pH 8.0)
- Sample to be purified

Materials:

- 1.7 mL Microcentrifuge Tubes
- 5 mL Snap-cap Tubes
- 1 mL Syringe
- 19G Needle

Equipment:

- Superose Chromatography Column (30 × 1 cm)
- Bio-Rad Chromatography System

Procedures:

1) Equilibrate the column with running buffer (10 mM Tris-HCl, pH 8.0/0.2 mM EDTA) and allow the baseline to become stable. Once the baseline is stable, autozero the meter view program and the UV Monitor.
2) Load 1mL of the phage-DOXIL pH7.5 into the injection port.
3) Run the sample through the column with 0.25mL/min running buffer collecting fractions every 10min using the fraction collector in 15mL snapcap tubes. The UV monitor was set at an AUFS of 0.1 to detect the presence of sample.
4) Column was run for ~2.5 hours collecting fractions. Once the run was complete the column was allowed to purge for 1hour before running the next sample.
5) Fractions were stored at 4°C for further analysis.

4.2.2. Ultrafiltration Cassettes

Reagents:

- Ethanol (70%), 10 mL

Materials:

- Microcentrifuge tubes, sterile, 1.7 mL
- NanoSep Filter Devices, 100K (Pall #OD100C34)

Equipment:

- Microfuge 18 Centrifuge: (Beckman Coulter)

Procedures:

1) To a labeled 100K NanoSep centrifugal filter device, add 100 µL 70% ethanol to sterilize.
2) Centrifuge tubes at 14,000 x g (Beckman Microfuge 18; ~12,000 rpm) for 5 minutes.
3) Add 200 µL of sterile dH2O to rinse the device and centrifuge at 14,000 x g (Beckman Microfuge 18; ~12,000 rpm) for 5 minutes.
4) Remove the flow through and discard.
5) Transfer appropriate sample to the labeled 100K NanoSep centrifugal filter device.
6) Add 300 µL of 1X PBS to each sample and mix gently.
7) Centrifuge samples at 14,000 x g (Beckman Microfuge 18; ~12,000 rpm) for 10 minutes.
8) Remove the flow through (free doxorubicin) and return the filter to the tube.
9) Add 300 µL of 1X PBS to each sample again and mix gently.
10) Centrifuge samples at 14,000 x g (Beckman Microfuge 18; ~12,000 rpm) for 5 minutes.
11) Transfer each sample to a sterile, labeled 0.65 mL microcentrifuge tube.

4.3. Nanomedicine Physicochemical Characterization Assays

4.3.1. Size Distribution

Reagents:

- Assay Buffer (10 mM Tris-HCl/0.2 mM EDTA, pH 8.0)
- Liposome Preparation

Materials:

- Cuvettes, polystyrene 1 x 1 x 4.5 cm: (Sarstedt #67-754)

Equipment:

- P-20 Pipette: (Gilson)
- ZetaSizer ZS90: (Malvern)

Procedures:

1) Pipette appropriate volume into a plastic sizing cuvette. Typically 10 µL of preparation is diluted into 990 µL of assay buffer or alternative solvent (1X PBS).
2) Wipe the front and back of the cuvette with a Kemwipe and place the cuvette in the sample holder of the ZetaSizer with the notch facing forward.
3) Measure size distribution with the default parameters. Voltage and attenuation parameters are determined automatically.
4) After running the sample, discard samples in doxorubicin waste containers and the cuvettes in the glassware box.

4.3.2. Zeta Potential

Reagents:

- Assay Buffer (10 mM Tris-HCl/0.2 mM EDTA, pH 8.0)
- Liposome Preparation

Materials:

- Cuvettes, polystyrene 1 x 1 x 4.5 cm: (Sarstedt #67-754)

Equipment:

- P-20 Pipette: (Gilson)
- ZetaSizer ZS90: (Malvern)
- Zeta Dip Cell, Aqueous: (Malvern #ZEN1002 lot #MAL1056915)

Procedures:

1) Pipette appropriate volume into a plastic sizing cuvette. Typically 10 µL of preparation is diluted into 990 µL of assay buffer or alternative solvent.
2) Place the zeta dip cell into the cuvette with the mountains on the dip cell facing the notch in the cuvette. Make sure no air bubbles get trapped in the dip cell.
3) Wipe the front and back of the cuvette with a Kemwipe and place the cuvette in the sample holder of the ZetaSizer with the notch facing forward.
4) Measure zeta potential with the default parameters, except the cuvette type was changed to zeta dip cell. Voltage and attenuation parameters were determined automatically.

5) After running the sample, rinse the zeta dip cell under distilled water and dry with a Kemwipe. Discard samples in doxorubicin waste containers and the cuvettes in the glassware box.

4.3.3. Orientation Assay of pVIII Protein in Liposomes

Reagents:

- Phage protein-modified Liposomes
- Proteinase K (100 µg/mL)
- PMFS (30 mM)
- 1X TBS, pH 7.4
- $CaCl_2$ (2.5 mM)

Materials:

- 0.65mL Microcentrifuge Tubes

Equipment:

- Heat Block

Procedures:

1) Prepare two samples of isolated coat protein for a proteinase K treated sample and an untreated sample for each protein used for modification. For each sample dilute the volume of protein calculated above in equation 7 to a total volume of 10µL with 10mM cholate/10mM Tris-HCl, pH8.0/0.2mM EDTA in a 0.65mL microcentrifuge tube.
2) Prepare two samples of modified Doxil for a proteinase K treated sample and an untreated sample for each preparation of modified Doxil. For each sample place 1µL of concentrated, modified Doxil into 9µL of distilled water in a 0.65mL microcentrifuge tube and mix thoroughly.
3) For each untreated sample, add 20µL of distilled water to the sample and mix thoroughly.
4) For each treated sample, add 2.5µL of 2.5mM $CaCl_2$ solution to activate the proteinase K and 12.5µL 100µg/mL proteinase K. Mix thoroughly and incubate at room temperature for 1 hour.
5) To stop the proteinase K reaction, add 5µL of 30mM PMFS to each of the treated samples. Mix thoroughly and incubate at room temperature for 5 min to ensure complete inhibition of the reaction.
6) Run samples on SDS-PAGE and detect for protein by Western blotting with appropriate antibodies.

4.4. Cell Viability Assays

4.4.1. Mammalian Cell Viability Assay by MTT

MTT is a commonly used method to determine viability in mammalian cells after treatment with various cytotoxic agents. Various parameters can be adjusted based on the desired treatment or goal of the experiment. Briefly, MTT is added to metabolically active cells that will reduce the MTT to a formazan precipitate within the cells. After sufficient incubation with MTT, the formazan crystals are solubilized with SDS/HCl before absorbance measurement at 570 nm. Protocol is adapted from the procedures described in Molecular Probes Vybrant MTT Cell Proliferation Assay Kit #V-13154.

Reagents:

- MTT in 1X PBS (5 mg/mL or 12 mM):
- Minimal Essential Medium, without phenol red
- Sodium Dodecyl Sulfate, SDS:
- Hydrochloric acid, HCl (0.01 M)

Materials:

- 96-well Flat Bottom Plate, Cell Culture Treated: (Costar #3595)
- Microcentrifuge tubes, 1.7 mL
- Centrifuge tubes, 15 mL: (Corning #430052)

Equipment:

- P-20 Pipette: (Gilson)
- P-1000 Pipette: (Gilson)
- Balance, Analytical:
- Plate Reader: (BioTek Synergy H1)

Procedures:

1) Passage cells as described in the lab manual, seed a suitable concentration of viable cells in a 96 well cell culture treated plate and allow cells to attach for at least 6 hours in complete cell culture media in a 37ºC incubator with 5% CO_2. Incubate with any treatments for an appropriate timeframe.
2) Calculate the volume of MTT working stock required for experiment:

Number of	Volume per	Volume	Volume Medium	Volume MTT Stock	Total

Wells	Well (mL)	Medium (mL)	×105% (mL)	[10% Medium] (mL)	Volume (mL)
1	0.1	0.1	0.1	0.01	0.11
12	0.1	1.2	1.26	0.126	1.39
48	0.1	4.8	5.04	0.504	5.54
96	0.1	9.6	10.08	1.01	11.09
192	0.1	19.2	20.16	2.02	22.18

3) Prepare a working stock of MTT as calculated above in MEM or a related basal medium without added serum or phenol red.
4) Aspirate the spent medium from the cells in each well by vacuum or manual pipetting. Be careful not to aspirate any cells during medium removal.
5) Add 110 µL of MTT working stock to each well containing cells. Add 110 µL of MTT working stock to three untreated wells containing no cells for a background blank. A single pipette tip (or single tips on a multichannel pipette) can be used for addition of treatment as long as the tips do not contact the cells at the bottom of the wells.
6) Briefly agitate the plate to mix the components within the wells.
7) Incubate plate in a 37ºC incubator with 5% CO_2 for 4 hours (Shorter time periods down to 1 hour can be used, but decreased sensitivity will be observed).
8) Prepare fresh SDS-HCl working solution by adding 10 mL of 0.01 M HCl to 1 gram of SDS measured into a 15 mL centrifuge tube. Mix the solution by vortexing until the SDS has dissolved into solution. Gentle heating may be used to solubilize SDS if it is slow to dissolve.
9) Add 100 µL of SDS-HCl working solution to each well containing MTT and mix thoroughly. Be careful not to introduce foam/bubbles into the wells by vigorous mixing. If bubbles are present, they can be removed by popping them with a large gauge needle prior to reading.
10) Incubate the plate in a 37ºC incubator with 5% CO_2 for 4 hour (Longer times can be used up to 18 hours without significant loss of signal, however sensitivity is decreased depending on the cell type).
11) Measure absorbance at 570 nm with a reference wavelength of 690 nm with Synergy H1 plate reader.
12) Compute the average absorbance of blanks at 570 nm as follows:

$$\text{Average Blank}_{570\text{ nm}} = \frac{\sum \text{Blank}_{570\text{ nm}}}{\text{Number of Blanks}} \tag{29}$$

13) Subtract the average blank at 570 nm from every other well on the plate:

$$\text{Blanked Sample}_{570\text{ nm}} = \text{Sample}_{570\text{ nm}} - \text{Average Blank}_{570\text{ nm}} \tag{30}$$

4.4.2. CellTiter Blue Assay

Reagents:

- CellTiter Blue, 20 mL: (Promega #G8080)
- Complete Cell Culture Medium
- Minimal Essential Medium (MEM) – without phenol red or L-Glutamine, (1X), 100 mL: (Gibco #51200-038)
- PBS, pH 7.2 w/o CaCl2 or MgCl2, (1X), 100 mL: (Gibco #20012-027)

Materials:

- 96-well Flat Bottom Plate, Cell Culture Treated: (Costar #3595)
- Microcentrifuge tubes, 1.7 mL
- Centrifuge tubes, 15 mL: (Corning #430052)

Equipment:

- Plate Reader: (BioTek Synergy H1)

Procedures:

1) Passage cells as described in the lab manual, seed a suitable concentration of viable cells in a 96 well cell culture treated plate and allow cells to attach for at least 6 hours in complete cell culture media in a 37ºC incubator with 5% CO_2. Incubate with any treatments for an appropriate timeframe.
2) Prepare serial dilutions (7 dilutions w/ 3 replicates per dilution) of each drug preparation in the appropriate complete cell culture medium.
3) Aspirate the medium from each of the wells using a vacuum with gentle suction.
4) Add 100 µL of each prepared sample into the corresponding well.
5) Incubate the 96-well plates in a 37ºC cell culture incubator with 5% CO2 for 24 hours.
6) After 24 hours, aspirate the culture medium containing drug treatments and replace with 100 µL of fresh culture medium and return to a 37ºC cell culture incubator with 5% CO2 for an additional 48 hours of washout.
7) Prepare working solution of resazurin reagent by diluting 4 mL of stock CellTiter Blue into 20 mL of 1X MEM without phenol red and mix thoroughly by vortexing.
8) Aspirate the culture medium from the treated cells in each of the 96-well plates.

9) Pipette 120 μL of resazurin working solution into each of the wells.

10) Gently shake the plate for ~10 seconds to create a homogeneous mixture.

11) Incubate in a 37ºC cell culture incubator with 5% CO2 for 1 hour.

12) Using the BioTek Synergy H1 plate reader, shake the plate for 10 seconds before reading the fluorescence at an excitation wavelength of 560 nm and an emission wavelength of 590 nm.

13) Return the plates into a 37ºC cell culture incubator with 5% CO2 for an additional 2-3 hours (3-4 hour total incubation) and repeat the fluorescent measurement as previously.

14) Calculate the average untreated, Triton X-100, and empty wells. Subtract the average of the empty wells from each of the samples. Calculate the percent viable for each sample according to the following formula:

$$\text{Viable } (\%) = \frac{(\text{Blanked Sample} - \text{Average Triton X-100})}{(\text{Average Untreated})} \times 100 \quad (31)$$

15) Calculate the average, standard deviation, and margin of error for each set of sample replicates. Plot the average percent viable cells versus the concentration of drug added on a x-y scatter plot.

REFERENCES

Abdella, B.R. & Fisher, J., 1985. A chemical perspective on the anthracycline antitumor antibiotics. *Environmental health perspectives*, 64, pp.4–18.

Ali, H.R. et al., 2014. Association between CD8+ T-cell infiltration and breast cancer survival in 12,439 patients. *Annals of Oncology*, 25(8), pp.1536–1543.

An, P. et al., 2004. Suppression of tumor growth and metastasis by a VEGFR-1 antagonizing peptide identified from a phage display library. *International Journal of Cancer*, 111(2), pp.165–173.

Andreev, O.A., Engelman, D.M. & Reshetnyak, Y.K., 2010. pH-sensitive membrane peptides (pHLIPs) as a novel class of delivery agents. *Molecular membrane biology*, 27(7), pp.341–352.

Angelov, D. et al., 2006. Nucleolin is a histone chaperone with FACT-like activity and assists remodeling of nucleosomes. *The EMBO journal*, 25(8), pp.1669–1679.

Antony, A.C., 1996. Folate receptors. *Annual review of nutrition*, 16, pp.501–521.

Arap, W., Pasqualini, R. & Ruoslahti, E., 1998a. Cancer treatment by targeted drug delivery to tumor vasculature in a mouse model. *Science*, 279(5349), pp.377–380.

Arap, W., Pasqualini, R. & Ruoslahti, E., 1998b. Cancer treatment by targeted drug delivery to tumor vasculature in a mouse model. *Science*, 279(5349), pp.377–380.

Arora, A. & Scholar, E.M., 2005. Role of tyrosine kinase inhibitors in cancer therapy. *The Journal of pharmacology and experimental therapeutics*, 315(3), pp.971–979.

Attarwala, H., 2010. Role of antibodies in cancer targeting. *Journal of natural science, biology, and medicine*, 1(1), pp.53–56.

Bae, Y.H. & Park, K., 2011. Targeted drug delivery to tumors: myths, reality and possibility. *Journal of Controlled Release*, 153(3), pp.198–205.

Baluk, P., Hashizume, H. & McDonald, D.M., 2005. Cellular abnormalities of blood vessels as targets in cancer. *Current opinion in genetics & development*, 15(1), pp.102–111.

Baylin, S.B. et al., 2001. Aberrant patterns of DNA methylation, chromatin formation and gene expression in cancer. *Human molecular genetics*, 10(7), pp.687–692.

Bazzoni, G. & Dejana, E., 2004. Endothelial cell-to-cell junctions: molecular organization and role in vascular homeostasis. *Physiological reviews*, 84(3), pp.869–901.

Bechara, C. & Sagan, S., 2013. Cell-penetrating peptides: 20 years later, where do we stand? *FEBS Letters*, 587(12), pp.1693–1702.

Bedi, D. et al., 2013. Targeted delivery of siRNA into breast cancer cells via phage fusion proteins. *Molecular Pharmaceutics*, 10(2), pp.551–559.

Bedi, D., Gillespie, J.W. & Petrenko, V.A., 2014. Selection of pancreatic cancer cell-binding landscape phages and their use in development of anticancer nanomedicines. *Protein Engineering, Design & Selection*, 27(7), pp.235–243.

Berlin, C. et al., 1995. alpha 4 integrins mediate lymphocyte attachment and rolling under physiologic flow. *Cell*,

80(3), pp.413–422.

Bertrand, N. et al., 2014. Cancer nanotechnology: the impact of passive and active targeting in the era of modern cancer biology. *Advanced drug delivery reviews*, 66, pp.2–25.

Bélizaire, A.-K. et al., 2003. Identification of a murine ICAM-1-specific peptide by subtractive phage library selection on cells. *Biochemical and biophysical research communications*, 309(3), pp.625–630.

Bignold, L.P., 2006. Alkylating agents and DNA polymerases. *Anticancer research*, 26(2B), pp.1327–1336.

Bijlsma, M.F. & van Laarhoven, H.W.M., 2015. The conflicting roles of tumor stroma in pancreatic cancer and their contribution to the failure of clinical trials: a systematic review and critical appraisal. *Cancer metastasis reviews*, 34(1), pp.97–114.

Bode, S.A. et al., 2015. Enzyme-Activatable Cell-Penetrating Peptides through a Minimal Side Chain Modification. *Bioconjugate chemistry*, 26(5), pp.850–856.

Boudreau, N.J. & Jones, P.L., 1999. Extracellular matrix and integrin signalling: the shape of things to come. *The Biochemical journal*, 339 (Pt 3), pp.481–488.

Brigati, J.R. & Petrenko, V.A., 2005. Thermostability of landscape phage probes. *Analytical and Bioanalytical Chemistry*, 382(6), pp.1346–1350.

Brigati, J.R. et al., 2008. Phage display for generating peptide reagents. In J. E. Coligan et al., eds. *Current Protocols in Protein Science*. New Jersey: John Wiley & Sons, Inc., pp. 1–27.

Brooks, H., Lebleu, B. & Vives, E., 2005. Tat peptide-mediated cellular delivery: back to basics. *Advanced drug delivery reviews*, 57(4), pp.559–577.

Buggins, T.R., Dickinson, P.A. & Taylor, G., 2007. The effects of pharmaceutical excipients on drug disposition. *Advanced drug delivery reviews*, 59(15), pp.1482–1503.

Burrell, R.A. et al., 2013. The causes and consequences of genetic heterogeneity in cancer evolution. *Nature*, 501(7467), pp.338–345.

Calzolari, A. et al., 2007. Transferrin receptor 2 is frequently expressed in human cancer cell lines. *Blood cells, molecules & diseases*, 39(1), pp.82–91.

Carboni, E. et al., 2014. Particle margination and its implications on intravenous anticancer drug delivery. *AAPS PharmSciTech*, 15(3), pp.762–771.

Carson-Walter, E.B. et al., 2001. Cell surface tumor endothelial markers are conserved in mice and humans. *Cancer Research*, 61(18), pp.6649–6655.

Cerchia, L. & de Franciscis, V., 2010. Targeting cancer cells with nucleic acid aptamers. *Trends in biotechnology*, 28(10), pp.517–525.

Chan, K.-S., Koh, C.-G. & Li, H.-Y., 2012. Mitosis-targeted anti-cancer therapies: where they stand. *Cell death & disease*, 3, p.e411.

Chan, K.S. et al., 2009. Identification, molecular characterization, clinical prognosis, and therapeutic targeting of human bladder tumor-initiating cells. *Proceedings of the National Academy of Sciences*, 106(33), pp.14016–14021.

Chang, C.Y. et al., 1999. Dissection of the LXXLL nuclear receptor-coactivator interaction motif using

combinatorial peptide libraries: discovery of peptide antagonists of estrogen receptors alpha and beta. *Molecular and cellular biology*, 19(12), pp.8226–8239.

Chen, F.L., Xia, W. & Spector, N.L., 2008. Acquired resistance to small molecule ErbB2 tyrosine kinase inhibitors. *Clinical cancer research : an official journal of the American Association for Cancer Research*, 14(21), pp.6730–6734.

Chen, J. & Weiss, W.A., 2015. Alternative splicing in cancer: implications for biology and therapy. *Oncogene*, 34(1), pp.1–14.

Chen, Z.G., 2010. Small-molecule delivery by nanoparticles for anticancer therapy. *Trends in Molecular Medicine*, 16(12), pp.594–602.

Chlebowski, R.T., 1979. Adriamycin (doxorubicin) cardiotoxicity: a review. *The Western journal of medicine*, 131(5), pp.364–368.

Cho, Y. et al., 2003. CD4+ and CD8+ T cells cooperate to improve prognosis of patients with esophageal squamous cell carcinoma. *Cancer Research*, 63(7), pp.1555–1559.

Christian, S., 2003. Nucleolin expressed at the cell surface is a marker of endothelial cells in angiogenic blood vessels. *Journal of Cell Biology*, 163(4), pp.871–878.

Christiansen, M.N. et al., 2014. Cell surface protein glycosylation in cancer. *Proteomics*, 14(4-5), pp.525–546.

Corti, A. & Curnis, F., 2011. Isoaspartate-dependent molecular switches for integrin-ligand recognition. *Journal of Cell Science*, 124(Pt 4), pp.515–522.

Corti, A. et al., 2008. The neovasculature homing motif NGR: more than meets the eye. *Blood*, 112(7), pp.2628–2635.

Couet, J. et al., 1997. Identification of peptide and protein ligands for the caveolin-scaffolding domain: Implications for the interaction of caveolin with caveolae-associated proteins. *The Journal of biological chemistry*, 272(10), pp.6525–6533.

Croce, C.M., 2009. Causes and consequences of microRNA dysregulation in cancer. *Nature reviews. Genetics*, 10(10), pp.704–714.

Daniels, T.R. et al., 2012. The transferrin receptor and the targeted delivery of therapeutic agents against cancer. *Biochimica et biophysica acta*, 1820(3), pp.291–317.

Daniels, T.R., Delgado, T., Helguera, G., et al., 2006a. The transferrin receptor part II: targeted delivery of therapeutic agents into cancer cells. *Clinical immunology (Orlando, Fla.)*, 121(2), pp.159–176.

Daniels, T.R., Delgado, T., Rodríguez, J.A., et al., 2006b. The transferrin receptor part I: Biology and targeting with cytotoxic antibodies for the treatment of cancer. *Clinical immunology (Orlando, Fla.)*, 121(2), pp.144–158.

Das, P.M. & Singal, R., 2004. DNA methylation and cancer. *Journal of clinical oncology : official journal of the American Society of Clinical Oncology*, 22(22), pp.4632–4642.

Davis, M.E. et al., 2010. Evidence of RNAi in humans from systemically administered siRNA via targeted nanoparticles. *Nature*, 464(7291), pp.1067–1070.

Dehouck, B. et al., 1997. A new function for the LDL receptor: transcytosis of LDL across the blood-brain barrier. *Journal of Cell Biology*, 138(4), pp.877–889.

Denisova, G. et al., 2009. Characterizing complex polysera produced by antigen-specific immunization through the use of affinity-selected mimotopes. *PloS one*, 4(4), p.e5309.

DeSantis, C.E. et al., 2014. Cancer treatment and survivorship statistics, 2014. *CA: A Cancer Journal for Clinicians*, 64(4), pp.252–271.

Desgrosellier, J.S. & Cheresh, D.A., 2010. Integrins in cancer: biological implications and therapeutic opportunities. *Nature reviews. Cancer*, 10(1), pp.9–22.

Deutscher, S.L., 2010. Phage display in molecular imaging and diagnosis of cancer. *Chemical Reviews*, 110(5), pp.3196–3211.

Di Segni, A., Farin, K. & Pinkas-Kramarski, R., 2008. Identification of nucleolin as new ErbB receptors- interacting protein. *PloS one*, 3(6), p.e2310.

Dixon, J. et al., 1994. Expression of aminopeptidase-n (CD 13) in normal tissues and malignant neoplasms of epithelial and lymphoid origin. *Journal of clinical pathology*, 47(1), pp.43–47.

Dobrovolskaia, M.A. & McNeil, S.E., 2007. Immunological properties of engineered nanomaterials. *Nature nanotechnology*, 2(8), pp.469–478.

Duffy, M.J., 1996. Proteases as prognostic markers in cancer. *Clinical cancer research : an official journal of the American Association for Cancer Research*, 2(4), pp.613–618.

Early Breast Cancer Trialists' Collaborative Group (EBCTCG), 2005. Effects of chemotherapy and hormonal therapy for early breast cancer on recurrence and 15-year survival: an overview of the randomised trials. *Lancet*, 365(9472), pp.1687–1717.

Fagbohun, O.A., 2010. *Landscape Phage-Targeted Drug Delivery to Breast Cancer Cells*. Auburn University, AL: Auburn University.

Fagbohun, O.A. et al., 2012. Landscape phages and their fusion proteins targeted to breast cancer cells. *Protein Engineering, Design & Selection*, 25(6), pp.271–283.

Falo, L.D. et al., 1992. Serum proteases alter the antigenicity of peptides presented by class I major histocompatibility complex molecules. *Proceedings of the National Academy of Sciences*, 89(17), pp.8347–8350.

Fang, J., Nakamura, H. & Maeda, H., 2011. The EPR effect: Unique features of tumor blood vessels for drug delivery, factors involved, and limitations and augmentation of the effect. *Advanced drug delivery reviews*, 63(3), pp.136–151.

Fang, M. et al., 2014. Collagen as a double-edged sword in tumor progression. *Tumour biology : the journal of the International Society for Oncodevelopmental Biology and Medicine*, 35(4), pp.2871–2882.

Fani, M. et al., 2006. Comparative evaluation of linear and cyclic 99mTc-RGD peptides for targeting of integrins in tumor angiogenesis. *Anticancer research*, 26(1A), pp.431–434.

Feig, C. et al., 2012. The pancreas cancer microenvironment. *Clinical cancer research : an official journal of the American Association for Cancer Research*, 18(16), pp.4266–4276.

Ferrari, M., 2005. Cancer nanotechnology: opportunities and challenges. *Nature reviews. Cancer*, 5(3), pp.161–171.

Ferretti, S. et al., 2009. Tumor interstitial fluid pressure as an early-response marker for anticancer therapeutics. *Neoplasia (New York, N.Y.)*, 11(9), pp.874–881.

Fisher, R., Larkin, J. & Swanton, C., 2012. Inter and intratumour heterogeneity: a barrier to individualized medical therapy in renal cell carcinoma? *Frontiers in oncology*, 2, p.49.

Florent, J.-C. & Monneret, C., 2008. Doxorubicin Conjugates for Selective Delivery to Tumors. In K. Krohn, ed. *Topics in Current Chemistry*. Berlin: Springer, pp. 99–140.

Fraire, A.E. et al., 1987. Lung cancer heterogeneity. Prognostic implications. *Cancer*, 60(3), pp.370–375.

Fukasawa, K. et al., 2006. Aminopeptidase N (APN/CD13) is selectively expressed in vascular endothelial cells and plays multiple roles in angiogenesis. *Cancer letters*, 243(1), pp.135–143.

Gabizon, A. & Papahadjopoulos, D., 1988. Liposome formulations with prolonged circulation time in blood and enhanced uptake by tumors. *Proceedings of the National Academy of Sciences*, 85(18), pp.6949–6953.

Gabizon, A. et al., 1994. Prolonged circulation time and enhanced accumulation in malignant exudates of doxorubicin encapsulated in polyethylene-glycol coated liposomes. *Cancer Research*, 54(4), pp.987–992.

Gabizon, A., Shmeeda, H. & Barenholz, Y., 2003. Pharmacokinetics of pegylated liposomal Doxorubicin: review of animal and human studies. *Clinical pharmacokinetics*, 42(5), pp.419–436.

Galm, U. et al., 2005. Antitumor antibiotics: bleomycin, enediynes, and mitomycin. *Chemical Reviews*, 105(2), pp.739–758.

Gandra, N. et al., 2013. Virus-mimetic cytoplasm-cleavable magnetic/silica nanoclusters for enhanced gene delivery to mesenchymal stem cells. *Angewandte Chemie International Edition*, 52(43), pp.11278–11281.

Gardner, E.R. et al., 2008. Randomized crossover pharmacokinetic study of solvent-based paclitaxel and nab-paclitaxel. *Clinical cancer research : an official journal of the American Association for Cancer Research*, 14(13), pp.4200–4205.

Gasparini, G., Brooks, P.C. & Biganzoli, E., 1998. Vascular integrin alpha (v) beta3: a new prognostic indicator in breast cancer. *Clinical Cancer ...*.

Gentile, F., Curcio, A., et al., 2008a. The margination propensity of spherical particles for vascular targeting in the microcirculation. *Journal of nanobiotechnology*, 6, p.9.

Gentile, F., Ferrari, M. & Decuzzi, P., 2008b. The transport of nanoparticles in blood vessels: the effect of vessel permeability and blood rheology. *Annals of biomedical engineering*, 36(2), pp.254–261.

Giancotti, F.G., 1997. Integrin signaling: specificity and control of cell survival and cell cycle progression. *Current opinion in cell biology*, 9(5), pp.691–700.

Ginisty, H. et al., 1999. Structure and functions of nucleolin. *Journal of Cell Science*, 112 (Pt 6), pp.761–772.

Ginisty, H., Amalric, F. & Bouvet, P., 1998. Nucleolin functions in the first step of ribosomal RNA processing. *The EMBO journal*, 17(5), pp.1476–1486.

Gottlieb, T.A. et al., 1993. Actin microfilaments play a critical role in endocytosis at the apical but not the basolateral surface of polarized epithelial cells. *Journal of Cell Biology*, 120(3), pp.695–710.

Gray, B.P., McGuire, M.J. & Brown, K.C., 2013. A liposomal drug platform overrides Peptide ligand targeting to a cancer biomarker, irrespective of ligand affinity or density. *PloS one*, 8(8), p.e72938.

Grodzinski, P., Silver, M. & Molnar, L.K., 2006. Nanotechnology for cancer diagnostics: promises and challenges. *Expert review of molecular diagnostics*, 6(3), pp.307–318.

Gross, A.L., Gillespie, J.W. & Petrenko, V.A., Selection of Promiscuous Tumor Targeting Phage Proteins.

Gullino, P.M., Clark, S.H. & Grantham, F.H., 1964. The Interstitial Fluid of Solid Tumors. *Cancer Research*, 24, pp.780–794.

Gupta, B., Levchenko, T.S. & Torchilin, V.P., 2005. Intracellular delivery of large molecules and small particles by cell-penetrating proteins and peptides. *Advanced drug delivery reviews*, 57(4), pp.637–651.

Gutierrez, C. & Schiff, R., 2011. HER2: biology, detection, and clinical implications. *Archives of pathology & laboratory medicine*, 135(1), pp.55–62.

Ha, T.-Y., 2009. The role of regulatory T cells in cancer. *Immune network*, 9(6), pp.209–235.

Habashy, H.O. et al., 2010. Transferrin receptor (CD71) is a marker of poor prognosis in breast cancer and can predict response to tamoxifen. *Breast cancer research and treatment*, 119(2), pp.283–293.

Haglund, K., Di Fiore, P.P. & Dikic, I., 2003. Distinct monoubiquitin signals in receptor endocytosis. *Trends in biochemical sciences*, 28(11), pp.598–603.

Hamzeh-Mivehroud, M., Mahmoudpour, A. & Dastmalchi, S., 2012. Identification of new peptide ligands for epidermal growth factor receptor using phage display and computationally modeling their mode of binding. *Chemical biology & drug design*, 79(3), pp.246–259.

Hansen, S.H., Sandvig, K. & van Deurs, B., 1993. Clathrin and HA2 adaptors: effects of potassium depletion, hypertonic medium, and cytosol acidification. *Journal of Cell Biology*, 121(1), pp.61–72.

Haraguchi, N. et al., 2010. CD13 is a therapeutic target in human liver cancer stem cells. *The Journal of clinical investigation*, 120(9), pp.3326–3339.

Hartmann, L.C. et al., 2007. Folate receptor overexpression is associated with poor outcome in breast cancer. *International Journal of Cancer*, 121(5), pp.938–942.

Hartsock, A. & Nelson, W.J., 2008. Adherens and tight junctions: structure, function and connections to the actin cytoskeleton. *Biochimica et biophysica acta*, 1778(3), pp.660–669.

Hashida, H. et al., 2002. Aminopeptidase N is involved in cell motility and angiogenesis: its clinical significance in human colon cancer. *Gastroenterology*, 122(2), pp.376–386.

Healy, J.M. et al., 1995. Peptide ligands for integrin alpha v beta 3 selected from random phage display libraries. *Biochemistry*, 34(12), pp.3948–3955.

Heldin, C.-H. et al., 2004. High interstitial fluid pressure - an obstacle in cancer therapy. *Nature reviews. Cancer*, 4(10), pp.806–813.

Heuser, J.E. & Anderson, R.G., 1989. Hypertonic media inhibit receptor-mediated endocytosis by blocking clathrin-coated pit formation. *Journal of Cell Biology*, 108(2), pp.389–400.

Hirschmann-Jax, C. et al., 2004. A distinct “side population” of cells with high drug efflux capacity in human tumor cells. *Proceedings of the National Academy of Sciences*, 101(39), pp.14228–14233.

Ho, I.A., Lam, P.Y. & Hui, K.M., 2004. Identification and characterization of novel human glioma-specific peptides to potentiate tumor-specific gene delivery. *Human Gene Therapy*, 15(8), pp.719–732.

Hofmann, M. et al., 2006. Lowering of tumor interstitial fluid pressure reduces tumor cell proliferation in a xenograft tumor model. *Neoplasia (New York, N.Y.)*, 8(2), pp.89–95.

Holbro, T., Civenni, G. & Hynes, N.E., 2003. The ErbB receptors and their role in cancer progression. *Experimental cell research*, 284(1), pp.99–110.

Hovanessian, A.G. et al., 2010. Surface expressed nucleolin is constantly induced in tumor cells to mediate calcium-dependent ligand internalization. *PloS one*, 5(12), p.e15787.

Howell, S.M. et al., 2014. Serum stable natural peptides designed by mRNA display. *Scientific Reports*, 4, p.6008.

Hrkach, J. et al., 2012. Preclinical development and clinical translation of a PSMA-targeted docetaxel nanoparticle with a differentiated pharmacological profile. *Science translational medicine*, 4(128), p.128ra39.

Huang, J. et al., 2012. MimoDB 2.0: a mimotope database and beyond. *Nucleic Acids Research*, 40, pp.D271–D277.

Huang, Y. et al., 2006. The angiogenic function of nucleolin is mediated by vascular endothelial growth factor and nonmuscle myosin. *Blood*, 107(9), pp.3564–3571.

Hufton, S.E. et al., 2000. Development and application of cytotoxic T lymphocyte-associated antigen 4 as a protein scaffold for the generation of novel binding ligands. *FEBS Letters*, 475(3), pp.225–231.

Huttenlocher, A. & Horwitz, A.R., 2011. Integrins in cell migration. *Cold Spring Harbor perspectives in biology*, 3(9), p.a005074.

Hynes, N.E. & Lane, H.A., 2005. ERBB receptors and cancer: the complexity of targeted inhibitors. *Nature reviews. Cancer*, 5(5), pp.341–354.

Hynes, R.O., 2002. Integrins: bidirectional, allosteric signaling machines. *Cell*, 110(6), pp.673–687.

Ikeda, N. et al., 2003. Clinical significance of aminopeptidase N/CD13 expression in human pancreatic carcinoma. *Clinical cancer research : an official journal of the American Association for Cancer Research*, 9(4), pp.1503–1508.

Immordino, M.L. et al., 2004. Preparation, characterization, cytotoxicity and pharmacokinetics of liposomes containing lipophilic gemcitabine prodrugs. *Journal of Controlled Release*, 100(3), pp.331–346.

Ishida, T. & Kiwada, H., 2008. Accelerated blood clearance (ABC) phenomenon upon repeated injection of PEGylated liposomes. *International journal of pharmaceutics*, 354(1-2), pp.56–62.

Ishida, T. et al., 2003. Accelerated clearance of a second injection of PEGylated liposomes in mice. *International journal of pharmaceutics*, 255(1-2), pp.167–174.

Ishii, K. et al., 2001. Aminopeptidase N regulated by zinc in human prostate participates in tumor cell invasion. *International Journal of Cancer*, 92(1), pp.49–54.

Ivanenkov, V.V. & Menon, A.G., 2000. Peptide-mediated transcytosis of phage display vectors in MDCK cells. *Biochemical and biophysical research communications*, 276(1), pp.251–257.

Iwasaki, T. et al., 2015. Cellular uptake and in vivo distribution of polyhistidine peptides. *Journal of Controlled Release*, 210, pp.115–124.

Jayanna, P.K., Bedi, D., DeInnocentes, P.A., et al., 2010a. Landscape phage ligands for PC3 prostate carcinoma cells. *Protein Engineering, Design & Selection*, 23(6), pp.423–430.

Jayanna, P.K., Bedi, D., Gillespie, J.W., et al., 2010b. Landscape phage fusion protein-mediated targeting of nanomedicines enhances their prostate tumor cell association and cytotoxic efficiency. *Nanomedicine: Nanotechnology, Biology, and Medicine*, 6(4), pp.538–546.

Jayanna, P.K., Torchilin, V.P. & Petrenko, V.A., 2009. Liposomes targeted by fusion phage proteins. *Nanomedicine: Nanotechnology, Biology, and Medicine*, 5(1), pp.83–89.

Kalli, K.R. et al., 2008. Folate receptor alpha as a tumor target in epithelial ovarian cancer. *Gynecologic oncology*, 108(3), pp.619–626.

Kamada, H. et al., 2007. Creation of novel cell-penetrating peptides for intracellular drug delivery using systematic phage display technology originated from Tat transduction domain. *Biological & pharmaceutical bulletin*, 30(2), pp.218–223.

Kamen, B.A. & Smith, A.K., 2004. A review of folate receptor alpha cycling and 5-methyltetrahydrofolate accumulation with an emphasis on cell models in vitro. *Advanced drug delivery reviews*, 56(8), pp.1085–1097.

Kaye, S.B., 1998. New antimetabolites in cancer chemotherapy and their clinical impact. *British journal of cancer*, 78 Suppl 3, pp.1–7.

Kelly, K.A. & Jones, D.A., 2003. Isolation of a colon tumor specific binding peptide using phage display selection. *Neoplasia (New York, N.Y.)*, 5(5), pp.437–444.

Kelly, K.A. et al., 2005. Detection of vascular adhesion molecule-1 expression using a novel multimodal nanoparticle. *Circulation research*, 96(3), pp.327–336.

Kennecke, H. et al., 2010. Metastatic behavior of breast cancer subtypes. *Journal of clinical oncology : official journal of the American Society of Clinical Oncology*, 28(20), pp.3271–3277.

Kluza, E. et al., 2012. Dual-targeting of αvβ3 and galectin-1 improves the specificity of paramagnetic/fluorescent liposomes to tumor endothelium in vivo. *Journal of Controlled Release*, 158(2), pp.207–214.

Knez, K. et al., 2013. Affinity comparison of p3 and p8 peptide displaying bacteriophages using surface plasmon resonance. *Analytical Chemistry*, 85(21), pp.10075–10082.

Kobayashi, T. et al., 2011. In vitro selection of a peptide inhibitor of human IL-6 using mRNA display. *Molecular biotechnology*, 48(2), pp.147–155.

Koivunen, E., Wang, B. & Ruoslahti, E., 1994. Isolation of a highly specific ligand for the alpha 5 beta 1 integrin from a phage display library. *Journal of Cell Biology*, 124(3), pp.373–380.

Koivunen, E., Wang, B. & Ruoslahti, E., 1995. Phage libraries displaying cyclic peptides with different ring sizes: ligand specificities of the RGD-directed integrins. *Biotechnology*, 13(3), pp.265–270.

Komarova, Y. & Malik, A.B., 2010. Regulation of endothelial permeability via paracellular and transcellular transport pathways. *Annual review of physiology*, 72, pp.463–493.

Kontermann, R.E., 2012. Dual targeting strategies with bispecific antibodies. *mAbs*, 4(2), pp.182–197.

Kraft, S. et al., 1999. Definition of an unexpected ligand recognition motif for alphav beta6 integrin. *The Journal of biological chemistry*, 274(4), pp.1979–1985.

Krag, D.N. et al., 2006. Selection of tumor-binding ligands in cancer patients with phage display libraries. *Cancer Research*, 66(15), pp.7724–7733.

Krust, B. et al., 2011. Targeting surface nucleolin with multivalent HB- 19 and related Nucant pseudopeptides results in distinct inhibitory mechanisms depending on the malignant tumor cell type. *BMC Cancer*, 11(1), p.333.

Kung, V.T. & Redemann, C.T., 1986. Synthesis of carboxyacyl derivatives of phosphatidylethanolamine and use as an efficient method for conjugation of protein to liposomes. *Biochimica et biophysica acta*, 862(2), pp.435–439.

Kuzmicheva, G.A., Jayanna, P.K., Eroshkin, A.M., et al., 2009a. Mutations in fd phage major coat protein modulate affinity of the displayed peptide. *Protein Engineering, Design & Selection*, 22(10), pp.631–639.

Kuzmicheva, G.A., Jayanna, P.K., Sorokulova, I.B., et al., 2009b. Diversity and censoring of landscape phage libraries. *Protein Engineering, Design & Selection*, 22(1), pp.9–18.

LaBarge, M.A., 2010. The Difficulty of Targeting Cancer Stem Cell Niches. *Clinical Cancer Research*, 16(12), pp.3121–3129.

Lampugnani, M.G. & Dejana, E., 2007. Adherens junctions in endothelial cells regulate vessel maintenance and angiogenesis. *Thrombosis research*, 120 Suppl 2, pp.S1–6.

Lankveld, D.P. et al., 2011. Blood clearance and tissue distribution of PEGylated and non-PEGylated gold nanorods after intravenous administration in rats. *Nanomedicine: Nanotechnology, Biology, and Medicine*, 6(2), pp.339–349.

Lapeyre, B., Bourbon, H. & Amalric, F., 1987. Nucleolin, the major nucleolar protein of growing eukaryotic cells: an unusual protein structure revealed by the nucleotide sequence. *Proceedings of the National Academy of Sciences*, 84(6), pp.1472–1476.

Lee, D.-H. et al., 2014. Glutathione PEGylated liposomal methylprednisolone (2B3-201) attenuates CNS inflammation and degeneration in murine myelin oligodendrocyte glycoprotein induced experimental autoimmune encephalomyelitis. *Journal of neuroimmunology*, 274(1-2), pp.96–101.

Lee, T.-Y. et al., 2007. Peptide-mediated targeting to tumor blood vessels of lung cancer for drug delivery. *Cancer Research*, 67(22), pp.10958–10965.

Li, H., Fan, X. & Houghton, J., 2007a. Tumor microenvironment: the role of the tumor stroma in cancer. *Journal of cellular biochemistry*, 101(4), pp.805–815.

Li, M.W.M., Mruk, D.D. & Cheng, C.Y., 2012. Gap junctions and blood-tissue barriers. *Advances in experimental medicine and biology*, 763, pp.260–280.

Li, R. et al., 2003. Use of phage display to probe the evolution of binding specificity and affinity in integrins. *Protein Engineering*, 16(1), pp.65–72.

Li, W., Suez, I. & Szoka, F.C., 2007b. Reconstitution of the M13 major coat protein and its transmembrane peptide segment on a DNA template. *Biochemistry*, 46(29), pp.8579–8591.

Liu, J.K. et al., 2014. Phage display discovery of novel molecular targets in glioblastoma-initiating cells. *Cell death and differentiation*, 21(8), pp.1325–1339.

Liu, Y. et al., 2011. Dual targeting folate-conjugated hyaluronic acid polymeric micelles for paclitaxel delivery. *International journal of pharmaceutics*, 421(1), pp.160–169.

Lockman, P.R. et al., 2004. Nanoparticle surface charges alter blood-brain barrier integrity and permeability. *Journal of drug targeting*, 12(9-10), pp.635–641.

Longmire, M., Choyke, P.L. & Kobayashi, H., 2008. Clearance properties of nano-sized particles and molecules as imaging agents: considerations and caveats. *Nanomedicine: Nanotechnology, Biology, and Medicine*, 3(5), pp.703–717.

Lopez-Tarruella, S. & Schiff, R., 2007. The dynamics of estrogen receptor status in breast cancer: re-shaping the paradigm. *Clinical cancer research : an official journal of the American Association for Cancer Research*, 13(23), pp.6921–6925.

Loughrey, H., Bally, M.B. & Cullis, P.R., 1987. A non-covalent method of attaching antibodies to liposomes. *Biochimica et biophysica acta*, 901(1), pp.157–160.

Lowman, H.B. et al., 1998. Molecular mimics of insulin-like growth factor 1 (IGF-1) for inhibiting IGF-1: IGF-binding protein interactions. *Biochemistry*, 37(25), pp.8870–8878.

Lu, P. et al., 2011. Extracellular matrix degradation and remodeling in development and disease. *Cold Spring Harbor perspectives in biology*, 3(12).

Lukyanova, N.Y. et al., 2009. Molecular profile and cell cycle in MCF-7 cells resistant to cisplatin and doxorubicin. *Experimental oncology*, 31(2), pp.87–91.

Luque-García, J.L. et al., 2010. Differential protein expression on the cell surface of colorectal cancer cells associated to tumor metastasis. *Proteomics*, 10(5), pp.940–952.

Madani, F. et al., 2011. Mechanisms of cellular uptake of cell-penetrating peptides. *Journal of biophysics (Hindawi Publishing Corporation : Online)*, 2011, p.414729.

Maheshwari, G. et al., 2000. Cell adhesion and motility depend on nanoscale RGD clustering. *Journal of Cell Science*, 113, pp.1677–1686.

Mamot, C. et al., 2012. Tolerability, safety, pharmacokinetics, and efficacy of doxorubicin-loaded anti-EGFR immunoliposomes in advanced solid tumours: a phase 1 dose-escalation study. *The lancet oncology*, 13(12), pp.1234–1241.

Mandava, S. et al., 2004. RELIC--a bioinformatics server for combinatorial peptide analysis and identification of protein-ligand interaction sites. *Proteomics*, 4(5), pp.1439–1460.

Manning, M., Chrysogelos, S. & Griffith, J., 1981. Mechanism of coliphage M13 contraction: intermediate structures trapped at low temperatures. *Journal of virology*, 40(3), pp.912–919.

Markman, J.L. et al., 2013. Nanomedicine therapeutic approaches to overcome cancer drug resistance. *Advanced drug delivery reviews*, 65(13-14), pp.1866–1879.

Martin, T.A. & Jiang, W.G., 2009. Loss of tight junction barrier function and its role in cancer metastasis. *Biochimica et biophysica acta*, 1788(4), pp.872–891.

Maruta, F. et al., 2002. Identification of FGF receptor-binding peptides for cancer gene therapy. *Cancer gene therapy*, 9(6), pp.543–552.

Marvin, D.A., Symmons, M.F. & Straus, S.K., 2014. Structure and assembly of filamentous bacteriophages. *Progress in Biophysics and Molecular Biology*, 114, pp.80–122.

Mathers, C., Fat, D.M. & Boerma, J.T., 2008. The global burden of disease: 2004 update.

Matsumura, Y. et al., 2004. Phase I and pharmacokinetic study of MCC-465, a doxorubicin (DXR) encapsulated in PEG immunoliposome, in patients with metastatic stomach cancer. *Annals of Oncology*, 15(3), pp.517–525.

McGuire, M.J. et al., 2014. Identification and characterization of a suite of tumor targeting peptides for non-small cell lung cancer. *Scientific Reports*, 4, p.4480.

McIntosh, D.P. et al., 2002. Targeting endothelium and its dynamic caveolae for tissue-specific transcytosis in vivo: a pathway to overcome cell barriers to drug and gene delivery. *Proceedings of the National Academy of Sciences*, 99(4), pp.1996–2001.

Menrad, A. et al., 1993. Biochemical and functional characterization of aminopeptidase N expressed by human melanoma cells. *Cancer Research*, 53(6), pp.1450–1455.

Modok, S., Mellor, H.R. & Callaghan, R., 2006. Modulation of multidrug resistance efflux pump activity to overcome chemoresistance in cancer. *Current opinion in pharmacology*, 6(4), pp.350–354.

Molenaar, T.J.M. et al., 2002. Specific inhibition of P-selectin-mediated cell adhesion by phage display-derived peptide antagonists. *Blood*, 100(10), pp.3570–3577.

Moore, N. & Lyle, S., 2011. Quiescent, slow-cycling stem cell populations in cancer: a review of the evidence and discussion of significance. *Journal of oncology*, 2011.

Moreno-Layseca, P. & Streuli, C.H., 2014. Signalling pathways linking integrins with cell cycle progression. *Matrix biology : journal of the International Society for Matrix Biology*, 34, pp.144–153.

Morita, Y. et al., 2006. Selection and properties for the recognition of P19 embryonic carcinoma stem cells. *Biotechnology progress*, 22(4), pp.974–978.

Mount, J.D. et al., 2004. Cell targeted phagemid rescued by preselected landscape phage. *Gene*, 341, pp.59–65.

Muller, P.Y. & Milton, M.N., 2012. The determination and interpretation of the therapeutic index in drug development. *Nature reviews. Drug discovery*, 11(10), pp.751–761.

Muller, W.A., 2009. Mechanisms of transendothelial migration of leukocytes. *Circulation research*, 105(3), pp.223–230.

Murayama, O., Nishida, H. & Sekiguchi, K., 1996. Novel peptide ligands for integrin alpha 6 beta 1 selected from a phage display library. *Journal of biochemistry*, 120(2), pp.445–451.

Nabi, I.R. & Le, P.U., 2003. Caveolae/raft-dependent endocytosis. *Journal of Cell Biology*, 161(4), pp.673–677.

Naito, Y. et al., 1998. CD8+ T cells infiltrated within cancer cell nests as a prognostic factor in human colorectal cancer. *Cancer Research*, 58(16), pp.3491–3494.

Naiyer, M.M. et al., 2013. Identification and characterization of a human IL-10 receptor antagonist. *Human immunology*, 74(1), pp.28–31.

Newton-Northup, J.R., Figueroa, S.D. & Deutscher, S.L., 2011. Streamlined in vivo selection and screening of human prostate carcinoma avid phage particles for development of peptide based in vivo tumor imaging agents. *Combinatorial chemistry & high throughput screening*, 14(1), pp.9–21.

Nobs, L. et al., 2004. Current methods for attaching targeting ligands to liposomes and nanoparticles. *Journal of pharmaceutical sciences*, 93(8), pp.1980–1992.

Nowell, P.C., 1976. The clonal evolution of tumor cell populations. *Science*, 194(4260), pp.23–28.

Oldenburg, K.R. et al., 1992. Peptide ligands for a sugar-binding protein isolated from a random peptide library. *Proceedings of the National Academy of Sciences*, 89(12), pp.5393–5397.

Oleinika, K. et al., 2013. Suppression, subversion and escape: the role of regulatory T cells in cancer progression. *Clinical and experimental immunology*, 171(1), pp.36–45.

Olofsson, L., Ankarloo, J. & Nicholls, I.A., 1998. Phage viability in organic media: insights into phage stability. *Journal of Molecular Recognition*, 11, pp.91–93.

Oyama, Tsukasa et al., 2006. Isolation of multiple cell-binding ligands from different phage displayed-peptide libraries. *Biosensors & bioelectronics*, 21(10), pp.1867–1875.

Oyama, Tsuksa et al., 2003. Isolation of lung tumor specific peptides from a random peptide library: generation of diagnostic and cell-targeting reagents. *Cancer letters*, 202(2), pp.219–230.

Paolino, D. et al., 2010. Gemcitabine-loaded PEGylated unilamellar liposomes vs GEMZAR: biodistribution, pharmacokinetic features and in vivo antitumor activity. *Journal of Controlled Release*, 144(2), pp.144–150.

Park, J.W. et al., 2002. Anti-HER2 immunoliposomes: enhanced efficacy attributable to targeted delivery. *Clinical cancer research : an official journal of the American Association for Cancer Research*, 8(4), pp.1172–1181.

Parton, R.G., Joggerst, B. & Simons, K., 1994. Regulated internalization of caveolae. *Journal of Cell Biology*, 127(5), pp.1199–1215.

Pasqualini, R. et al., 2000. Aminopeptidase N is a receptor for tumor-homing peptides and a target for inhibiting angiogenesis. *Cancer Research*, 60(3), pp.722–727.

Petrenko, V.A., 2008. Landscape Phage as a Molecular Recognition Interface for Detection Devices. *Microelectronics journal*, 39(2), pp.202–207.

Petrenko, V.A. & Jayanna, P.K., 2014. Phage protein-targeted cancer nanomedicines. *FEBS Letters*, 588(2), pp.341–349.

Petrenko, V.A. & Smith, G.P., 2005. *Phage Display In Biotechnology and Drug Discovery* S. S. Sidhu & C. R. Geyer, eds., Bo Raton, FL: CRC Press.

Petrenko, V.A. & Smith, G.P., 2000. Phages from landscape libraries as substitute antibodies. *Protein Engineering*, 13(8), pp.589–592.

Petrenko, V.A. et al., 1996. A library of organic landscapes on filamentous phage. *Protein Engineering*, 9(9), pp.797–801.

Petri, B. & Bixel, M.G., 2006. Molecular events during leukocyte diapedesis. *The FEBS journal*, 273(19), pp.4399–4407.

Petros, R.A. & DeSimone, J.M., 2010. Strategies in the design of nanoparticles for therapeutic applications. *Nature reviews. Drug discovery*, 9(8), pp.615–627.

Pfaff, M. et al., 1994. Selective recognition of cyclic RGD peptides of NMR defined conformation by alpha IIb beta 3, alpha V beta 3, and alpha 5 beta 1 integrins. *The Journal of biological chemistry*, 269(32), pp.20233–20238.

Phan, A. et al., 2007. Open label phase I study of MBP-426, a novel formulation of oxaliplatin, in patients with advanced or metastatic solid tumors. *Molecular Cancer*.

Pidgeon, C. & Hunt, C.A., 1981. Calculating number and surface area of liposomes in any suspension. *Journal of pharmaceutical sciences*, 70(2), pp.173–176.

Pollaro, L. & Heinis, C., 2010. Strategies to prolong the plasma residence time of peptide drugs. *MedChemComm*.

Pommier, Y., 2006. Topoisomerase I inhibitors: camptothecins and beyond. *Nature reviews. Cancer*, 6(10), pp.789–802.

Popkov, M. et al., 1998. Multidrug-resistance drug-binding peptides generated by using a phage display library. *European Journal of Biochemistry*, 251(1-2), pp.155–163.

Prabhakar, U. et al., 2013. Challenges and key considerations of the enhanced permeability and retention effect for nanomedicine drug delivery in oncology. In Cancer research. pp. 2412–2417.

Pytela, R., Pierschbacher, M.D. & Ruoslahti, E., 1985. Identification and isolation of a 140 kd cell surface glycoprotein with properties expected of a fibronectin receptor. *Cell*, 40(1), pp.191–198.

Qin, B. et al., 2011. Identification of a LNCaP-specific binding peptide using phage display. *Pharmaceutical research*, 28(10), pp.2422–2434.

Rajotte, D. et al., 1998. Molecular heterogeneity of the vascular endothelium revealed by in vivo phage display. *The Journal of clinical investigation*, 102(2), pp.430–437.

Rangel, R. et al., 2007. Impaired angiogenesis in aminopeptidase N-null mice. *Proceedings of the National Academy of Sciences*, 104(11), pp.4588–4593.

Recht, L. et al., 1990. Transferrin receptor in normal and neoplastic brain tissue: implications for brain-tumor immunotherapy. *Journal of neurosurgery*, 72(6), pp.941–945.

Richard, J.P. et al., 2003. Cell-penetrating peptides. A reevaluation of the mechanism of cellular uptake. *The Journal of biological chemistry*, 278(1), pp.585–590.

Riihimäki, M. et al., 2012. Death causes in breast cancer patients. *Annals of Oncology*, 23(3), pp.604–610.

Ringhieri, P. et al., 2015. Liposomal doxorubicin doubly functionalized with CCK8 and R8 peptide sequences for selective intracellular drug delivery. *Journal of peptide science : an official publication of the European Peptide Society*, 21(5), pp.415–425.

Roberts, W.G. & Palade, G.E., 1997. Neovasculature induced by vascular endothelial growth factor is fenestrated. *Cancer Research*, 57(4), pp.765–772.

Romanov, V.I., Durand, D.B. & Petrenko, V.A., 2001. Phage display selection of peptides that affect prostate carcinoma cells attachment and invasion. *The Prostate*, 47(4), pp.239–251.

Ross, J.F., Chaudhuri, P.K. & Ratnam, M., 1994. Differential regulation of folate receptor isoforms in normal and malignant tissues in vivo and in established cell lines. Physiologic and clinical implications. *Cancer*, 73(9), pp.2432–2443.

Ruoslahti, E., 1996. RGD and other recognition sequences for integrins. *Annual review of cell and developmental biology*, 12, pp.697–715.

Ruoslahti, E., 2002. Specialization of tumour vasculature. *Nature reviews. Cancer*, 2(2), pp.83–90.

Ruoslahti, E., 2000. Targeting tumor vasculature with homing peptides from phage display. *Seminars in cancer biology*, 10(6), pp.435–442.

Ryschich, E. et al., 2004. Transferrin receptor is a marker of malignant phenotype in human pancreatic cancer and in neuroendocrine carcinoma of the pancreas. *European journal of cancer (Oxford, England : 1990)*, 40(9), pp.1418–1422.

Sahay, G., Alakhova, D.Y. & Kabanov, A.V., 2010. Endocytosis of nanomedicines. *Journal of Controlled Release*, 145(3), pp.182–195.

Saiki, I. et al., 1993. Role of aminopeptidase N (CD13) in tumor-cell invasion and extracellular matrix degradation. *International Journal of Cancer*, 54(1), pp.137–143.

Samoylova, T.I. et al., 2003. Phage probes for malignant glial cells. *Molecular Cancer Therapeutics*, 2(11), pp.1129–1137.

Sanna, V., Pala, N. & Sechi, M., 2014. Targeted therapy using nanotechnology: focus on cancer. *International journal of nanomedicine*, 9, pp.467–483.

Sapra, P. & Allen, T.M., 2002. Internalizing antibodies are necessary for improved therapeutic efficacy of antibody-targeted liposomal drugs. *Cancer Research*, 62(24), pp.7190–7194.

Sato, E. et al., 2005. Intraepithelial CD8+ tumor-infiltrating lymphocytes and a high CD8+/regulatory T cell ratio are associated with favorable prognosis in ovarian cancer. *Proceedings of the National Academy of Sciences*, 102(51), pp.18538–18543.

Saul, J.M., Annapragada, A.V. & Bellamkonda, R.V., 2006. A dual-ligand approach for enhancing targeting selectivity of therapeutic nanocarriers. *Journal of Controlled Release*, 114(3), pp.277–287.

Schuurhuis, G.J. et al., 1993. Changes in subcellular doxorubicin distribution and cellular accumulation alone can largely account for doxorubicin resistance in SW-1573 lung cancer and MCF-7 breast cancer multidrug resistant tumour cells. *British journal of cancer*, 68(5), pp.898–908.

Schwind, P. et al., 1992. Subtilisin removes the surface layer of the phage fd coat. *European Journal of Biochemistry*, 210(2), pp.431–436.

Scott, J.K. et al., 1992. A family of concanavalin A-binding peptides from a hexapeptide epitope library. *Proceedings of the National Academy of Sciences*, 89(12), pp.5398–5402.

Seki, T., Fang, J. & Maeda, H., 2009. Enhanced delivery of macromolecular antitumor drugs to tumors by nitroglycerin application. *Cancer science*, 100(12), pp.2426–2430.

Senoo, H. & Hata, R., 1994. Extracellular matrix regulates cell morphology, proliferation, and tissue formation. *Kaibogaku zasshi. Journal of anatomy*, 69(6), pp.719–733.

Senzer, N. et al., 2013. Phase I study of a systemically delivered p53 nanoparticle in advanced solid tumors. *Molecular Therapy*, 21(5), pp.1096–1103.

Senzer, N.N. et al., 2009. Abstract C36: MBP-426, a novel liposome-encapsulated oxaliplatin, in combination with 5-FU/leucovorin (LV): Phase I results of a Phase I/II study in gastro- …. *Molecular Cancer*.

Shen, Q. et al., 2010. Myosin light chain kinase in microvascular endothelial barrier function. *Cardiovascular research*, 87(2), pp.272–280.

Shroff, K. & Kokkoli, E., 2012. PEGylated liposomal doxorubicin targeted to α5β1-expressing MDA-MB-231 breast cancer cells. *Langmuir : the ACS journal of surfaces and colloids*, 28(10), pp.4729–4736.

Shukla, S., Ohnuma, S. & Ambudkar, S.V., 2011. Improving cancer chemotherapy with modulators of ABC drug transporters. *Current drug targets*, 12(5), pp.621–630.

Siegel, R. et al., 2014. Cancer Statistics, 2014. *CA: A Cancer Journal for Clinicians*, 64(1), pp.9–29.

Siegel, R.L., Miller, K.D. & Jemal, A., 2015. Cancer statistics, 2015. *CA: A Cancer Journal for Clinicians*, 65(1), pp.5–29.

Singh, I., 2006. Textbook of human histology.

Slamon, D.J. et al., 1989. Studies of the HER-2/neu proto-oncogene in human breast and ovarian cancer. *Science*, 244(4905), pp.707–712.

Smith, G.P., 1993. Surface display and peptide libraries. *Gene*, 128, pp.1–2.

Smith, G.P. & Petrenko, V.A., 1997. Phage Display. *Chemical Reviews*, 97(2), pp.391–410.

Smith, G.P., Petrenko, V.A. & Matthews, L.J., 1998. Cross-linked filamentous phage as an affinity matrix. *Journal of immunological methods*, 215(1-2), pp.151–161.

Soekarjo, M. et al., 1996. Thermodynamics of the membrane insertion process of the M13 procoat protein, a lipid bilayer traversing protein containing a leader sequence. *Biochemistry*, 35(4), pp.1232–1241.

Sonaje, K. et al., 2012. Opening of epithelial tight junctions and enhancement of paracellular permeation by chitosan: microscopic, ultrastructural, and computed-tomographic observations. *Molecular Pharmaceutics*, 9(5), pp.1271–1279.

Spidlen, J. et al., 2012. FlowRepository: a resource of annotated flow cytometry datasets associated with peer-reviewed publications. *Cytometry. Part A : the journal of the International Society for Analytical Cytology*, 81(9), pp.727–731.

Spruijt, R.B., Wolfs, C.J. & Hemminga, M.A., 1989. Aggregation-related conformational change of the membrane-associated coat protein of bacteriophage M13. *Biochemistry*, 28(23), pp.9158–9165.

Srivastava, M. & Pollard, H.B., 1999. Molecular dissection of nucleolin's role in growth and cell proliferation: new insights. *FASEB journal : official publication of the Federation of American Societies for Experimental Biology*, 13(14), pp.1911–1922.

Stapleton, S. et al., 2013. Tumor perfusion imaging predicts the intra-tumoral accumulation of liposomes. *Journal of Controlled Release*, 172(1), pp.351–357.

Strebhardt, K. & Ullrich, A., 2008. Paul Ehrlich's magic bullet concept: 100 years of progress. *Nature reviews. Cancer*, 8(6), pp.473–480.

SUN, L. et al., 2007. Radiolabeling and Biodistribution of a Nasopharyngeal Carcinoma-targeting Peptide Identified by in vivo Phage Display. *Acta Biochimica et Biophysica Sinica*, 39(8), pp.624–632.

Sun, X. et al., 2010. Phage display-derived peptides for osteosarcoma imaging. *Clinical cancer research : an official journal of the American Association for Cancer Research*, 16(16), pp.4268–4277.

Suzuki, H. et al., 2013. Epigenetic alteration and microRNA dysregulation in cancer. *Frontiers in genetics*, 4, p.258.

Suzuki, M. et al., 1981. A new approach to cancer chemotherapy: selective enhancement of tumor blood flow with angiotensin II. *Journal of the National Cancer Institute*, 67(3), pp.663–669.

Tajrishi, M.M., Tuteja, R. & Tuteja, N., 2011. Nucleolin: The most abundant multifunctional phosphoprotein of nucleolus. *Communicative & integrative biology*, 4(3), pp.267–275.

Tan, B.T. et al., 2006. The cancer stem cell hypothesis: a work in progress. *Laboratory investigation; a journal of technical methods and pathology*, 86(12), pp.1203–1207.

Tang, B. et al., 2013. Screening of a specific peptide binding to VPAC1 receptor from a phage display peptide library. *PloS one*, 8(1), p.e54264.

Taurin, S., Nehoff, H. & Greish, K., 2012. Anticancer nanomedicine and tumor vascular permeability; Where is the missing link? *Journal of Controlled Release*, 164(3), pp.265–275.

Taverner, A. et al., 2015. Enhanced paracellular transport of insulin can be achieved via transient induction of myosin light chain phosphorylation. *Journal of Controlled Release*, 210, pp.189–197.

Tokuhara, T., 2006. Clinical Significance of Aminopeptidase N in Non-Small Cell Lung Cancer. *Clinical Cancer Research*, 12(13), pp.3971–3978.

Torchilin, V., 2011. Tumor delivery of macromolecular drugs based on the EPR effect. *Advanced drug delivery reviews*, 63(3), pp.131–135.

Torchilin, V.P., 2008. Tat peptide-mediated intracellular delivery of pharmaceutical nanocarriers. *Advanced drug delivery reviews*, 60(4-5), pp.548–558.

Tsai, M.-J. et al., 2014. Tumor microenvironment: a new treatment target for cancer. *ISRN biochemistry*, 2014, p.351959.

Tsutsui, S. et al., 2002. Prognostic value of c-erbB2 expression in breast cancer. *Journal of surgical oncology*, 79(4), pp.216–223.

Tu, X. et al., 2009. Screening and identification of a peptide specifically targeted to NCI-H1299 cells from a phage display peptide library. *Molecular Medicine Reports*, 2(6), pp.1005–1010.

Tuma, P.L. & Hubbard, A.L., 2003. Transcytosis: crossing cellular barriers. *Physiological reviews*, 83(3), pp.871–932.

Venables, J.P., 2004. Aberrant and alternative splicing in cancer. *Cancer Research*, 64(21), pp.7647–7654.

Ventola, C.L., 2012. The nanomedicine revolution: part 1: emerging concepts. *P & T : a peer-reviewed journal for formulary management*, 37(9), pp.512–525.

Vercauteren, D. et al., 2010. The use of inhibitors to study endocytic pathways of gene carriers: optimization and pitfalls. *Molecular Therapy*, 18(3), pp.561–569.

Vescio, R.A. et al., 1990. The distinction of small cell and non-small cell lung cancer by growth in native-state histoculture. *Cancer Research*, 50(18), pp.6095–6099.

Vestweber, D., 2008. VE-cadherin: the major endothelial adhesion molecule controlling cellular junctions and blood vessel formation. *Arteriosclerosis, thrombosis, and vascular biology*, 28(2), pp.223–232.

Visvader, J.E., 2011. Cells of origin in cancer. *Nature*, 469(7330), pp.314–322.

Visvader, J.E. & Lindeman, G.J., 2008. Cancer stem cells in solid tumours: accumulating evidence and unresolved questions. *Nature reviews. Cancer*, 8(10), pp.755–768.

Wakankar, A.A. & Borchardt, R.T., 2006. Formulation considerations for proteins susceptible to asparagine deamidation and aspartate isomerization. *Journal of pharmaceutical sciences*, 95(11), pp.2321–2336.

Wang, Jie et al., 2011a. Improving delivery and efficacy of nanomedicines in solid tumors: role of tumor priming. *Nanomedicine: Nanotechnology, Biology, and Medicine*, 6(9), pp.1605–1620.

Wang, Jing et al., 2012a. Selective photothermal therapy for breast cancer with targeting peptide modified gold nanorods. *Dalton Transactions*, 41(36), pp.11134–11144.

Wang, L H, Rothberg, K.G. & Anderson, R.G., 1993. Mis-assembly of clathrin lattices on endosomes reveals a regulatory switch for coated pit formation. *Journal of Cell Biology*, 123(5), pp.1107–1117.

Wang, Rongrong et al., 2012b. Application of poly(ethylene glycol)-distearoylphosphatidylethanolamine (PEG-DSPE) block copolymers and their derivatives as nanomaterials in drug delivery. *International journal of nanomedicine*, 7, pp.4185–4198.

Wang, Suwei et al., 2004. Doxorubicin induces apoptosis in normal and tumor cells via distinctly different mechanisms. intermediacy of H(2)O(2)- and p53-dependent pathways. *The Journal of biological chemistry*, 279(24), pp.25535–25543.

Wang, Tao et al., 2014. Enhanced tumor delivery and antitumor activity in vivo of liposomal doxorubicin modified with MCF-7-specific phage fusion protein. *Nanomedicine: Nanotechnology, Biology, and Medicine*, 10(2), pp.421–430.

Wang, Tao et al., 2011b. In vitro optimization of liposomal nanocarriers prepared from breast tumor cell specific phage fusion protein. *Journal of drug targeting*, 19(8), pp.597–605.

Wang, Tao, D'Souza, G.G.M., et al., 2010a. Enhanced binding and killing of target tumor cells by drug-loaded liposomes modified with tumor-specific phage fusion coat protein. *Nanomedicine: Nanotechnology, Biology, and Medicine*, 5(4), pp.563–574.

Wang, Tao, Petrenko, V.A. & Torchilin, V.P., 2010b. Paclitaxel-loaded polymeric micelles modified with MCF-7 cell-specific phage protein: enhanced binding to target cancer cells and increased cytotoxicity. *Molecular Pharmaceutics*, 7(4), pp.1007–1014.

Wang, Tao, Yang, S., et al., 2010c. Cytoplasmic delivery of liposomes into MCF-7 breast cancer cells mediated by cell-specific phage fusion coat protein. *Molecular Pharmaceutics*, 7(4), pp.1149–1158.

Wang, Weiqin et al., 2015. Cell-penetrating Peptides for Cancer-targeting Therapy and Imaging. *Current cancer drug targets*, 15(4), pp.337–351.

Weerakkody, D. et al., 2013. Family of pH (low) insertion peptides for tumor targeting. *Proceedings of the National Academy of Sciences*, 110(15), pp.5834–5839.

Wiig, H. et al., 2010. Interstitial fluid: the overlooked component of the tumor microenvironment? *Fibrogenesis & tissue repair*, 3, p.12.

Wu, C. et al., 2008a. A peptide-based carrier for intracellular delivery of proteins into malignant glial cells in vitro. *Journal of Controlled Release*, 130(2), pp.140–145.

Wu, P. et al., 2000. Identification of novel prostate-specific antigen-binding peptides modulating its enzyme activity. *European Journal of Biochemistry*, 267(20), pp.6212–6220.

Wu, X. et al., 2008b. Identification and characterization of a novel peptide ligand of Tie2 for targeting gene therapy. *Acta Biochimica et Biophysica Sinica*, 40(3), pp.217–225.

Xie, J., Lee, S. & Chen, X., 2010. Nanoparticle-based theranostic agents. *Advanced drug delivery reviews*, 62(11), pp.1064–1079.

Yang, H.-W. et al., 2012. Cooperative dual-activity targeted nanomedicine for specific and effective prostate cancer therapy. *ACS nano*, 6(2), pp.1795–1805.

Yao, L., Daniels, J., Danniels, J., et al., 2013a. pHLIP peptide targets nanogold particles to tumors. *Proceedings of the National Academy of Sciences*, 110(2), pp.465–470.

Yao, L., Daniels, J., Wijesinghe, D., et al., 2013b. pHLIP®-mediated delivery of PEGylated liposomes to cancer cells. *Journal of Controlled Release*, 167(3), pp.228–237.

Yuan, F. et al., 1995. Vascular permeability in a human tumor xenograft: molecular size dependence and cutoff size. *Cancer Research*, 55(17), pp.3752–3756.

Zacher, A.N. et al., 1980. A new filamentous phage cloning vector: fd-tet. *Gene*, 9(1-2), pp.127–140.

Zang, L. et al., 2009. Screening and identification of a peptide specifically targeted to NCI-H1299 from a phage display peptide library. *Cancer letters*, 281(1), pp.64–70.

Zhang, J. et al., 2014. Mechanism study of cellular uptake and tight junction opening mediated by goblet cell-specific trimethyl chitosan nanoparticles. *Molecular Pharmaceutics*, 11(5), pp.1520–1532.

Zhang, X.-X., Eden, H.S. & Chen, X., 2012. Peptides in cancer nanomedicine: drug carriers, targeting ligands and protease substrates. *Journal of Controlled Release*, 159(1), pp.2–13.

Zhang, Y. et al., 2010. [Screening and identification of CD13-binding peptides with phage display peptide library]. *Nan fang yi ke da xue xue bao = Journal of Southern Medical University*, 30(4), pp.827–830.

Zhao, H. et al., 2013. Enhanced binding to and killing of hepatocellular carcinoma cells in vitro by melittin when linked with a novel targeting peptide screened from phage display. *Journal of peptide science : an official publication of the European Peptide Society*, 19(10), pp.639–650.

Zhu, G.H. et al., 2003. [Screening of short peptides that bind specifically to osteosarcoma cells by phage-displayed peptide library]. *Di Yi Jun Yi Da Xue Bao*, 23(1), pp.12–15.

Zolnik, B.S. et al., 2010. Nanoparticles and the immune system. *Endocrinology*, 151(2), pp.458–465.

Zwicke, G.L., Mansoori, G.A. & Jeffery, C.J., 2012. Utilizing the folate receptor for active targeting of cancer nanotherapeutics. *Nano reviews*, 3.